Applications of Effective Field Theory to Electron Scattering

Thesis by
Luca R. Diaconescu

In Partial Fulfillment of the Requirements
for the Degree of
Doctor of Philosophy

California Institute of Technology
Pasadena, California

2005

(Defended January 7, 2005)

Acknowledgements

I would like to take this opportunity to thank all those who have made it possible for me to undertake and complete this work. My advisors, Robert McKeown, Michael Ramsey-Musolf, and Bira van Kolck, have provided a great deal of guidance and advice throughout my years at Caltech. They were also very understanding and supportive of my family needs, for which I am very grateful. I would also like to thank Rocco Schiavilla who provided advice, software, and computing resources for my first project.

Throughout my many years of study, my family has been very patient and supportive. My parents, Andi and Pia, have given me the desire and the opportunity to undertake this project. The support and love of my wife Magda have provide me with the inspiration and the will to fulfill it.

Finally, I would like to acknowledge the financial support I received from Nortel Networks.

Abstract

In this work two calculations are presented. In the first, we compute the vector analyzing power (VAP) for the elastic scattering of transversely polarized electrons from protons at low energies, using an effective theory of electrons, protons, and photons. We study all contributions through second order in E/M, where E and M are the electron energy and nucleon mass, respectively. The leading order VAP arises from the imaginary part of the interference of one- and two-photon exchange amplitudes. Sub-leading contributions are generated by the nucleon magnetic moment and charge radius, as well as recoil corrections to the leading-order amplitude. Working to $\mathcal{O}(E/M)^2$, we obtain a prediction for A_n that is free of unknown parameters and that agrees with the recent measurement of the VAP in backward angle ep scattering.

In the second part of this thesis the longitudinal asymmetry due to Z^0 exchange is calculated in quasi-elastic electron-deuteron scattering at momentum transfers $|Q^2| \simeq 0.1$ GeV^2 relevant for the SAMPLE experiment. The deuteron and pn scattering-state wave functions are obtained from solutions of a Schrödinger equation with the Argonne v_{18} potential. Electromagnetic and weak neutral one- and two-nucleon currents are included in the calculation. The two-nucleon currents of pion range are shown to be identical to those derived in Effective Field Theory. The results indicate that two-body contributions to the asymmetry are small ($\simeq 0.2\%$) around the quasi-elastic peak, but become relatively more significant ($\simeq 3\%$) in the high-energy wing of the quasi-elastic peak.

Contents

List of Figures

List of Tables

Chapter 1

Introduction

Over the years considerable effort has been put into the understanding of nuclear structure. In the Standard Model, the fundamental theory that governs the strong interaction is Quantum Chromodynamics (QCD), a renormalizable gauge theory.

QCD is a theory with asymptotic freedom, where the coupling constant is small in the high-energy regime and large at low energies. As a consequence, perturbative treatments break down in the low-energy region, where the nuclei reside. To circumvent this problem, special methods for working within the theory at low energy must be employed. The direct approach is to numerically solve the functional integrals on a lattice of space-time points. The second method is to base the field theory description on the physically observed degrees of freedom in a way that reflects the symmetries of the underlying fundamental theory. Such an approach is referred to as an effective field theory (EFT) (see [1], [2], [3]), and it is the subject of this work.

Two different computations that make use of EFT are presented in this work. In the first computation, the vector analyzing power (VAP) in electron proton scattering is computed. This work was published in Physical Review C70, 2004, 054003 (nucl-th/0405044). For this computation, an EFT with the pionic degrees of freedom integrated out is used. To leading order, the VAP arises from the interference of one- and two-photon exchange amplitudes. The calculation done to second order in p/M (where p is a small external momenta and M is the nucleon

mass) is free of unknown parameters and was compared against existing measurements. The calculation is found to be in agreement with the VAP measurement performed by the SAMPLE collaboration [4] and resolves a discrepancy with the potential scattering computation of [5]. At the higher energies used in VAP measurements performed at Mainz [6], the calculation was no longer able to match the experimental results. This is not unexpected since at those higher energies one expects the low energy expansion obtained from the EFT to break down. This points to the need to include more degrees of freedom (e.g., π's) in the EFT for the larger energy regime.

In the second computation, the two-body contribution to the parity violating (PV) asymmetry in electron deuteron scattering is computed. This work was published in Physical Review C63, 2001, 044007 (nucl-th/0011034). An effective theory with nucleons and pions as degrees of freedom is required in order to obtain the one- and two-body current operators. These operators are then used in conjunction with a successful phenomenological model in order to numerically compute the PV asymmetry. The calculation is performed at $Q^2 = 0.1 GeV^2$, which is relevant to the SAMPLE experiment [7] where the meson exchange current contribution to the PV asymmetry was a theoretical unknown. At the time this calculation was performed, a discrepancy between the SAMPLE measurement and the existing theoretical models existed. This work was undertaken in order to investigate if the meson exchange currents can account for this discrepancy. The results show that the two-body contributions to the PV asymmetry are small ($\simeq$ 0.2%) around the quasi-elastic peak, but become relatively more significant ($\simeq$ 3%) in the high-energy wing of the quasi-elastic peak. This is too small a contribution to account for the discrepancy in question. This discrepancy was later resolved by a re-evaluation of the experimental data [8].

1.1 Effective Field Theory

To illustrate how one obtains the effective field theory from the underlying fundamental theory, a brief description of how to construct the pion-nucleon Lagrangian is outlined. An effective field theory has two main features: it maintains the symmetry properties of the underlying fundamental theory, and it has an expansion parameter, typically a small momentum or small mass scale, which permits calculation to a given order in the theory to be performed in a systematic way. In EFT, the small expansion parameter arises from the separation of scales between the small momenta and masses involved and the characteristic scale of the EFT. In the case of QCD the characteristic mass for chiral symmetry is $\Lambda_\chi \simeq 1GeV$, and we immediately note that $m_\pi << \Lambda_\chi$. Thus, if the external momenta (p) involved in the process are small, both ratios m_π/Λ_χ and p/Λ_χ are small, and provide the small expansion parameter that an EFT requires.

We begin the discussion by first looking at chiral symmetry. Consider a free, massless spin 1/2 Dirac field:

$$L = i\bar{\Psi}\gamma_\mu\partial^\mu\Psi \tag{1.1}$$

We can define the projectors:

$$P_{R,L} = \frac{1 \pm \gamma_5}{2} \tag{1.2}$$

and the projected fields:

$$\Psi_{R,L} = P_{R,L}\Psi \tag{1.3}$$

Substituting these back into the Lagrangian of equation 1.1 we get:

$$L = i(\bar{\Psi}_R\gamma_\mu\partial^\mu\Psi_R + \bar{\Psi}_L\gamma_\mu\partial^\mu\Psi_L) \tag{1.4}$$

Since the left-handed and right-handed fermions do not communicate, they both

have a global $U(1)$ symmetry as can be seen by applying $U(1)$ transformations separately on the fields:

$$\begin{aligned} \Psi_R &\rightarrow e^{i\epsilon_R}\Psi_R \\ \Psi_L &\rightarrow e^{i\epsilon_L}\Psi_L \end{aligned} \tag{1.5}$$

The conserved currents for the Lagrangian of 1.1 are:

$$\begin{aligned} j^i_\mu &= \bar{\Psi}_i\gamma_\mu\Psi_i \\ V_\mu &= \bar{\Psi}\gamma_\mu\Psi \\ A_\mu &= \bar{\Psi}\gamma_\mu\gamma^5\Psi \end{aligned} \tag{1.6}$$

where $i = R, L$. Looking at the effect of the $U(1)_L \times U(1)_R$ transformation on the original field Ψ,

$$\Psi = \Psi_R + \Psi_L \rightarrow e^{i\epsilon_R}\Psi_R + e^{i\epsilon_L}\Psi_L = e^{i(\frac{\epsilon_R+\epsilon_L}{2}+\frac{\epsilon_R-\epsilon_L}{2}\gamma^5)}\Psi = e^{i(\epsilon_V+\epsilon_A\gamma^5)}\Psi_L \tag{1.7}$$

where:

$$\begin{aligned} \epsilon_V &= \frac{1}{2}(\epsilon_R + \epsilon_L) \\ \epsilon_A &= \frac{1}{2}(\epsilon_R - \epsilon_L) \end{aligned} \tag{1.8}$$

Invariance of the Lagrangian under Eq. 1.7 is called chiral symmetry.

Let us now look at the effect of a mass term in the Lagrangian of Eq. 1.1 on chiral symmetry. We have:

$$\bar{\Psi}M\Psi = \bar{\Psi}_L M\Psi_R + \bar{\Psi}_R M\Psi_L \tag{1.9}$$

which clearly breaks the symmetry.

We can now proceed and investigate chiral symmetry for the QCD Lagangian.

$$L_{QCD} = -\frac{1}{g^2} G^a_{\mu\nu} G^{\mu\nu,a} + i\bar{q}\gamma^\mu(\partial_\mu - iG_\mu)q - \bar{q}Mq \tag{1.10}$$

where G_μ is the gluon field, $G^a_{\mu\nu}$ is the gluon field strength tensor and $M = diag(m_u, m_d, m_s, \ldots)$ contains the quark masses. In the calculations presented in this work, we will only consider nucleons and pions as the degrees of freedom. As such, we will restrict the discussion here to u and d quarks. From our brief look at chiral symmetry we know that the mass term will break the symmetry. Furthermore, since the u and d masses are quite small, we will ignore the mass term and rewrite Eq. 1.10 as:

$$L = i(\bar{q}_R\gamma_\mu\partial^\mu q_R + \bar{q}_L\gamma_\mu\partial^\mu q_L) \tag{1.11}$$

This Lagrangian has $SU(2)_R \times SU(2)_L \times U(1)_R \times U(1)_L$ symmetry. We have briefly discussed the U(1) symmetry, which is of no interest from now on. The field transformation for the $SU(2)_R \times SU(2)_L$ are:

$$\begin{aligned} q_R &\rightarrow e^{i\epsilon^a_R T^a} q_R \\ q_L &\rightarrow e^{i\epsilon^a_L T^a} q_L \end{aligned} \tag{1.12}$$

where we have defined:

$$T^a = \frac{\tau^a}{2} \tag{1.13}$$

with τ^a being the generators for the $SU(2)$ group.

The conserved currents for the $SU(2)_R \times SU(2)_L$ are given by:

$$\begin{aligned} V^a_\mu &= \bar{q}\gamma_\mu T^a q \\ A^a_\mu &= \bar{q}\gamma_\mu\gamma^5 T^a q \end{aligned} \tag{1.14}$$

From the above, we expect chiral symmetry to be manifest in the particle spectrum

of QCD as degenerate hadron doublets of opposite parity. This is not the case (e.g. there are no neutral meson doublets of opposite parity), but there is approximate flavor $SU(2)_V$ symmetry in the hadron spectrum. The chiral symmetry must therefore be spontaneously broken to its vectorial subgroup. The three Goldstone bosons that appear in the process are the pions.

The goal now is to construct effective low energy Lagrangians that contain only pion and nucleon degrees of freedom that reflect the spontaneously broken chiral symmetry. We must thus construct the most general Lagrangian with chiral symmetry broken down to the $SU_V(2)$ subgroup.

One starts with constructing the pion field matrix:

$$U = e^{\frac{i\pi^a \tau^a}{f}} \tag{1.15}$$

where f is a constant with dimension of mass. The pion field matrix transforms linearly under chiral transformations:

$$U' = RUL^+ \tag{1.16}$$

with the R and L given by:

$$\begin{aligned} L &= e^{-i\alpha_L^a T^a} \\ R &= e^{-i\alpha_R^a T^a} \end{aligned} \tag{1.17}$$

To obtain the transformation for the unbroken $SU(2)_V$ group we must set $\alpha_L = \alpha_R$, whereas the broken axial $SU(2)_A$ transformations are obtained by $\alpha_L = -\alpha_R$.

Since in the construction of the Lagrangian we need kinetic terms, a covariant derivative on the chiral pion field is also required. The covariant derivative must transform linearly under chiral $SU(2)_R \times SU(2)_L$.

$$\begin{aligned} D_\mu U &\rightarrow LD_\mu UR^+ \\ D^\mu U^+ &\rightarrow RD^\mu UL^+ \end{aligned} \tag{1.18}$$

and it includes the external vector and axial fields:

$$D_\mu U = \frac{i\tau \cdot \partial_\mu \pi}{f} + iU(v_\mu - a_\mu) - i(v_\mu + a_\mu)U + \dots \tag{1.19}$$

Since we have constructed a pion field matrix and a covariant derivative, we can write the desired Lagrangian for massless pion fields:

$$L = \frac{f^2}{4} Tr[D^\mu U^+ D_\mu U] + \dots \tag{1.20}$$

where the ... represent higher order terms. We see that by direct substitution of the covariant derivative into Eq. 1.20 we obtain the expected kinetic term for the pions : $\partial_\mu \pi \partial^\mu \pi^+$. From the first term in the Lagrangian of Eq. 1.20 we can also work out the Feynman rule for the pion axial-source interaction to be $f\delta^{ab}\epsilon \cdot k$, and from this we can identify the parameter f as the pion decay constant $f_\pi = 93MeV$.

We can now turn our attention to the pion-nucleon system. We first collect the proton and neutron in the field:

$$N = \begin{pmatrix} p \\ n \end{pmatrix} \tag{1.21}$$

Further, we define the field u and its transformation as follows:

$$\begin{aligned} u^2 &= U \\ u'^2 &= U' = RUL^+ \end{aligned} \tag{1.22}$$

Requiring the field u to transform as:

$$Ru = u'K \tag{1.23}$$

or

$$u' \to LuK^+ \quad = \quad KuR^+ \tag{1.24}$$

sets K as a highly nonlinear function:

$$K = \sqrt{LU^+R^+}R\sqrt{U} \tag{1.25}$$

Next we make the nucleon transform as an $SU(2)$ field:

$$N' \to KN \tag{1.26}$$

where all the chiral nature of the transformation is contained in the function K. As before, a covariant derivative must also be constructed:

$$\begin{aligned} D_\mu N &= \partial_\mu N + \Gamma_\mu N \\ \Gamma_\mu &= \frac{1}{2}[u^+, \partial_\mu u] \end{aligned} \tag{1.27}$$

The above covariant derivative transforms homogeneously under chiral transformations:

$$D'_\mu = KD_\mu K^+ \tag{1.28}$$

At this point, the most general Lagrangian up to one derivative can be written down:

$$L = i\bar{N}D_\mu\gamma^\mu N + g_A\bar{N}A_\mu\gamma^\mu\gamma_5 N - m\bar{N}N + \ldots \tag{1.29}$$

where A_μ is an axial vector field built from the u's:

$$A_\mu = \frac{i}{2}\{u^+, D_\mu u\} = \frac{\partial_\mu \pi}{f_\pi} + \ldots \tag{1.30}$$

and g_A is the bare axial coupling.

At this point we notice that the large mass associated with the nucleon is going to present a problem when performing the systematic expansion since it is of the same order as the characteristic mass of the EFT. To circumvent this issue, one may write Eq. 1.29 in the extreme non-relativistic limit and integrate out the heavy degrees of freedom. To accomplish this goal, the heavy degrees of freedom must first be factored out by making use of the velocity four-vector v as described in [2]. The velocity four-vector allows one to write the four-momenta of heavy particle of mass M as:

$$p_\mu = Mv_\mu + l_\mu \tag{1.31}$$

with l being a small residual momentum and $v^2 = 1$. We can now write the velocity projection operator and construct its eigenstates:

$$\begin{aligned} P_{v\pm} &= \frac{1 \pm \gamma_\mu v^\mu}{2} \\ N &= e^{-imv\cdot x}(H + h) \\ H &= e^{imv\cdot x} P_{v+} N \\ h &= e^{imv\cdot x} P_{v-} N \end{aligned} \tag{1.32}$$

Substituting back into Eq. 1.29, we obtain:

$$L = i\bar{H}AH + \bar{h}BH + \bar{H}\gamma_0 B^+ \gamma_0 h - \bar{h}Ch + \ldots \tag{1.33}$$

Where the operators A, B, and C are:

$$\begin{aligned} A &= i(v\cdot D) + g_A(u\cdot S) + \ldots \\ B &= i\not{D}^T - \frac{1}{2} g_A (v\cdot u)\gamma_5 + \ldots \\ C &= i(v\cdot D) + 2m + g_A(u\cdot S) + \ldots \end{aligned} \tag{1.34}$$

with $\not{D}^T = \gamma^\mu(g_{\mu\nu} - v_\mu v_\nu)D^\nu$ and the $\ldots$ representing higher order terms. Inte-

grating out the heavy degrees of freedom the Lagrangian becomes:

$$L = i\bar{H}(A + \gamma_0 B^+ \gamma_0 B)H \tag{1.35}$$

Next, we make use of the simplifications of the Dirac algebra in the heavy mass formulation (again, see [2]) and change notation from H to N, in order to write the leading order pion-nucleon Lagrangian:

$$\begin{aligned} L &= \bar{H} iD \cdot v H + g_A \bar{H}(A \cdot S)H \\ A &= i(v \cdot D) \end{aligned} \tag{1.36}$$

All the effective Lagrangians that also include higher-order terms used in this work are obtained in a similar fashion. Their derivations will not be presented here, but references will be given to the relevant papers at the appropriate places throughout the thesis.

1.2 Vector Analyzing Power in Electron-Proton Scattering

The first computation presented deals with the vector analyzing power (VAP), A_n, in polarized electron-proton scattering. The scattering of transversely polarized electrons from protons has recently become a topic of considerable interest in nuclear physics. The VAP is a time-reversal (T) odd, parity (P) even correlation between the electron spin and the independent momenta associated with the scattering process:

$$A_n \sim \epsilon^{\mu\nu\alpha\beta} P_\mu S_\nu K_\alpha K'_\beta \tag{1.37}$$

where S, P, and K (K') denote the electron spin, initial proton momentum, and incident (scattered) electron momentum, respectively. A non-zero VAP cannot arise at leading order in quantum electrodynamics (QED), but could be generated by new T-odd, P-even interactions involving electrons and quarks. Searches for

such interactions have been carried out in neutron and nuclear β-decay as well as nuclear γ-decays [9, 10, 11]. Indirect constraints may also be obtained from limits on the permanent electric dipole moments of neutral atoms under various assumptions regarding the pattern of symmetry-breaking [12, 13, 14, 15, 16]. The sensitivity of direct searches for T-odd, P-even interactions is generally limited by the presence of QED "final state interactions" (FSIs) that break the T-symmetry between initial and final states and give rise to non-vanishing T-odd, P-even observables. Uncertainties in theoretical calculations of these final state interactions would cloud the interpretation of a sufficiently precise T-odd, P-even measurement in terms of new interactions. Observations of T-odd, P-even correlations in nuclear γ-decays are consistent with theoretical calculations of QED final state interactions [17], while T-odd, P-even searches in neutron β-decay have yet to reach the sensitivity needed to discern these effects.

Recently, the SAMPLE collaboration has reported a non-zero measurement of the VAP in polarized, elastic electron-proton scattering [4], making it the first non-zero result for any T-odd, P-even observable in any electron scattering process. The result has received widespread attention, as it differs substantially from the simplest theoretical estimate of QED final state contributions that neglects proton recoil and internal structure [5]. While one might speculate that this difference reflects the presence of new physics, a more likely explanation lies in elements of nucleon structure omitted from the simplest treatments of QED FSIs.

If so, then the SAMPLE result, as well as other VAP measurements that have been completed or are under consideration, could have important implications for the interpretation of other precision observables involving hadrons that require computation of exchange QED corrections to the leading order amplitude.

The most interesting such observable is the ratio of proton electromagnetic form factors obtained via Rosenbluth separation in elastic *ep* scattering [18]. The reason for this is that, currently, there is a discrepancy between the G_{E_p}/G_{M_p} obtained through the Rosenbluth separation technique versus the one obtained using Generalized Parton Distributions. A two-photon exchange contribution might be

able to resolve this discrepancy. Another set of observables where such a contribution could be of interest are higher-order "box graph" contributions to weak interaction observables [19]. Here, γZ and W^+W^- "box diagrams" are, in several cases, the leading unknown contributors. Finally, QED final state interactions must be accurately computed in direct searches for T-odd, P-even effects. In each of these instances, a calculation of QED corrections requires a realistic and sufficiently precise treatment of hadronic intermediate states, particularly those arising in two-photon exchange amplitudes, $\mathcal{M}_{\gamma\gamma}$, or the analogous amplitudes involving the exchange of one heavy gauge boson and one photon. Since the leading QED contribution to A_n arises from Im $\mathcal{M}_{\gamma\gamma}$, experimental measurements of the VAP provide an important test of theoretical calculations of $\mathcal{M}_{\gamma\gamma}$ needed for the interpretation of other measurements.

At the same time, the VAP provides a new window on nucleon structure, as $\mathcal{M}_{\gamma\gamma}$ probes the doubly virtual Compton scattering (VVCS) amplitude. In recent years, virtual Compton scattering (VCS) on the proton has become an important tool in probing the internal structure of the proton. VCS involves the coupling of one virtual and one real photon to a hadronic system. In the case of the proton, the VCS cross section is sensitive to the generalized polarizabilities of the proton, and its measurement should provide insight in the proton structure [20]. In practice, however, this cross section includes Bethe-Heitler (BH) amplitudes associated with radiation of a real photon from the electrons. Proper treatment of the cross section must therefore be taken in order to obtain a correct interpretation of the measurement. In contrast, the process involving the coupling of two virtual photons to the hadronic system is immune to background BH amplitudes and, thus, offers an alternative to VCS in probing the proton structure.

With the aforementioned motivation in mind, we study the VAP in the framework of an effective theory of low-energy ep scattering. Since the SAMPLE measurement corresponds to kinematics close to the pion electroproduction threshold, we consider only the electron, photon, and nucleon as dynamical degrees of freedom. In this respect, our analysis corresponds to the use of heavy baryon chiral

perturbation theory with the pions integrated out. To make the treatment systematic, we expand A_n in powers of p/M, where p is either the incident electron energy (E) or mass (m) and M is the nucleon mass. Working to second order in p/M, we obtain all contributions to A_n that arise uniquely from one-loop, two-photon exchange amplitudes and obtain a prediction that is free from any unknown parameters. We also write down the leading, non-renormalizable T-odd, P-even *eepp* operators whose interference with $\mathcal{M}_\gamma$ can generate a non-zero VAP and show that they contribute at $\mathcal{O}(p/M)^4$.

We find that inclusion of all one-loop effects through $\mathcal{O}(p/M)^2$ in $\mathcal{M}_{\gamma\gamma}$ as well as all terms in $\mathcal{M}_\gamma$ through this order is sufficient to resolve the disagreement between the SAMPLE result and the simplest potential scattering predictions. This resolution follows from several effects that occur beyond leading order in p/M: recoil corrections to the pure charge scattering result obtained in Ref. [5], the nucleon isovector magnetic moment, and the proton charge radius. In the absence of dynamical pions, contributions from the nucleon polarizability arise at higher order than we consider here and appear unnecessary to account for the experimental result. Given that the incident electron energy E is of the same order as m_π, we have no *a priori* reason to expect agreement of our computation with experiment. What it suggests, however, is that for this kinematic regime, pions play a less important role in the VVCS amplitude than one might naively expect. Future, low-energy A_n measurements, taken over a broader range in q^2 and scattering angle than the SAMPLE measurement, would provide additional, useful tests of this conclusion.

We also consider A_n at forward scattering angles and energies somewhat higher than those of the SAMPLE experiment. Results for this kinematic domain have been reported by the A4 Collaboration at the MAMI facility in Mainz [6]. Although we would not expect our framework to be reliable in this kinematic regime, where the electron energy E is much closer to M, it is nonetheless instructive to compare with the Mainz results as a way of pointing to the physics that may be operative in this domain. Indeed, we find substantial disagreement (5σ for the

$Q^2 = 0.106 GeV^2$ point and 3σ for the $Q^2 = 0.230 GeV^2$ point) with the Mainz data [6]. The culprit could be that going to the Mainz kinematics exceeds the limit of validity of our effective theory, and that we must include additional dynamical degrees of freedom such as the π or $\Delta(1230)$ resonance, or both. Inclusion of such degrees of freedom will result in the need of computing Feynaman diagrams containing multiple loops. In such a case, one would be required to compute both real and imaginary contributions from the loop integrals. As such, future studies using alternative methods such as dispersion relations may be needed to explore this kinematic domain.

Finally, we also consider A_n for polarized Møller scattering. The VAP for this process has been measured by the E158 Collaboration at SLAC [21], and theoretical computations given in Refs. [22, 23, 24]. Our computation agrees with these earlier $A_n(ee)$ calculations, providing a useful cross-check on our study of the VAP for ep scattering.

1.3 Parity-Violating Electron-Deuteron Scattering

The purpose of the second computation is to compute a theoretical value for the electron-deuteron scattering parity-violating asymmetry including two-nucleon currents. This theoretical value is of interest for the interpretation of the SAMPLE experiment. The SAMPLE Collaboration measured the longitudinal asymmetry in polarized elastic electron scattering on the proton [7] and polarized quasi-elastic electron scattering on the deuteron [25]. In the experiment, elastically scattered electrons are detected in the backward direction ($130^o \leq \theta \leq 170^0$) by a large solid-angle air Cerenkov detector consisting of ten mirrors which image the target onto ten 8-inch photomultiplier tubes.

The asymmetries measured by the experiment are sensitive to the nucleon's form factors:

$$A = \left[\frac{-G_F Q^2}{4\sqrt{2}\alpha}\right] \frac{\epsilon G_E^\gamma G_E^Z + \tau G_M^\gamma G_M^Z - (1 - 4\sin^2\theta_W)\epsilon' G_M^\gamma G_A^e}{\epsilon (G_E^\gamma)^2 + \tau (G_M^\gamma)^2} \quad (1.38)$$

where ϵ,τ and ϵ' are kinematic quantities. One then gets the strange form factors from the flavor structure of the electroweak coupling and isospin symmetry of the nucleon:

$$G^s_{E,M} = (1 - 4\sin^2\theta_W)G^{\gamma,p}_{E,M} - G^{\gamma,n}_{E,M} - G^{Z,p}_{E,M} \tag{1.39}$$

Thus, if one performs the PV measurement for both electron-proton and electron-neutron scattering and if other effects are under control, the two measurements can be used to determine the values of the strange form factors. Neglecting two-nucleon current effects, preliminary results at the time this calculation was performed were in disagreement with theoretical predictions, in particular for the axial contribution [26]. This discrepancy has later disappeared through a re-analysis of the data [8]. This calculation was, thus, undertaken in order to better understand the size of the two-body effects in the quasi-elastic electron deuteron scattering. The computation uses EFT to obtain the two-body leading order long-range current operators, which are then combined with a phenomenological model of the initial and final state.

Neutral charge and current one-nucleon operators are well-known (see, for example, Ref. [27]). The contribution of such operators to the asymmetry was computed at various momentum transfers in Ref. [28]. Several theoretical issues were studied in detail. For the kinematical region relevant to SAMPLE, final-state interactions were found to be important. It was also found that (except for very low momentum transfers) the asymmetry in the vicinity of the quasi-elastic peak is fairly independent of the choice of two-nucleon (NN) potential.

Two-nucleon charge and current operators have also been studied to some extent. Electromagnetic heavy-meson exchange contributions were considered in Ref. [29]. They were shown to be unimportant in a calculation of the asymmetry that neglected final-state interactions. In Ref. [30], an impulse approximation modified to incorporate gauge invariance was employed. The effects of parity-violating NN interactions on the deuteron wave function were found to be small.

Pion-exchange currents were included in the computation of the asymmetry, but only in the electromagnetic sector.

In the present work these earlier calculations are extended. The leading one-body and two-boy currents are calculated using EFT [3, 31]. For the two-body currents we consider pion-exchange diagrams for both the electromagnetic and weak contributions. These currents are then incorporated in a successful phenomenological model [32]. The phenomenological model is used for two purposes. First, it allowed for the generation of the result in a timely fashion and second, it allowed for the inclusion of some higher order terms. If contributions from these higher order terms turns out to be significant one would then need to go back to the EFT and systematically compute higher order terms (see Section 3.3.2 for further discussion).

Within the model, the one-nucleon currents considered here include phenomenological form factors and have the same form as those in Ref. [27]. In addition, the model used can include effects from heavier mesons evaluated using the Riska prescription [33]. Such contributions are beyond the leading-order contributions obtained from EFT. As such, to make the connection between these effects and EFT, higher-order terms in the diagrams considered and new diagrams must be included in the EFT computation. Since including these contributions has no significant impact on the final result, the relevant EFT diagrams will not be computed. Finally, the asymmetry is calculated with deuteron and final-state wave functions obtained from a realistic potential, the Argonne v_{18} model [34].

Since this calculation was performed, more work has been done on the subject. A new operator that was not considered in this work is presented in Ref. [35]. Calculations that consider parity violation arising from hadronic PV were shown to be small and are reported in Ref. [36] and Ref. [37].

The results for the kinematical region of interest to SAMPLE are presented. (The calculation can be repeated at other momentum transfers, such as those of the lower energy SAMPLE experiment [38] [8] and JLab's G0 experiment [39].) The effects of two-body currents on the asymmetry, both near the quasi-elastic

peak where one-body processes should dominate and away from the quasi-elastic peak where these two-body currents could be important, have been studied. The results show that most of the two-nucleon contributions to the asymmetry are due to currents of pion range and, therefore, dominated by the leading operators. Near the quasi-elastic peak, two-body currents give a small contribution to the asymmetry. Away from the peak, they become more important and can increase the magnitude of the asymmetry by as much as 3%. The contribution to the asymmetry associated with the electromagnetic-axial current interference response function is about 20%. The overall effect of two-nucleon currents on the data of the SAMPLE experiment is indeed small, but not negligible, and has been incorporated in the data analysis [26].

Chapter 2

The Vector Analyzing Power in Elastic Electron-Proton Scattering

2.1 Introduction

An introduction to this study of the vector analyzing power in elastic electron proton scattering was presented in Section 1.2 and is discussed in detail in this chapter. The work presented here was published in Physical Review C70, 2004, 054003 (nucl-th/0405044).

The chapter is organized as follows: in Section 2.2, we discuss general features of the VAP and our approach to the computation. Section 2.3 provides details of the calculation. In Section 2.4, we give numerical results and discuss their significance, while Section 2.5 presents our conclusions. Technical details are provided in the Appendices.

2.2 General Considerations

We are interested in computing the VAP in elastic *ep* scattering:

$$A_n = \frac{d\sigma_\uparrow - d\sigma_\downarrow}{d\sigma_\uparrow + d\sigma_\downarrow} = \frac{2\mathrm{Im}\ \mathcal{M}^*_{\gamma\gamma}\mathcal{M}_\gamma}{|\mathcal{M}_\gamma|^2} \tag{2.1}$$

where $d\sigma_{\uparrow(\downarrow)}$ is the differential cross section for scattering of electrons with incident spin parallel (anti-parallel) to $\vec{K} \times \vec{K}'$. In a phase convention where the single

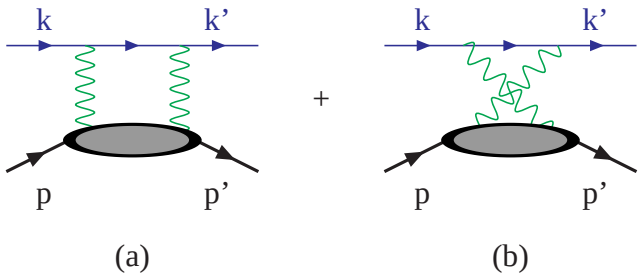

Figure 2.1: Two photon exchange diagrams. The wavy lines indicate virtual photons, while k (k') and p (p') denote the initial (final) electron and proton momenta, respectively.

γ-exchange amplitude $\mathcal{M}_\gamma$ is purely real, A_n requires a non-vanishing imaginary part of $\mathcal{M}_{\gamma\gamma}$[1]. To compute the latter, one must consider both the box and crossed-box diagrams of Figure 2.1. Simple power-counting arguments indicate that the contribution to $\mathcal{M}_{\gamma\gamma}$ arising from the leading-order γp couplings is ultraviolet finite but infrared divergent. Thus, in general, one must also compute the contributions to A_n arising from the bremsstrahlung diagrams of Figure 2.2. As we show by explicit calculation in Appendix A, however, the bremsstrahlung contribution to A_n vanishes identically, while $\mathrm{Im}\mathcal{M}_{\gamma\gamma}$ is infrared finite. The resulting, leading-order contribution to A_n is $\mathcal{O}(p/M)^0$.

Additional contributions to $\mathcal{M}_{\gamma\gamma}$ arise from higher-order operators that couple one or more virtual photons to the proton and electron. We neglect the latter since they are suppressed by additional powers of the fine structure constant[2]. In contrast, the γp operators are induced by strong interactions and have couplings of

[1] By $\mathrm{Im}\mathcal{M}_{\gamma\gamma}$, we mean the coefficients of the various products of fermion bilinears, $\bar{e}\Gamma e\bar{N}\Gamma' N$, *etc.* that appear in the amplitude.

[2] For high energy scattering, these higher-order QED contributions may receive logarithmic enhancements [24].

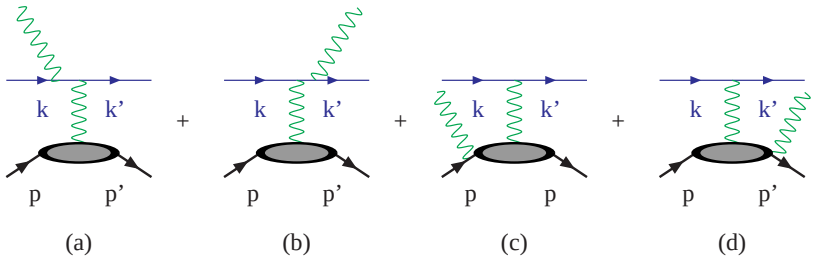

Figure 2.2: Bremsstrahlung contributions.

order e. In order to treat their contributions systematically, we adopt an effective theory framework since we cannot compute the operator coefficients from first principles in Quantum Chromodynamics. The natural framework for doing so is heavy baryon chiral perturbation theory (HBχPT), which provides a systematic expansion in powers of p/Λ_χ and p/M, where $\Lambda_\chi = 4\pi F_\pi$ is the scale of chiral symmetry-breaking and p is an external momentum or mass with magnitude much less than M and Λ_χ. In the present case, where we integrate out the pions, we take $p = E$ or m (where E and m are the energy and mass of the incoming electron) and use M as the heavy scale. For the kinematics of the SAMPLE experiment, $E >> m$. Since there are no hard collinear infrared singularities in Im $\mathcal{M}_{\gamma\gamma}$, we may drop all power corrections involving the electron mass and obtain our result as an expansion in E/M.

The leading terms in heavy baryon Lagrangian for nucleons and photons relevant to our computation are:

$$\mathcal{L}_{N\gamma} \quad = \quad \bar{B}_v i v\cdot D B_v + \frac{1}{2M}\bar{B}_v\left[(v\cdot D)^2 - D^2\right]B_v$$

$$+\frac{e\mu}{2M}\epsilon_{\mu\nu\alpha\beta}F^{\mu\nu}v^{\alpha}\bar{B}_v S^{\beta}B_v - \frac{eC_r}{M^2}\bar{B}_v v_\mu B_v \partial_\lambda F^{\mu\lambda} + \cdots \tag{2.2}$$

where B_v is the field for a heavy proton of velocity v_μ, where $D_\mu = \partial_\mu - ieA_\mu$, and where we have shown explicitly all γp interactions through $\mathcal{O}(p^2)$. The latter arise from the subleading kinetic term in Eq. 2.2 as well as from the operators containing the field strength, $F^{\mu\nu}$. The coefficient $\mu = 2.793$ is the proton magnetic moment, while C_r determines the proton Sachs, or electric, radius:

$$C_r = \frac{M^2}{6}\langle r^2\rangle_E = M^2\frac{dG_E^p(t)}{dt}|_{t=0} \tag{2.3}$$

where $t = q^2$. The experimental value for $\langle r^2\rangle_E = 0.743$ fm^2 [40, 41] implies $C_r = 2.81$. When included in the loop diagrams of Figure 2.1, these interactions generate contributions to the ep amplitude $\mathcal{M}_\gamma$ and $\mathcal{M}_{\gamma\gamma}$ through order $(p/M)^2$ relative to the leading term. To this order, operators associated with the nucleon polarizability (see Figure 2.4) do not contribute, as they are given by

$$\frac{\alpha}{M^3}F^{\mu\nu}F_{\mu\nu}\bar{B}_v B_v \tag{2.4}$$

and thus occur at $\mathcal{O}(p^3)$ in $\mathcal{L}_{N\gamma}$ when the pion is treated as heavy. Furthermore, as can be seen from Figure 2.4, there is no way to cut this diagram and end up with on-shell intermediate states. As such, we conclude that there is no absorptive contribution from the loop integral, thus, even if we were to include the polarizability it would not contribute to the VAP.

Higher-order contributions to A_n can also arise from effective T-odd, P-even $eeNN$ interactions. The origin of such operators could be either physics that we have integrated out, such as contributions to $\mathcal{M}_{\gamma\gamma}$ from πN or Δ intermediate states, or explicit T-odd, P-even interactions arising from new physics. As shown in Appendix B, there exist no Hermitian, four-fermion operators at dimension six that contribute to A_n. The lowest dimension T-odd, P-even four-fermion operators have dimension seven and would nominally contribute to A_n at $\mathcal{O}(p/M)^3$. We show, however, that contributions from these operators vanish to this order and

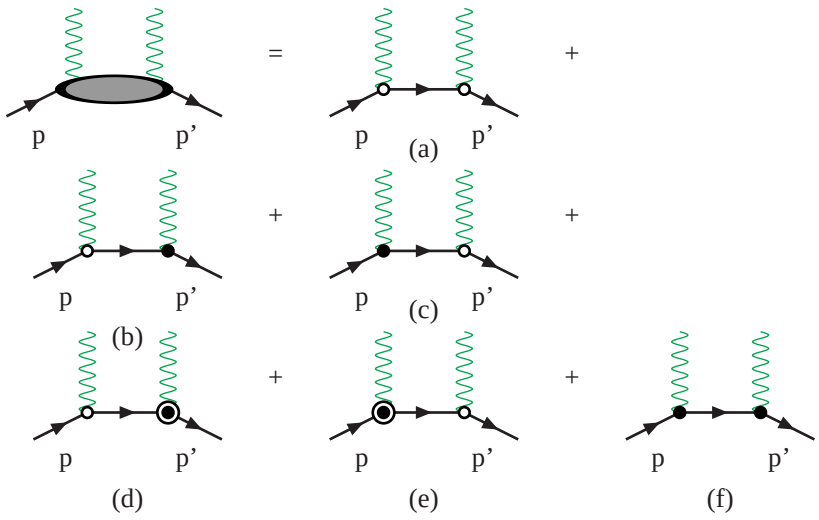

Figure 2.3: Contributions to the VVCS amplitude appearing in Figure 2.1. Open circles indicate the leading order γN couplings, solid circles indicate the contributions from $O(p/M)$ corrections to the leading couplings, such as the magnetic moment and recoil corrections. The $O(p/M)^2$ corrections arising from the charge radius are denoted by a solid circle inside an open circle.

first arise at $\mathcal{O}(p/M)^4$. Since we truncate our analysis at two orders lower, we may neglect these operators and obtain a parameter-free prediction for the VAP. Nevertheless, we discuss these operators briefly in Section 2.4 when considering the possible size of neglected, higher-order contributions.

As we show in detail in Section 2.3, the leading one-loop contributions to A_n– generated by two $\mathcal{O}(p)$ γp insertions in the VVCS amplitude (Figure 2.3a)–are finite, non-analytic in p, and occur at $\mathcal{O}(p/M)^0$, whereas those generated by the dimension seven T-odd, P-even operators arise at $\mathcal{O}(p/M)^4$. Thus, the leading contributions are uniquely determined from the one-loop calculation. Similarly, contributions to $\mathcal{M}_{\gamma\gamma}$ involving one $\mathcal{O}(p)$ and one $\mathcal{O}(p^2)$ γp interaction (Figure 2.3b, c) contribute to A_n at $\mathcal{O}(p/M)$, are also finite and non-analytic in p, and

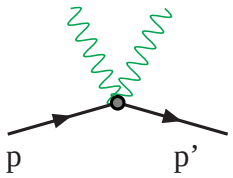

Figure 2.4: Polarizabilty diagrams. This appears at $O(p/M)^3$ and is not included in the computation.

are unique to the loop calculation. The $\mathcal{O}(p/M)^2$ loop contributions arise either from two $\mathcal{O}(p^2)$ γp operators (*e.g.*, two insertions of the nucleon magnetic moment operator, Figure 2.3d) or one $\mathcal{O}(p)$ and one $\mathcal{O}(p^3)$ term (*viz*, the proton charge radius). We find, however, that the $\mathcal{O}(p/M)^2$ components of $\mathcal{M}_{\gamma\gamma}$ arise only from the γp magnetic moment interaction as well as from recoil order terms in $\mathcal{L}_{N\gamma}$. Contributions to $\mathcal{M}_{\gamma\gamma}$ from the proton charge radius vanish, though it does contribute to A_n as a higher-order term in $\mathcal{M}_\gamma$.

2.3 Two-Photon Exchange

The evaluation of four-point functions for general kinematics does not readily lend itself to evaluation using standard Feynman parameterization in the loop integrals. Alternate methods for evaluating these integrals that do not rely explicitly on Feynman parameters have been worked out in Refs. [42, 43] and have become standard. In the present case, where we are interested in backward angle scattering at nonzero q^2, we would ideally like to use this formalism. However, the form of

the heavy-baryon propagator does not permit one to adopt the t'Hooft-Passarino-Veltmann formulation directly.

We circumvent these difficulties by carrying out the computation with relativistic baryon propagators and by expanding our result in powers of p/M. Doing so allows us to evaluate the loop integrals using the standard formulation of Refs. [42, 43]. It has been shown in other contexts [44] that doing so allows one to recover the heavy-baryon result so long as the external momenta are sufficiently small. Moreover, our loop results are entirely non-analytic in p and, thus, must match the corresponding non-analytic results obtained with heavy-baryon propagators. To the order of our analysis, there exist no four-fermion operators that could account for differences between relativistic and non-relativistic treatments of A_n.

The one-loop $\mathcal{M}_{\gamma\gamma}$ is nominally infrared singular and must, therefore, be regulated with an IR regulator such as a photon mass. On general grounds, the regulator dependence should be cancelled by a corresponding dependence of the bremsstrahlung contribution to the spin-dependent cross section. As is well-known, such a cancellation occurs for unpolarized scattering cross section. In Appendix B, we work out the corresponding bremsstrahlung contribution to A_n and show that it vanishes identically. Consequently, $\mathrm{Im}\mathcal{M}_{\gamma\gamma}$ must be IR regulator-independent.

In general, the amplitude $\mathcal{M}_{\gamma\gamma}$ depends on each of the eleven integrals obtained in Ref. [43]. The imaginary part, however, depends on only four:

$$\begin{aligned} D_0 &= \frac{2\pi}{-t}\ln(\frac{-t}{\lambda^2})\frac{1}{\sqrt{\Lambda}}\Theta(s-(m+M)^2) \\ C_0(1,2,3) &= \frac{\pi}{\sqrt{\Lambda}}\ln(\frac{\Lambda}{s\lambda^2})\Theta(s-(m+M)^2) \\ C_0(1,3,4) &= C_0(1,2,3) = C_0 \\ B_0(1,3) &= \pi\frac{\sqrt{\Lambda}}{s}\Theta(s-(m+M)^2) \end{aligned} \tag{2.5}$$

where the three labels associated with the B_0 and C_0 functions indicate which propagators are used for the two-point and three-point integral as discussed in

Appendix C, λ is the photon mass, and:

$$\Lambda = s^2 - 2s(M^2 + m^2) + (M^2 - m^2)^2 \tag{2.6}$$

These integrals have been previously computed in Refs. [43, 45] (In [45] they are obtained by the use of dispersion techniques). The D_0 and C_0 loop integrals diverge as $\lambda \to 0$, but the combination:

$$2C_0 + D_0 t = \frac{2\pi}{\sqrt{\Lambda}} \ln(\frac{\Lambda}{-st})\Theta(s - (m+M)^2) \tag{2.7}$$

is finite in this limit and is the only combination of D_0 and C_0 integrals that is so. As such, the two-photon contribution to A_n must only contain terms proportional to this combination or to the B_0 integral.

In evaluating the loop contributions to A_n, it is most efficient to identify the terms in $\mathcal{M}_{\gamma\gamma}$ that generate the correlation of Eq. 1.37 by carrying out the Dirac algebra in the interference term $\mathrm{Im}\mathcal{M}_{\gamma\gamma}\ \mathcal{M}_\gamma^*$ before evaluating the momentum integrals.[3] After carrying out the momentum integration, the contribution from the box diagram of Figure 2.1a is:

$$\begin{aligned}
2\mathrm{Im}\mathcal{M}_{\gamma\gamma}^{\mathrm{box}}\mathcal{M}_\gamma^* &= -\frac{(4\pi\alpha)^2}{4\pi^4 t}\frac{16m\pi^2(4\pi\alpha)}{(\Lambda+st)}\epsilon^{\mu\nu\alpha\beta}P_\mu S_\nu K_\alpha K'_\beta \\
&\Bigg\{ \Big[4(M^2-m^2-3s)M^2R + \kappa[(6R+2)\Lambda - ((m^2-M^2-s)R+2s)t] \\
&+ \kappa^2 R\frac{1}{8M^2(\Lambda+st)}[2(3m^3+16M^2)\Lambda^2 \\
&+ \Lambda(11m^4 - 2(13M^2+8s)m^2 + 15M^4 + 11s^2 + 14M^2 s)t \\
&+ 4s(2m^4 - (5M^2+4s)M^2 + 3M^4 + 2s^2 - 3M^2 s)t^2]\Big](2C_0 + D_0 t) \\
&- 4\frac{\Lambda+ts}{\Lambda}(\kappa^2+4\kappa+2)B_0\Bigg\}
\end{aligned} \tag{2.8}$$

s, t, and u are the Mandelstaam variables, $\kappa = \mu - 1$ is the nucleon anomalous

[3] This procedure introduces no ambiguities because Im $\mathcal{M}_{\gamma\gamma}$ is finite to the order of our analysis.

magnetic moment and:

$$R - 1 = t\left[\frac{\kappa}{4M^2} - \frac{C_r}{M^2}\right] \tag{2.9}$$

To obtain the result consistent with our power counting, we expand Eq. 2.8 in powers of p/M up to second order relative to the leading term:

$$\begin{aligned}
\mathrm{Im}\mathcal{M}^{\mathrm{box}}_{\gamma\gamma}\mathcal{M}^{*}_{\gamma} &= -\frac{(4\pi\alpha)^2}{t}\frac{32\pi^2\alpha m M\epsilon^{\mu\nu\alpha\beta}P_\mu S_\nu K_\alpha K'_\beta}{\sqrt{E^2-m^2}[(E^2-m^2+t/4)+\frac{Et}{2M}+\frac{m^2t}{4M^2}]} \\
&\times \left\{\left[\ln\left[\frac{4(E^2-m^2)}{-t}\right] - 2E/M + (2E^2-m^2)/M^2\right]\right. \\
&\left[R + \frac{3E}{M} + \frac{2m^2}{M^2} + \frac{\kappa^2}{M^2}\frac{32(E^2-m^2)^2+t^2/2+10(E^2-m^2)t}{4(E^2-m^2)+t}\right. \\
&+ \left.\left.\frac{4\kappa}{M^2}(m^2-E^2)\right] - \frac{\kappa^2+4\kappa+2}{M^2}\left[(E^2-m^2)+\frac{t}{4}\right]\right\} \\
&\Theta\quad (s-(m+M)^2)
\end{aligned} \tag{2.10}$$

where the Θ-function arises from the integrals $2C_0 + 2D_0 t$ and B_0. Note that we have retained the m-dependence purely for illustrative purposes, as $m << E$ for the experiments of interest here. The corresponding contribution from the crossed-box diagram can be obtained by crossing symmetry with the replacement $s \to u$. In this case, the Θ-function vanishes, so only $\mathrm{Im}\mathcal{M}^{\mathrm{box}}_{\gamma\gamma}\mathcal{M}^{*}_{\gamma}$ contributes.

In the expression 2.10, the terms that go as powers of E/M or m/M but do not contain factors of κ or C_r arise purely from recoil effects. The proton charge radius contributes solely via $\mathcal{M}_\gamma$. Although it also contributes to the absorptive part of $\mathcal{M}_{\gamma\gamma}$, the resulting terms do not contribute to the spin-dependent correlation of Eq. 1.37. Including the magnetic moment, charge radius, and recoil-order terms in $\mathcal{M}_\gamma$ along with the loop contributions in Eq. 2.10 leads to the following expression for the VAP:

$$\begin{aligned}
A_n &= -\frac{2\alpha t m}{\sqrt{E^2-m^2}[(E^2-m^2+t/4)+\frac{Et}{2M}+\frac{m^2t}{4M^2}]}\vec{S}\cdot\vec{K}\times\vec{K}' \\
&\times \left\{\left[\ln\left[\frac{4(E^2-m^2)}{-t}\right] - 2E/M + (2E^2-m^2)/M^2\right]\right.
\end{aligned}$$

$$\begin{aligned}
&\Bigg[\quad R + \frac{3E}{M} + \frac{2m^2}{M^2} + \frac{\kappa^2}{M^2}\frac{32(E^2-m^2)^2 + t^2/2 + 10(E^2-m^2)t}{4(E^2-m^2)+t} \\
&+ \quad \frac{4\kappa}{M^2}(m^2-E^2)\Bigg] - \frac{\kappa^2+4\kappa+2}{M^2}\left[(E^2-m^2)+\frac{t}{4}\right]\Bigg\} \\
&\times \quad \Bigg[(8E^2+4t)R^2 + \frac{4Et}{M} \\
&+ \quad t\frac{t+2m^2+2\kappa(t+2m^2)+\kappa^2[t+4(m^2-E^2)]/2}{M^2}\Bigg]^{-1}
\end{aligned} \tag{2.11}$$

Dropping all terms that go as powers of E/M, m/M, or t/M^2 yields the result obtained in Ref. [5] that was obtained for scattering from an infinitely heavy, point-like proton.

2.4 Results and Discussion

The expression for A_n given in Eq. (2.11) provides a parameter-free prediction for low-energy electron scattering. In Figure 2.5 and Figure 2.6, we plot A_n as a function of energy for fixed laboratory frame scattering angles $\theta = 146.1^\circ$ (Figure 2.5) and $\theta = 30^\circ$ (Figure 2.6), while in Figure 2.7 we show the VAP for fixed energy $E = 192$ MeV while varying θ. In all cases, the leading-order calculation is shown for comparison. In Figure 2.7, the relative importance of the recoil, magnetic moment, and charge radius contributions are also indicated.

The result obtained in the SAMPLE measurement is also shown. While the leading-order calculation overestimates the magnitude of A_n by a factor of roughly four, inclusion of the higher-order terms considered here produces agreement with the experimental value. Interestingly, there appears to be scant evidence that dynamical pions or the Δ play a significant role in A_n for this kinematic region ($E = 192$ MeV), despite one's expectation that they might.

At higher energies, our result for A_n cannot be considered reliable, since the convergence of the effective theory expansion breaks down for $E \sim M$. The A4 collaboration at Mainz has measured A_n at $E = 570.3$ MeV and $E = 854.3$ MeV and $25^\circ \leq \theta \leq 35^\circ$. Results for the higher-energy VAP have been reported in Ref. [6]. A comparison with our computation indicates that the experimental values for

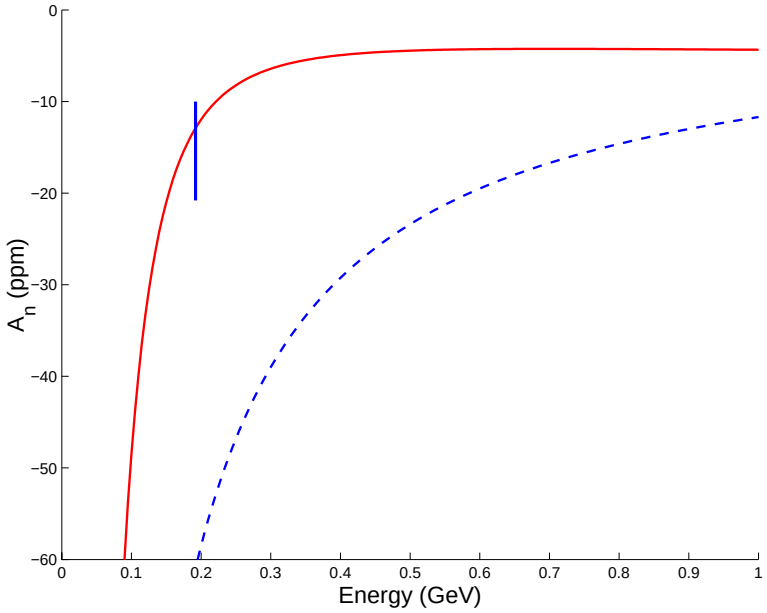

Figure 2.5: VAP vs. energy for fixed scattering angle, $\theta = 146.1°$. The dashed blue line is the leading-order result, and the solid red line shows the full calculation. The SAMPLE result [4] is also shown at $E = 192$ MeV.

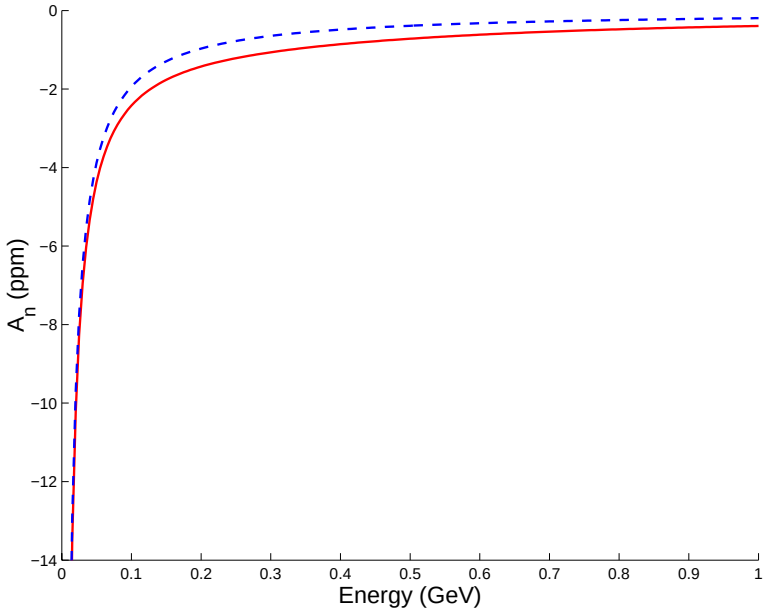

Figure 2.6: VAP vs. energy for fixed scattering angle, $\theta = 30°$. The dashed blue line is the leading-order result, and the solid red line shows the full calculation.

forward-angle scattering and higher energies are substantially larger in magnitude than we are able to obtain via the low-energy expansion to $\mathcal{O}(E/M)^2$. Presumably, a resummation of higher-order contributions in E/M using non-perturbative techniques, such as dispersion relations, would be required to compute reliably A_n in this domain [18, 46, 47, 48, 49]. We would also expect that inclusion of nucleon resonances and pions as explicit degrees of freedom would be needed to account for the experimental results.

One indication of the possible strength of these higher-order contributions may be given by considering the T-odd, P-even dimension seven operators. As shown in Appendix B, there exist two $d = 7$ operators that could, in principle, contribute. From an explicit calculation, we find that only one of the two–$\mathcal{O}_{eN}^{7a}$–leads to a non-vanishing A_n. Here, it is useful to consider the form of this operator for relativistic proton fields, N:

$$\mathcal{O}_{eN}^{7a} = \frac{\alpha^2 C_{7a}}{M^3} \bar{e}\sigma^{\mu\nu}\gamma_5(\overrightarrow{D} + \overleftarrow{D})_\nu e \; \bar{N}\gamma_5\gamma_\mu N \tag{2.12}$$

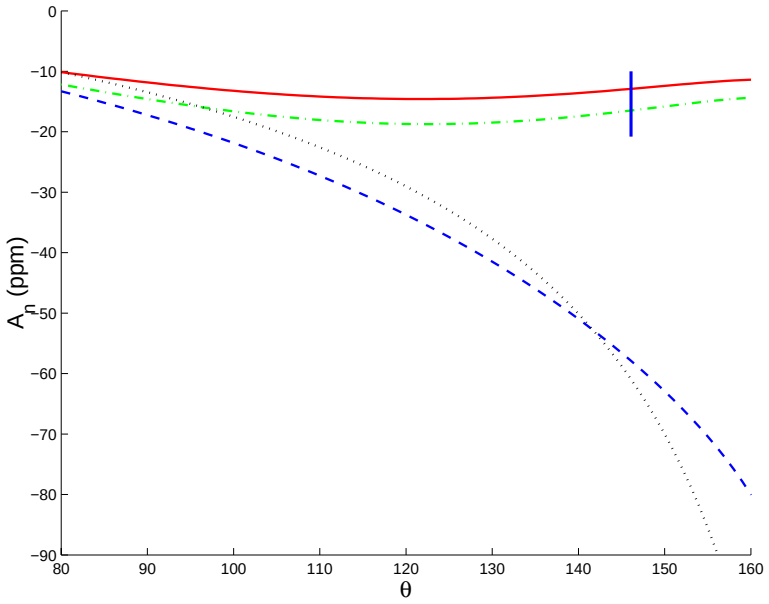

Figure 2.7: VAP vs. scattering angle for the SAMPLE kinematics ($E = 192$ MeV). The dotted black line gives the leading-order result, the blue dashed line adds the recoil corrections, the green dash-dotted line adds the magnetic corrections, and the solid red line shows the full calculation through $\mathcal{O}(p/M)^2$.

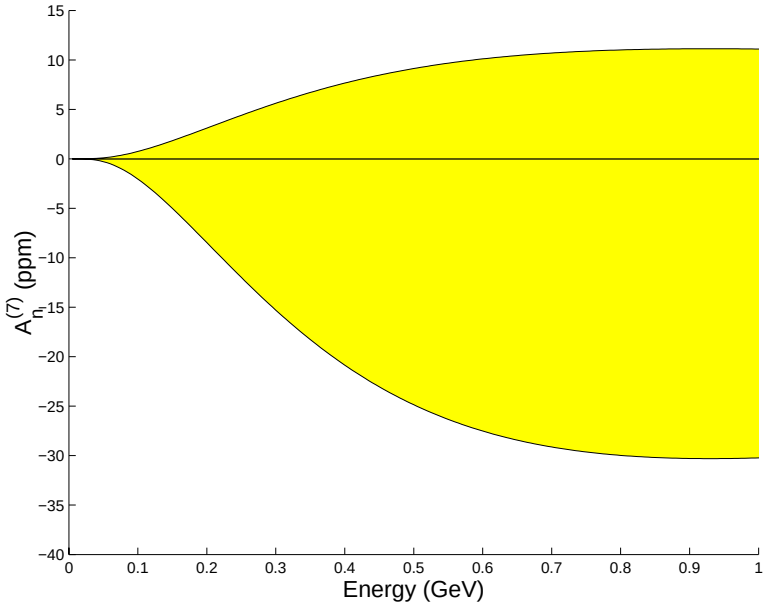

Figure 2.8: Possible contribution from the dimension seven, T-odd, P-even operator $\mathcal{O}_{eN}^{7a}$ to the backward angle VAP ($\theta = 146.1^\circ$).

Re-writing this operator in terms of the heavy fields B_v leads to:

$$\tilde{\mathcal{O}}_{eN}^{7a} = -2\frac{\alpha^2 C_{7a}}{M^2}\bar{e}\sigma^{\mu\nu}\gamma_5(\overleftarrow{D} + \overrightarrow{D})_\nu e\ \bar{B}_v S_\mu^v B_v \tag{2.13}$$

where S_μ^v is the nucleon spin. The contribution from $\tilde{\mathcal{O}}_{eN}^{7a}$ to the interference amplitude Im $\tilde{\mathcal{M}}_{eN}^{7a}\ \mathcal{M}_\gamma^*$ goes as $\epsilon^{\mu\nu\alpha\beta}S_\mu v_\nu v_\alpha K'_\beta$ and, thus, vanishes. On the other hand, using the relativistic form of the operator, $\mathcal{O}_{eN}^{7a}$, leads to the correlation $\epsilon^{\mu\nu\alpha\beta}S_\mu P_\nu P'_\alpha K'_\beta$ that is non-vanishing for $P \neq P'$. The resulting contribution to the VAP is:

$$A_n^{(7)} = \frac{\alpha C_{7a}}{4\pi}\frac{t^2|\vec{K}||\vec{K}'|\sin\theta}{M^2[8M^2E^2 + 2(2E+M)tM + t^2]} \tag{2.14}$$

a result that is $\mathcal{O}(p/M)^4$. In short, the only heavy baryon operators that can contribute involve either fields with two different velocities (*viz*, B_v and $B_{v'}$) whose contribution requires non-zero proton recoil, or dimension eight operators involving the B_v fields only and carrying an additional p/M recoil suppression.

The SAMPLE result for A_n allows for a non-vanishing, but small, coefficient for the leading, higher-order T-odd, P-even operator. Using the relativistic operator $\mathcal{O}_{eN}^{7a}$ for illustration and including the loop contributions through $\mathcal{O}(p/M)^2$ leads to $C_{7a} = 3.07 \pm 6.64$. Naive dimensional analysis would have suggested a magnitude for C_{7a} or order unity, so the SAMPLE results do not appear to imply the presence of any unnatural hadronic scale physics. We may now use this range for C_{7a} to estimate the possible size of higher-order effects at other kinematics. The resulting band is shown in Figure 2.8 for backward angles ($\theta = 146.1^\circ$) and in Figure 2.9 for forward angles ($\theta = 30^\circ$). For the Mainz measurement at $E = 570$ MeV and $\theta = 30^\circ$, we find $-2.0 \leq A_n^{(7)} \leq 0.7$ ppm, while $A_n^{\rm loop} = -0.64$ ppm. Thus, one might expect the impact of the physics we have integrated out to grow in importance relative to the loop effects considered here as the energy of the beam is increased, and it appears reasonable to expect a magnitude of a few ppm at the Mainz kinematics. We caution, however, that the precise value obtained in our calculation is unlikely to be correct in this energy regime, where the convergence of the E/M expansion is slow at best.

As a final comparison, we also consider A_n in fixed target, polarized Møller scattering. The VAP for this process has been measured at SLAC by the E158 collaboration [21], and one expects results to be forthcoming in the near future. Calculations of this quantity have been performed by several authors [22, 23, 24]. As a cross-check on our VAP for *ep* scattering, we carry out the analogous calculation here. It can be performed completely relativistically without performing an expansion in electron energy. However, since we are now dealing with identical particles in the final state, we need to compute the interference between tree diagrams in Figure 2.10b and the box diagrams of Figure 2.10a. For the SLAC measurement, one has $E = 46$ GeV. Performing the calculation in the center of mass frame we obtain:

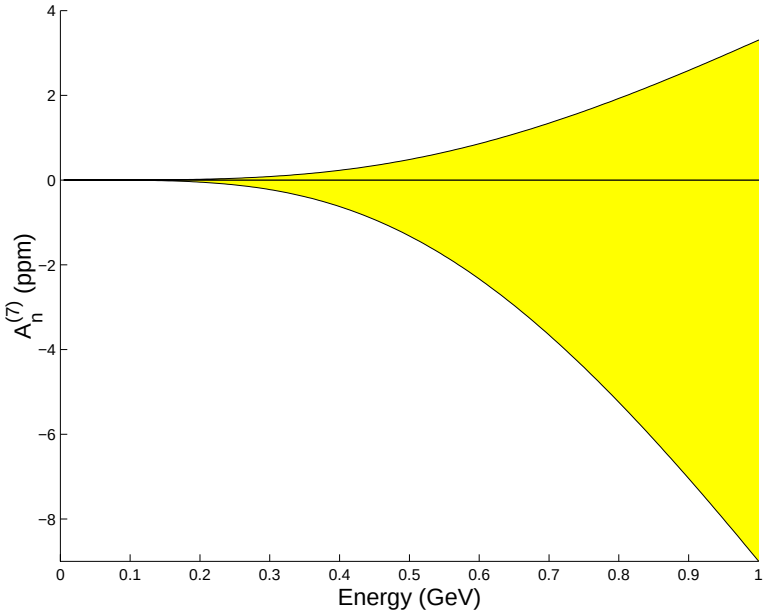

Figure 2.9: Possible contribution from $\mathcal{O}_{eN}^{7a}$ to the VAP at $\theta = 30°$, given constraints on the operator coefficient C_{7a} implied by the SAMPLE result.

$$\begin{aligned}
\frac{d\sigma^{\uparrow}}{d\Omega} - \frac{d\sigma^{\downarrow}}{d\Omega} &= -\frac{\alpha^3}{8}\frac{m}{\sqrt{s}}\sin\theta\sqrt{1-\frac{4m^2}{s}} \\
&\quad \Bigg[\; 3(s-4m^2)\Bigg(t(u-s+2m^2)\ln\left(\frac{-t}{s-4m^2}\right) \\
&\quad -u(t-s+2m^2)\ln\left(\frac{-u}{s-4m^2}\right)\Bigg) - 2(t-u)tu\Bigg] \\
\frac{d\sigma^{\uparrow}}{d\Omega} + \frac{d\sigma^{\downarrow}}{d\Omega} &= \frac{\alpha^2}{2st^2u^2}\Big[(t^2+tu+u^2)^2 + 4m^2(m^2-t-u)(t^2-tu+u^2)\Big]
\end{aligned} \tag{2.15}$$

Our results are in agreement with those of Refs. [22, 23, 24].[4] The resulting asymmetry is plotted in Figure 2.11 and agrees with the corresponding figure in Ref. [24] (note that in Ref. [24], the VAP is plotted vs. $\cos\theta$ rather than vs. θ as

[4] In Ref. [24], $\mathcal{O}(\alpha^2)$ contributions arising from initial and final state radiation effects were also computed. The corresponding contributions for the *ep* VAP are smaller than the hadronic uncertainties arising at $\mathcal{O}(\alpha)$, so we do not consider them.

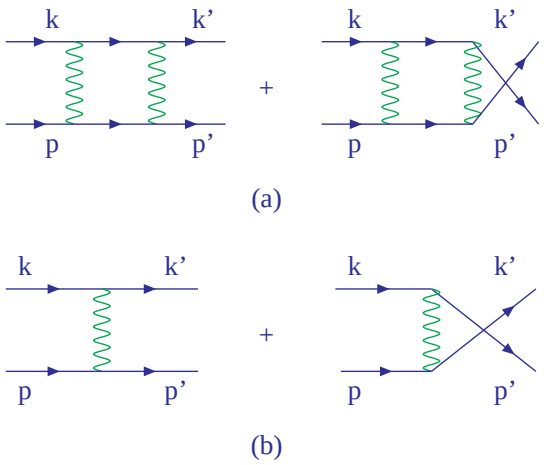

Figure 2.10: Diagrams contributing to the VAP for Møller scattering.

we do here).

2.5 Conclusions

In this study, we have computed the low-energy, backward-angle VAP using an effective theory involving electrons, photons, and protons and have obtained a parameter-free prediction through $\mathcal{O}(p/M)^2$. The VAP to this order is determined entirely by the imaginary part of the interference between the two-photon exchange, one-loop amplitude and the tree-level one-photon-exchange amplitude. In the limit that $M \to \infty$, our result exactly reproduces the VAP obtained in Ref. [5] for scattering from a structureless, infinitely heavy proton that over predicts the magnitude of A_n at the kinematics of the SAMPLE experiment. We find that inclusion of all contributions through $\mathcal{O}(p/M)^2$ leads to agreement with the experiment and leaves little room for important effects arising from dynamical pions or nucleon resonances at these energies. The leading counterterm contributions arise at $\mathcal{O}(p/M)^4$ and are consistent with zero. Thus, the SAMPLE measurement provides no evidence for unusual hadronic physics effects at these scales. The data

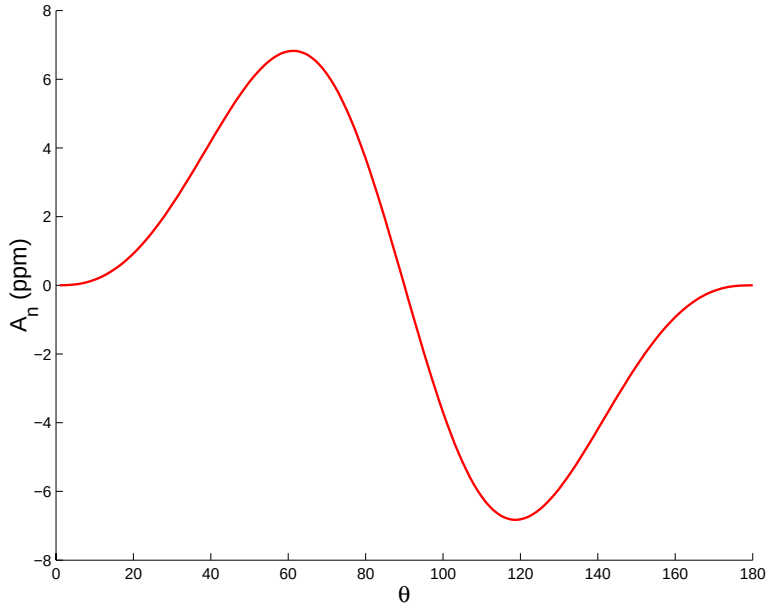

Figure 2.11: The Møller VAP vs. CM scattering angle at the E158 kinematics.

also constrain the magnitude of the counterterm coefficients to be of natural size and lead one to expect the VAP as measured by the A4 collaboration at Mainz to be at most of the order of a few ppm. Given the range of validity of our effective theory, however, we cannot produce a reliable prediction for VAP at the Mainz energies.

In this context, the results of the SAMPLE measurement have notable consequences for studies of weak interaction processes. In the case of both neutron β-decay and parity-violating ep scattering, theoretical consideration of final state QED corrections to the leading-order weak amplitudes is important for the interpretation of various measurements [19]. To the extent that these measurements involve relatively low lepton energies, an analogous effective field theory computation of one-loop graphs involving the exchange of one weak vector boson and one photon should be reliable at the $\sim 20\%$ level relative to the size of other $\mathcal{O}(\alpha)$ corrections. Future, more precise measurements of the VAP at low-energies and over a range of angles would provide important tests of this provisional assessment.

One might also ask how competitive the SAMPLE measurement is with other direct searches for new T-odd, P-even interactions. As discussed in Refs. [12, 13], direct searches are most relevant in symmetry-breaking scenarios wherein parity is broken at or above the scale for the breakdown of T. Existing direct searches imply that $\alpha_T \lesssim$ few $\times 10^{-3}$, where α_T is the ratio of a typical T-odd, P-even nuclear matrix element to those of the residual strong interaction. When translated into bounds on generic, dimension seven operator coefficients C_7 [under the normalization of Eq. (2.12)], one obtains $|C_7| \lesssim 2$. The sensitivity of the SAMPLE measurement is comparable. Given that conventional, hadronic final state effects that have been integrated out in our computation naturally imply a value of C_{7a} with a magnitude of order unity, it appears unlikely that one will be able to circumvent the corresponding theoretical hadronic uncertainties as needed to make the VAP a direct probe of new physics. On the other hand, low-energy studies of A_n could provide important information for the theoretical interpretation of other precision, electroweak observables.

Appendix A: Bremsstrahlung Computation

Here, we show that the Bremsstrahlung amplitudes corresponding to Figure 2.2 give a vanishing contribution to the VAP. The amplitudes are:

$$\begin{aligned}
\mathcal{M}^a &= \frac{-i}{q^2}\bar{u}(K')(ie)\gamma_\mu \frac{i(\not{K}-\not{l})+m)}{(K-l)^2-m^2}(ie)\gamma^\alpha\epsilon_\alpha \frac{1+\gamma_5\not{S}}{2}u(K)\bar{u}(p')(ie)\gamma^\mu u(p) \\
\mathcal{M}^b &= \frac{-i}{q^2}\bar{u}(K')(ie)\gamma^\alpha\epsilon_\alpha \frac{i(\not{K}'+\not{l})+m)}{(K'+l)^2-m^2}(ie)\gamma_\mu \frac{1+\gamma_5\not{S}}{2}u(K)\bar{u}(p')(ie)\gamma_\mu u(p) \\
\mathcal{M}^c &= \frac{-i}{q^2}\bar{u}(K')(ie)\gamma^\mu u(K)\bar{u}(p')(ie)\gamma^\mu \frac{i(\not{p}'+\not{l})+M)}{(p'+l)^2-M^2}(ie)\gamma^\alpha\epsilon_\alpha u(p) \\
\mathcal{M}^d &= \frac{-i}{q^2}\bar{u}(K')(ie)\gamma^\mu u(K)\bar{u}(p')(ie)\gamma^\alpha\epsilon_\alpha \frac{i(\not{p}-\not{l})+M)}{(p-l)^2-M^2}(ie)\gamma^\mu u(p) \qquad (2.16)
\end{aligned}$$

Here, l_μ is the radiated photon momentum. The square of the invariant amplitude:

$$\mathcal{M}^{\mathcal{B}} = \left|\mathcal{M}^a + \cdots + \mathcal{M}^d\right|^2 \qquad (2.17)$$

depends on ten different products of leptonic and hadronic tensors. The leptonic tensors are:

$$
\begin{aligned}
L^{aa}_{\mu\nu} &= Tr[(\not{K}' + m)\gamma_\mu \frac{(\not{K} - \not{l} + m)}{(K-l)^2 - m^2}\gamma_\alpha \frac{1+\gamma_5 \not{S}}{2}(\not{K} + m)\gamma_\beta \frac{(\not{K} - \not{l} + m)}{(K-l)^2 - m^2}\gamma_\nu]\epsilon^\alpha \epsilon^{*\beta} \\
L^{ab}_{\mu\nu} &= Tr[(\not{K}' + m)\gamma_\mu \frac{(\not{K} - \not{l} + m)}{(K-l)^2 - m^2}\gamma_\alpha \frac{1+\gamma_5 \not{S}}{2}(\not{K} + m)\gamma_\nu \frac{(\not{K}' + \not{l} + m)}{(K'+l)^2 - m^2}\gamma_\beta]\epsilon^\alpha \epsilon^{*\beta} \\
L^{ac}_{\mu\nu} &= Tr[(\not{K}' + m)\gamma_\mu \frac{(\not{K} - \not{l} + m)}{(K-l)^2 - m^2}\gamma_\alpha \frac{1+\gamma_5 \not{S}}{2}(\not{K} + m)\gamma_\nu]\epsilon^\alpha \\
L^{ad}_{\mu\nu} &= L^{ac}_{\mu\nu} \\
L^{bb}_{\mu\nu} &= Tr[(\not{K}' + m)\gamma_\alpha \frac{(\not{K}' + \not{l} + m)}{(K'+l)^2 - m^2}\gamma_\mu \frac{1+\gamma_5 \not{S}}{2}(\not{K} + m)\gamma_\nu \frac{(\not{K}' + \not{l} + m)}{(K'+l)^2 - m^2}\gamma_\beta]\epsilon^\alpha \epsilon^{*\beta} \\
L^{bc}_{\mu\nu} &= Tr[(\not{K}' + m)\gamma_\alpha \frac{(\not{K}' + \not{l} + m)}{(K'+l)^2 - m^2}\gamma_\mu \frac{1+\gamma_5 \not{S}}{2}(\not{K} + m)\gamma_\nu]\epsilon^\alpha \\
L^{bd}_{\mu\nu} &= L^{bc}_{\mu\nu} \\
L^{cc}_{\mu\nu} &= Tr[(\not{K}' + m)\gamma_\mu \frac{1+\gamma_5 \not{S}}{2}(\not{K} + m)\gamma_\nu] \\
L^{cd}_{\mu\nu} &= L^{cc}_{\mu\nu} \\
L^{dd}_{\mu\nu} &= L^{cc}_{\mu\nu}
\end{aligned}
\tag{2.18}
$$

The corresponding hadronic tensors are:

$$
\begin{aligned}
H^{\mu\nu}_{aa} &= Tr[(\not{p}' + M)\gamma^\mu (\not{p} + M)\gamma^\nu] \\
H^{\mu\nu}_{ab} &= H^{\mu\nu}_{aa} \\
H^{\mu\nu}_{ac} &= Tr[(\not{p}' + M)\gamma^\mu (\not{p} + M)\gamma^\beta \frac{(\not{p} - \not{l} + M)}{(p-l)^2 - M^2}\gamma^\nu]\epsilon^*_\beta \\
H^{\mu\nu}_{ad} &= Tr[(\not{p}' + M)\gamma^\mu (\not{p} + M)\gamma^\nu \frac{(\not{p}' + \not{l} + M)}{(p'+l)^2 - M^2}\gamma^\beta]\epsilon^*_\beta \\
H^{\mu\nu}_{bb} &= H^{\mu\nu}_{aa} \\
H^{\mu\nu}_{bc} &= H^{\mu\nu}_{aa} \\
H^{\mu\nu}_{bd} &= H^{\mu\nu}_{ad} \\
H^{\mu\nu}_{cc} &= Tr[(\not{p}' + M)\gamma^\alpha \frac{(\not{p} - \not{l} + M)}{(p-l)^2 - M^2}\gamma^\mu (\not{p} + M)\gamma^\nu \frac{(\not{p} - \not{l} + M)}{(p-l)^2 - M^2}\gamma^\beta]\epsilon_\alpha \epsilon^*_\beta \\
H^{\mu\nu}_{cd} &= Tr[(\not{p}' + M)\gamma^\alpha \frac{(\not{p} - \not{l} + M)}{(p-l)^2 - M^2}\gamma^\mu (\not{p} + M)\gamma^\beta \frac{(\not{p}' + \not{l} + M)}{(p'+l)^2 - M^2}\gamma^\nu]\epsilon_\alpha \epsilon^*_\beta \\
H^{\mu\nu}_{dd} &= Tr[(\not{p}' + M)\gamma^\mu \frac{(\not{p}' + \not{l} + M)}{(p'+l)^2 - M^2}\gamma^\alpha (\not{p} + M)
\end{aligned}
$$

$$\gamma^\beta \frac{(\not{p}' + \not{l} + M)}{(p'+l)^2 - M^2}\gamma^\nu]\epsilon_\alpha \epsilon^*_\beta \tag{2.19}$$

We now need to compute:

$$\begin{aligned}
\mathcal{M}^{\mathcal{B}} &= \sum_{\text{pol}} \int d^4l \Bigg\{ \frac{1}{q^4} \Bigg[L^{aa}_{\mu\nu} H^{\mu\nu}_{aa} + L^{ab}_{\mu\nu} H^{\mu\nu}_{ab} + L^{ac} H^{\mu\nu}_{ac} + L^{ad}_{\mu\nu} H^{\mu\nu}_{ad} + L^{bb}_{\mu\nu} H^{\mu\nu}_{bb} \\
&+ L^{bc}_{\mu\nu} H^{\mu\nu}_{bc} + L^{bd}_{\mu\nu} H^{\mu\nu}_{bd} + L^{cc}_{\mu\nu} H^{\mu\nu}_{cc} + L^{cd}_{\mu\nu} H^{\mu\nu}_{cd} + L^{dd}_{\mu\nu} H^{\mu\nu}_{dd} \Bigg] + \text{h.c.} \Bigg\} \\
&= \sum_{\text{pol}} \int d^4l \Bigg\{ \frac{1}{q^4} \Bigg[(H^{\mu\nu}_{ac} + H^{\mu\nu}_{ad})(L^{ac}_{\mu\nu} + L^{ad}_{\mu\nu}) + H^{\mu\nu}_{aa}(L^{aa}_{\mu\nu} + L^{ab}_{\mu\nu} + L^{bb}_{\mu\nu}) \\
&+ L^{\mu\nu}_{cc}(H^{cc}_{\mu\nu} + H^{cd}_{\mu\nu} + H^{dd}_{\mu\nu}) \Bigg] + \text{h.c.} \Bigg\}
\end{aligned} \tag{2.20}$$

where the sum is over all polarizations of the radiated photon. We are only interested in the terms proportional to $\epsilon_{\alpha\beta\gamma\delta} S^\alpha k^\beta k'^\gamma p^\delta$. First the momentum integrals are investigated:

$$\begin{aligned}
i\pi^2 \mathcal{I}^{\mathcal{B}} = \int d^4l \; & \Bigg[\frac{1}{(p'+l)^2 - M^2} \frac{1}{(p'+l)^2 - M^2} + \frac{1}{(p'+l)^2 - M^2} \frac{1}{(p-l)^2 - M^2} \\
&+ \frac{1}{(p-l)^2 - M^2} \frac{1}{(p-l)^2 - M^2} + \frac{1}{(k'+l)^2 - m^2} \frac{1}{(k'+l)^2 - m^2} \\
&+ \dots \Bigg]
\end{aligned} \tag{2.21}$$

We can evaluate the generic two point integral as defined by:

$$\begin{aligned}
i\pi^2 B(p^2; m_1^2, m_2^2) &= \mu^{4-n} \\
&\int d^n q \; \Bigg[\frac{1}{q^2 + m_1^2 - i\epsilon} \times \frac{1}{(q+p)^2 + m_2^2 - i\epsilon} \Bigg]
\end{aligned} \tag{2.22}$$

We are only interested in the imaginary part of B. We find that above the physical treshold $s = -p^2 \geq (m_1 + m_2)^2$ this integral develops an imaginary part [50]:

$$\text{Im} B(p^2; m_1^2, m_2^2) = \pi \frac{\sqrt{\lambda(s, m_1^2, m_2^2)}}{s} \Theta(s - (m_1 + m_2)^2) \tag{2.23}$$

Evaluating the B functions for the kinematics involved here one finds that none of the integrals of Eq. 2.21 develop an imaginary part. As such, evaluating the traces and performing the integration, a result of the form:

$$\begin{aligned}\mathcal{M}^{\mathcal{B}} &= f_1(m,M,s,t,u) + f_2(m,M,s,t,u) i\epsilon_{\alpha\beta\gamma\delta} S^\alpha k^\beta k'^\gamma p^\delta + h.c. \\ &= 2f_1(m,M,s,t,u) \end{aligned} \tag{2.24}$$

is obtained. Hence, there is no contribution to A_n.

Appendix B: Local Operators

As discussed in the text, we are interested in computing the contribution to the VAP from local, four-fermion $eeNN$ operators. The lowest-dimension operators of this form have dimension six. First, we show by explicit calculation that all $d = 6$ operators give vanishing contributions to A_n. The most general form for the $d = 6$ operators are:

$$\mathcal{O}_{eN}^{6a} = \frac{\alpha^2}{M^2}\bar{e}(C_1 + C_2\gamma_5)e\bar{N}(C_1' + C_2'\gamma_5)N$$

$$\mathcal{O}_{eN}^{6b} = \frac{\alpha^2}{M^2}\bar{e}(C_3 + C_4\gamma_5)\gamma^\mu e\bar{N}(C_3' + C_4'\gamma_5)\gamma^\mu N \tag{2.25}$$

$$\mathcal{O}_{eN}^{6c} = \frac{\alpha^2}{M^2}\bar{e}(C_5 + C_6\gamma_5)\sigma^{\mu\nu} e\bar{N}(C_5' + C_6'\gamma_5)\sigma_{\mu\nu} N \tag{2.26}$$

where we have used relativistic nucleon fields N (the corresponding argument carries over straightforwardly in the heavy-baryon formalism). To make the above hermitian we require all the constants C_{eN}^i to be real. We now compute the interference of the amplitudes associated with these operators and the tree amplitude $\mathcal{M}_\gamma$, retaining only the desired structure $\epsilon_{\alpha\beta\gamma\delta} S^\alpha p^\beta K^\gamma K'^\delta$. The corresponding leptonic and hadronic tensors are:

$$L_{6a}^\mu = Tr[(\not{K}' + m)(C_1 + C_2\gamma_5)\frac{1+\gamma_5\not{S}'}{2}(\not{K} + m)\gamma^\mu]$$

$$L_{6b}^{\mu\nu} = Tr[(\not{K}' + m)(C_3 + C_4\gamma_5)\gamma^\nu\frac{1+\gamma_5\not{S}'}{2}(\not{K} + m)\gamma^\mu]$$

$$
\begin{aligned}
L_{6c}^{\mu\nu\alpha} &= Tr[(\not{K}' + m)(C_5 + C_6\gamma_5)\sigma^{\nu\alpha}\frac{1+\gamma_5\not{S}}{2}(\not{K} + m)\gamma^\mu] \\
H_{6a}^{\mu} &= Tr[(\not{p}' + m)(C_1' + C_2'\gamma_5)(\not{p} + m)\gamma^\mu] \\
H_{6b}^{\mu\nu} &= Tr[(\not{p}' + m)(C_3' + C_4'\gamma_5)\gamma^\mu(\not{p} + m)\gamma^\mu] \\
H_{6c}^{\mu\nu\alpha} &= Tr[(\not{p}' + m)(C_5' + C_6'\gamma_5)\sigma^{\mu\alpha}(\not{p} + m)\gamma^\mu] \\
\mathcal{M}_6\mathcal{M}_\gamma^* + \text{h.c.} &= \frac{(4\pi\alpha)\alpha^2}{tM^2} \\
&\quad \Big[\quad L_{6a}^{\mu} H_{\mu(6a)} + L_{6b}^{\mu\nu} H_{\mu\nu(6b)} + L_{6c}^{\mu\nu\alpha} H_{\mu\nu\alpha(6c)} \Big] + \text{h.c.} \quad (2.27)
\end{aligned}
$$

Evaluating the traces and keeping only the terms of interest we obtain:

$$
\begin{aligned}
\mathcal{M}_6\mathcal{M}_\gamma^* + \text{h.c.} &= i16\frac{(4\pi\alpha)\alpha^2}{tM^2} \\
&\quad (\quad C_1C_1'M - C_4C_4'm)\epsilon_{\alpha\beta\gamma\delta}S^\alpha p^\beta K^\gamma K'^\delta + \text{h.c.} \qquad (2.28)
\end{aligned}
$$

Since all the C's are real we see there is no contribution from dimension six terms. This result is as expected, as the operators $\mathcal{O}_{6a-c}$ are even under both T and P.

Now consider $d = 7$ operators. As for the $d = 6$ operators, all contributions from T-even P-even $d = 7$ operators will vanish. We may, however, write down two Hermitian T-odd, P-even $d = 7$ operators:

$$
\mathcal{O}_{eN}^{7a} = \frac{\alpha^2}{M^3}C_{7a}\bar{e}\gamma_5\sigma^{\mu\nu}(\overleftarrow{D} + \overrightarrow{D})_\nu e\bar{N}\gamma_5\gamma_\mu N \qquad (2.29)
$$

$$
\mathcal{O}_{eN}^{7b} = \frac{\alpha^2}{M^3}C_{7b}\bar{e}\gamma_5\gamma_\mu e\bar{N}\gamma_5\sigma^{\mu\nu}(\overleftarrow{D} + \overrightarrow{D})_\nu N \qquad (2.30)
$$

As before, we evaluate the interference of the above with $\mathcal{M}_\gamma$. The corresponding leptonic and hadronic tensors are:

$$
\begin{aligned}
L_{7a}^{\mu\nu} &= iTr[(\not{K}' + m)\gamma_5\sigma^{\mu\alpha}q_\alpha\frac{1+\gamma_5\not{S}}{2}(\not{K} + m)\gamma^\nu] \\
L_{7b}^{\mu\nu} &= Tr[(\not{K}' + m)\gamma_5\gamma^\mu\frac{1+\gamma_5\not{S}}{2}(\not{K} + m)\gamma^\nu] \\
H_{7a}^{\mu\nu} &= Tr[(\not{p}' + m)\gamma_5\gamma^\mu(\not{p} + m)\gamma^\nu] \\
H_{7b}^{\mu\nu} &= iTr[(\not{p}' + m)\gamma_5\sigma^{\mu\alpha}q^a(\not{p} + m)\gamma^\nu] \\
\mathcal{M}_7\mathcal{M}_\gamma^* + \text{h.c.} &= i\frac{(4\pi\alpha)\alpha^2}{tM^3}
\end{aligned}
$$

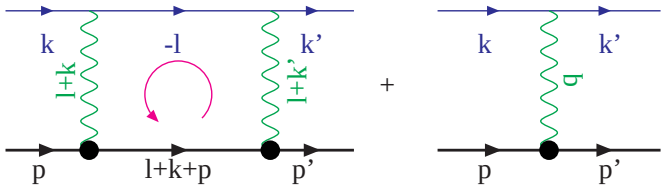

Figure 2.12: Momentum routing for the two-photon box graph integrals.

$$\left[\quad C_{7a} L_{7a}^{\mu\nu} H_{\mu\nu(7a)} + C_{7b} L_{7b}^{\mu\nu} H_{\mu\nu(7b)} \right] + \text{h.c.} \tag{2.31}$$

Evaluating the traces we note that only the $L_{7a}^{\mu\nu} H_{\mu\nu(7a)}$ contributes:

$$\mathcal{M}_7 \mathcal{M}_\gamma + \text{h.c.} \quad = \quad \frac{16(4\pi\alpha)\alpha^2 C_{7a}}{M^3} \epsilon_{\alpha\beta\gamma\delta} S^\alpha p^\beta k^\gamma k'^\delta \tag{2.32}$$

We are intrested in the contribution such a term gives to the VAP. Keeping only the leading piece of the tree amplitude we get:

$$A_n^{(7)} = \frac{\alpha C_{7a}}{4\pi} \frac{t^2 |\vec{K}||\vec{K}'| \sin\theta}{M^2[8M^2E^2 + 2(2E+M)tM + t^2]} \tag{2.33}$$

Appendix C: Loop Integrals

Here, we provide additional details about the computation of $\mathcal{M}_{\gamma\gamma}$. As noted in the text, the contribution from the crossed-box diagram vanishes, so we consider only $\text{Im}\mathcal{M}_{\gamma\gamma}^{\text{box}} \mathcal{M}_\gamma^*$. We may express the latter in terms of the leptonic and hadronic tensors:

$$
\begin{aligned}
L^{\mu\nu\alpha} &= \bar{u}(K')(ie)\gamma^{\mu}\frac{i(-\not{l}+m)}{l^2-m^2}(ie)\gamma^{\nu}\frac{1+\gamma_5\not{S}}{2}u(K)\bar{u}(K)(ie)\gamma^{\alpha}u(K') \\
H_{\mu\nu\alpha} &= \bar{u}(p')[ie(1+r(l+K')^2)\gamma_{\mu}-\frac{\kappa\sigma_{\mu\beta}}{2M}(l+K')^{\beta}]\frac{i(\not{l}+\not{K}'+\not{p}'+M)}{((l+K'+p')^2-M^2} \\
&\times [ie(1+r(l+K)^2)\gamma_{\nu}+\frac{\kappa\sigma_{\nu\delta}}{2M}(l+K)^{\delta}]u(p) \\
&\times \bar{u}(p)[ie(1+r(K-K')^2)\gamma_{\alpha}+\frac{\kappa\sigma_{\alpha\gamma}}{2M}(K-K')^{\gamma}]u(p') \\
\mathcal{M}^{\rm box}_{\gamma\gamma}\mathcal{M}^{*}_{\gamma} &= \int\frac{d^4l}{(2\pi)^2}L^{\mu\nu\alpha}\frac{-i}{(l+K')^2}\frac{-i}{(l+K)^2}\frac{-i}{(K-K')^2}H_{\mu\nu\alpha} \qquad (2.34)
\end{aligned}
$$

We define the loop integrals from above as follows:

$$
\begin{aligned}
i\pi^2 D_0 &= \int d^4l\frac{1}{(l^2-m^2)(l+K')^2[(l+K'+p')^2-M^2](l+K)^2} \\
i\pi^2 D_{\alpha} &= \int d^4l\frac{l_{\alpha}}{(l^2-m^2)(l+K')^2[(l+K'+p')^2-M^2](l+K)^2} \\
i\pi^2 D_{\alpha\beta} &= \int d^4l\frac{l_{\alpha}l_{\beta}}{(l^2-m^2)(l+K')^2[(l+K'+p')^2-M^2](l+K)^2} \\
i\pi^2 D_{\alpha\beta\gamma} &= \int d^4l\frac{l_{\alpha}l_{\beta}l_{\gamma}}{(l^2-m^2)(l+K')^2[(l+K'+p')^2-M^2](l+K)^2} \\
i\pi^2 D_{\alpha\beta\gamma\delta} &= \int d^4l\frac{l_{\alpha}l_{\beta}l_{\gamma}l_{\delta}}{(l^2-m^2)(l+K')^2[(l+K'+p')^2-M^2](l+K)^2} \qquad (2.35)
\end{aligned}
$$

In order to evaluate these integrals, we follow the methods of Refs. [42, 43], and our notation follows that of Ref. [43]. To this end, we need to compute the following three point functions:

$$
\begin{aligned}
i\pi^2 C_0(1,2,3) &= \int d^4l\frac{1}{(l^2-m^2)(l+K')^2[(l+K'+p')^2-M^2]} \\
i\pi^2 C_0(1,2,4) &= \int d^4l\frac{1}{(l^2-m^2)(l+K')^2(l+K)^2} \\
i\pi^2 C_0(1,3,4) &= \int d^4l\frac{1}{(l^2-m^2)[(l+K'+p')^2-M^2](l+K)^2} \\
i\pi^2 C_0(2,3,4) &= \int d^4l\frac{1}{(l+K')^2[(l+K'+p')^2-M^2](l+K)^2}
\end{aligned} \qquad (2.36)
$$

and two point functions:

$$\begin{aligned}
i\pi^2 B_0(1,2) &= \int d^4l \frac{1}{(l^2-m^2)(l+K')^2} \\
i\pi^2 B_0(1,3) &= \int d^4l \frac{1}{(l^2-m^2)[(l+K'+p')^2-M^2]} \\
i\pi^2 B_0(1,4) &= \int d^4l \frac{1}{(l^2-m^2)(l+K)^2} \\
i\pi^2 B_0(2,4) &= \int d^4l \frac{1}{(l+K')^2(l+K)^2} \\
i\pi^2 B_0(2,3) &= \int d^4l \frac{1}{(l+K')^2[(l+K'+p')^2-M^2]} \\
i\pi^2 B_0(3,4) &= \int d^4l \frac{1}{[(l+K'+p')^2-M^2](l+K)^2}
\end{aligned} \tag{2.37}$$

For all the B, C and D integrals above we are interested only in the imaginary part. The only two-, three-, and four-point integrals with non-vanishing imaginary parts are:

$$\begin{aligned}
\text{Im } D_0 &= \frac{2\pi}{-t}\ln(\frac{-t}{\lambda^2})\frac{1}{\sqrt{\Lambda}}\Theta(s-(m+M)^2) \\
\text{Im } C_0(1,2,3) &= \frac{\pi}{\sqrt{\Lambda}}\ln(\frac{\Lambda}{s\lambda^2})\Theta(s-(m+M)^2) \\
\text{Im } C_0(1,3,4) &= \text{Im}[C_0(1,2,3)] = C_0 \\
\text{Im } B_0(1,3) &= \pi\frac{\sqrt{\Lambda}}{s}\Theta(s-(m+M)^2)
\end{aligned} \tag{2.38}$$

In the above λ is the photon mass and $\Lambda = s^2 - 2s(M^2+m^2) + (M^2-m^2)^2$.

The four-point intergrals are evaluated using the Passarino and Veltman procedure. First one sets up the required framework for the calculation. For the

kinematics considered here, the Passarino and Veltman momenta and masses are:

$$\begin{array}{ll} p_1 = K & m_1 = m \\ p_2 = p & m_2 = 0 \\ p_3 = -p' & m_3 = M \\ p_4 = -K' & m_4 = 0 \end{array} \tag{2.39}$$

The f-functions are given by:

$$\begin{aligned} f_1 &= m_1^2 - m_2^2 - p_1^2 = 2m^2 \\ f_2 &= m_1^2 - m_2^2 + p_1^2 - p_5^2 = (s - M^2 - m^2) \\ f_3 &= m_2^2 - m_4^2 - p_4^2 + p_5^2 = -f_2 \end{aligned} \tag{2.40}$$

For space considerations not all the intermediate steps to obtain the integral coefficients are shown. The Passarino-Veltman R-functions will be shown only for the D_α integral:

$$\mathrm{Im}\begin{pmatrix} D_{11} \\ D_{12} \\ D_{13} \end{pmatrix} = X^{-1}\mathrm{Im}\begin{pmatrix} R_{20} \\ R_{21} \\ R_{22} \end{pmatrix} \tag{2.41}$$

where:

$$\begin{aligned} R_{20} &= \frac{1}{2}[f_1 D_0 + C_0(1,3,4) - C_0(2,3,4)] = \frac{1}{2}(2D_0 m^2 + C_0) \\ R_{21} &= \frac{1}{2}[f_2 D_0 + C_0(1,2,4) - C_0(1,3,4)] = \frac{1}{2}[2D_0(s - M^2 - m^2) - C_0] \\ R_{22} &= \frac{1}{2}[f_3 D_0 + C_0(1,2,3) - C_0(1,2,4)] \\ &= \frac{1}{2}[-2D_0(s - M^2 - m^2) + C_0] \end{aligned} \tag{2.42}$$

and where the inverse of the momentum matrix X is:

$$\begin{aligned} X^{-1} &= \begin{pmatrix} p_1^2 & p_1p_2 & p_1p_3 \\ p_1p_2 & p_2^2 & p_2p_3 \\ p_1p_3 & p_2p_3 & p_3^2 \end{pmatrix}^{-1} \\ &= \begin{pmatrix} \frac{4M^2-t}{\Lambda+ts} & \frac{3M^2+m^2-s-t}{\Lambda+ts} & \frac{M^2-m^2+s}{\Lambda+ts} \\ \frac{3M^2+m^2-s-t}{\Lambda+ts} & \frac{2(M^2+s+t)m^2-(s+t-M^2)^2-m^4}{t(\Lambda+ts)} & \frac{M^2-m^2}{\Lambda+ts}-\frac{1}{t} \\ \frac{M^2-m^2+s}{\Lambda+ts} & \frac{M^2-m^2}{\Lambda+ts}-\frac{1}{t} & \frac{s}{\Lambda+ts}-\frac{1}{t} \end{pmatrix} \end{aligned} \tag{2.43}$$

Puting things toghether we have:

$$D^\alpha = p_1^\alpha D_{11} + p_2^\alpha D_{12} + p_3^\alpha D_{13} \tag{2.44}$$

After performing the necessary algebra we obtain:

$$\begin{aligned} \mathrm{Im}[D_{11}] &= -\frac{D_0[2\Lambda+(m^2-M^2+s)t]-2C_0(s+M^2-m^2)}{2(\Lambda+ts)} \\ \mathrm{Im}[D_{12}] &= -\frac{D_0\Big[m^4+[t-2(M^2+s)]m^2+(M^2-s)(M^2-s-t)\Big]}{2(\Lambda+ts)} \\ &+ \frac{2C_0(m^2-M^2)}{2(\Lambda+ts)} \\ \mathrm{Im}[D_{13}] &= \frac{-D_0\Lambda+2C_0s}{2(\Lambda+ts)} \end{aligned} \tag{2.45}$$

Looking at the integral with two powers of momenta in the numerator we have:

$$\begin{aligned} D^{\alpha\beta} &= D_{21}p_1^\alpha p_1^\beta + D_{23}p_2^\alpha p_2^\beta + D_{23}p_3^\alpha p_3^\beta + D_{24}[p_1,p_2]^{\alpha\beta} \\ &+ D_{25}[p_1,p_3]^{\alpha\beta} + D_{26}[p_2,p_3]^{\alpha\beta} + D_{27}g^{\alpha\beta} \end{aligned} \tag{2.46}$$

where:

$$[a,b]^{\alpha\beta} = a^\alpha b^\beta + a^\beta b^\alpha \tag{2.47}$$

and after evaluating the coefficients we get:

$$
\begin{aligned}
\mathrm{Im}[D_{21}] &= \frac{2B_0(\Lambda+st)(-m^2+M^2+s)^2}{2\Lambda(\Lambda+st)^2} \\
&+ \frac{2C_0\Big[2\Lambda(m^2-2M^2-s)+[(m^2-M^2)^2-2sM^2-s^2]t\Big]}{2(\Lambda+st)^2} \\
&+ \frac{D_0\Big[2\Lambda^2+2\Lambda(m^2-2M^2+s)t+[m^4-2M^2m^2+(M^2-s)^2]t^2\Big]}{2(\Lambda+st)^2} \\
\mathrm{Im}[D_{22}] &= \frac{D_0\Lambda[2t^2-4(M^2-s)t+2\Lambda]}{4(\Lambda+st)^2} \\
&+ \frac{4C_0[(m^2-M^2)^2-2M^2(s+\Lambda)]}{4(\Lambda+st)^2} \\
&+ \frac{4B_0(\Lambda+st)}{\Lambda t}\Big[(s+t)m^4-2[(s+t)M^2+s^2]m^2 \\
&+ (M^2-s)^2s+(M^4+s^2)t\Big] \\
\mathrm{Im}[D_{23}] &= \frac{D_0\Lambda^3t+C_0\Lambda st(2\Lambda+st)t+2B_0s(\Lambda+st)(\Lambda+2st)}{2\Lambda(\Lambda+st)^2t} \\
\mathrm{Im}[D_{24}] &= \frac{2B_0(\Lambda+st)(m^2-M^2)(m^2-M^2-s)^2}{2\Lambda(\Lambda+st)^2} \\
&+ \frac{2C_0\Lambda\Big[\Lambda(m^2-3M^2)+[(m^2-M^2)^2-2sM^2]t\Big]}{2\Lambda(\Lambda+st)^2} \\
&+ \frac{D_0\Big[\Lambda^2+\Lambda(m^2-3M^2+2s)t+[m^4-2M^2m^2+(M^2-s)^2]t^2\Big]}{2\Lambda(\Lambda+st)^2} \\
\mathrm{Im}[D_{25}] &= \frac{D_0\Lambda[\Lambda+(m^2-M^2)t]}{2(\Lambda+st)^2} \\
&+ \frac{C_0[2\Lambda(m^2-M^2-2s)-s^2]}{2(\Lambda+st)^2} \\
&+ \frac{B_0(-m^2+M^2+s)(s+\Lambda)s}{\Lambda(\Lambda+st)^2} \\
\mathrm{Im}[D_{26}] &= \frac{2D_0\Lambda(\Lambda+m^2-M^2+s)+4C_0[\Lambda(m^2-M^2-s)-s^2t]}{4(\Lambda+st)^2} \\
&+ \frac{B_0s[\Lambda+(M^2-m^2+s)t]}{(\Lambda+st)\Lambda t} \\
\mathrm{Im}[D_{27}] &= \frac{(2C_0+D_0t)\Lambda}{4(\Lambda+ts)} \quad . \qquad (2.48)
\end{aligned}
$$

Looking at the integral with three powers of momenta in the numerator, we have:

$$\begin{aligned} D^{\alpha\beta\gamma} &= D_{31}p_1^\alpha p_1^\beta p_1^\gamma + D_{32}p_2^\alpha p_2^\beta p_2^\gamma + D_{33}p_3^\alpha p_3^\beta p_3^\gamma + D_{34}[p_1,p_1,p_2]^{\alpha\beta\gamma} \\ &+ D_{35}[p_1,p_1,p_3]^{\alpha\beta\gamma} + D_{36}[p_1,p_2,p_2]^{\alpha\beta\gamma} + D_{37}[p_1,p_3,p_3]^{\alpha\beta\gamma} \\ &+ D_{38}[p_2,p_2,p_3]^{\alpha\beta\gamma} + D_{39}[p_2,p_3,p_3]^{\alpha\beta\gamma} + D_{310}[p_1,p_2,p_3]^{\alpha\beta\gamma} \\ &+ D_{311}[p_1,g]^{\alpha\beta\gamma} + D_{312}[p_2,g]^{\alpha\beta\gamma} + D_{313}[p_3,g]^{\alpha\beta\gamma} \end{aligned} \tag{2.49}$$

After evaluating the coefficients we get:

$$\begin{aligned} \mathrm{Im}[D_{31}] &= -\frac{D_0}{2(\Lambda+st)^3}\Big[[(m^2-M^2)^3+s^3-3M^2s^2+3M^2(M^2-m^2)s]t^3 \\ &+ 3\Lambda(m^4-3M^2m^2+2M^4+s^2-3M^2s)t^2 \\ &+ 3\Lambda^2(m^2-3M^2+s)t+2\Lambda^3\Big] \\ &- \frac{2C_0}{2(\Lambda+st)^3}\Big[[(m^2-M^2)^3-s^3-3M^2s^2+3M^2(M^2-m^2)s]t^2 \\ &+ 3\Lambda(m^4-3M^2m^2+2M^4-s^2-3M^2s)t+3\Lambda^2(m^2-3M^2-s)\Big] \\ &- \frac{B_0}{2s\Lambda(\Lambda+st)^2}(m^2-M^2-s)\Big[m^8+(2s-4M^2)m^6 \\ &+ [6M^4-16sM^2+3s(t-4s)]m^4 \\ &+ [-4M^6+26sM^4+2s(10s-3t)M^2+14s^3]m^2 \\ &+ M^8-12M^6s-6M^2s^2t-s^3(5s+3t)+M^4s(16s+3t)\Big] \\ \mathrm{Im}[D_{32}] &= \frac{4D_0}{8(\Lambda+st)^3}\Big[-t^3[(m^2-M^2)^3+s^3-3M^2s^3+3M^2(M^2-m^2)s] \\ &- 3t^2\Lambda[M(m+M)-s][M(m-M)+s]+3t\Lambda^2(m^2-s)-\Lambda^3\Big] \\ &+ \frac{C_0}{(\Lambda+st)^3}\Big[[(m^2-M^2)^3-3M^2s^2+3M^2(M^2-m^2)s] \\ &+ 3\Lambda(m^2-M^2+2s)M^2-3\Lambda^2M^2\Big] \\ &+ \frac{B_0}{2(\Lambda+st)^2\Lambda st}\Big[-3s[(m^2-M^2)^3+s^3+2M^2(M^2-m^2)s]t^2 \\ &- \Lambda[(m^2-M^2)^3+6s^3+6M^2(M^2-m^2)s]t-3s^2\Lambda^2\Big] \\ \mathrm{Im}[D_{33}] &= -D_0\frac{\Lambda^3}{2(\Lambda+st)^3} \end{aligned}$$

$$
\begin{aligned}
&+ \quad \frac{C_0 s}{(\Lambda+st)^3}(3\Lambda^2+3st\Lambda+2s^2t^2) \\
&+ \quad \frac{B_0 s}{2}\Big[\frac{s(-\frac{3st}{\Lambda}-5)}{(\Lambda+st)^2}-\frac{3}{\Lambda t}\Big] \\
\mathrm{Im}[D_{34}] &= -\frac{D_0}{2(\Lambda+st)^3}\Big[\Lambda[(m^2-M^2+s)t^3+2m^4-7M^2m^2+5M^4+3s^2-8M^2s] \\
&+ \quad \Lambda^2(m^2-6M^2+3s)+\Lambda^3\Big] \\
&- \quad \frac{C_0}{2(\Lambda+st)^3}\Big[(m^2-6M^2)^2\Lambda^2+(2m^4-7M^2m^2+5M^4-8M^2s)\Lambda t \\
&+ \quad [(m^2-M^2)^3-3M^2s^2+3M^2(M^2-m^2)s]t^2\Big] \\
&- \quad \frac{B_0}{2s\Lambda(\Lambda+st)^3} \\
&\Big[\quad s^2t^2[3(m^2-M^2)^3-(m^2-5M^2)s^2-2(m^4+M^2m^2-2M^4)s] \\
&+ \quad st\Lambda[4(m^2-M^2)^3-(m^2-3M^2)s^2+3M^2(M^2-m^2)s] \\
&+ \quad \Lambda^2[(m^2-M^2)^3-(3m^2-7M^2)s^2+2(m^4-5M^2m^2+4M^4)s]\Big] \\
\mathrm{Im}[D_{35}] &= \frac{D_0}{2(\Lambda+st)^3}\Big[-\Lambda^3+(2m^2-3M^2)t\Lambda^2+[(m^2-M^2)^2-M^2s]t^2\Lambda\Big] \\
&+ \quad \frac{C_0}{2(\Lambda+st)^3}\Big[2[-sM^2+(m^2-M^2)^2-3s^2]t\Lambda \\
&- \quad [4m^2-6(M^2+s)]\Lambda^2-2s^3\Big] \\
&+ \quad \frac{B_0}{2\Lambda(\Lambda+st)^3}\Big[-[m^4-(2M^2+3s)m^2+M^4+5s^2+8M^2s]\Lambda^2 \\
&+ \quad 4(3M^2-2m^2+2s)s^2t\Lambda+[3s^2-(m^2-M^2)^2-2(m^2-2M^2)]st^2\Big] \\
\mathrm{Im}[D_{36}] &= \frac{D_0}{2(\Lambda+st)^3}\Big[-[(m^2-M^2)^3+s^3-3M^2s^2+3M^2(M^2-m^2)s]t^3 \\
&- \quad (m^4-5M^2m^2+4M^4+3s^2-7M^2s)\Lambda t^2+(4m^2-3s)\Lambda^2t-\Lambda^3\Big] \\
&+ \quad \frac{C_0}{(\Lambda+st)^3}\Big[[(m^2-M^2)^3+3M^2(M^2-m^2)s-3M^2s^2]t^2 \\
&- \quad (m^4-5M^2m^2+4M^4-7M^2s)\Lambda t-4M^2\Lambda^2\Big] \\
&+ \quad \frac{B_0}{2\Lambda(\Lambda+st)^3st}\Big[-2s^2(\Lambda+st)\Lambda^2 \\
&- \quad [(m-M^2)^3+4s^3+2M^2s^2+(m^4-8M^2m^2+7M^4)s]t\Lambda \\
&- \quad [3(m^2-M^2)^3+2s^3+2M^2s^2-(m^4+4M^2m^2-5M^4)s]st^2\Big]
\end{aligned}
$$

$$
\begin{aligned}
\mathrm{Im}[D_{37}] &= \frac{D_0}{2(\Lambda+st)^3}[\Lambda^3-(m^2-M^2)\Lambda^2 t] \\
&+ \frac{C_0}{(\Lambda+st)^3}[2t^2s^3+6s^2t\Lambda-2(m^2-M^2-3s)\Lambda^2] \\
&+ \frac{B_0}{2(\Lambda+st)^3\Lambda t}(\Lambda+st)s[-2\Lambda^2 \\
&+ (m^2-M^2-5s)st^2+3(m^2-M^2-3s)\Lambda t] \\
\mathrm{Im}[D_{38}] &= \frac{D_0}{2(\Lambda+st)^3}\Big[\Lambda^3+\Lambda^2 t(m^2-2M^2-2s) \\
&+ \Lambda[m^4+(s-2M^2)m^2+(M^2-s^2)t^2]\Big] \\
&+ \frac{C_0}{(\Lambda+st)^3}\Big[t^2s^3-(m^2-2M^2-s)\Lambda^2-\Lambda[(m^2-M^2)^2 \\
&- 2s^2+(m^2-2M^2)s]t\Big] \\
&+ \frac{B_0}{2(\Lambda+st)^3\Lambda t}\Big[3s\Lambda^3+[m^4-2(M^2+s)m^2+M^4+9s^2+4M^2s]t\Lambda^2 \\
&- s^2[(m^2-M^2)^2-3s^2+2(m^2-2M^2)s]t^3 \\
&- (4m^2-8M^2-9s)\Lambda s^2t^2\Big] \\
\mathrm{Im}[D_{39}] &= \frac{D_0}{2\Lambda(\Lambda+st)^3}\Lambda^3\Big[m^4+[t-2(M^2+s)]m^2+(M^2-s)(M^2-s-t)\Big] \\
&+ \frac{C_0}{2\Lambda(\Lambda+st)^3}[-2\frac{\Lambda}{t}(m^2-M^2-2s)+6s^2t\Lambda^2+2s^3t^2\Lambda] \\
&+ \frac{B_0}{2\Lambda(\Lambda+st)^3}[-\frac{3s\Lambda^3}{t}+s(-3m^2+3M^2+11s)\Lambda^2 \\
&+ s^2(4m^2-4M^2-13s)t\Lambda+s^3(m^2-M^2-5s)t^2] \\
\mathrm{Im}[D_{310}] &= \frac{D_0\Lambda}{4(\Lambda+st)^3}\Big[2\Lambda^2+[2(m^2-M^2)^2+s^2+(m^2-3M^2)s]t^2 \\
&+ (3m^2-5M^2+3s)t\Lambda\Big] \\
&+ \frac{2C_0}{4(\Lambda+st)^3}[2t^2s^3-2t(m^2-M^2)^2-5s^2 \\
&+ (m^2-3M^2s)\Lambda-(3m^2-5M^2-3s)\Lambda^2] \\
&+ \frac{B_0}{2\Lambda t(\Lambda+st)^3}\Big[2s\Lambda^3+[m^4-2(M^2+2s)m^2+M^4+7s^2+6M^2s]\Lambda^2 t \\
&- 2(3m^2-5M^2-45)\Lambda s^2t^2-s^2[(m^2-M^2)^2-3s^2+2(m^2-2M^2)s]t^3\Big]
\end{aligned}
$$

$$
\begin{aligned}
\mathrm{Im}[D_{311}] &= \frac{-2B_0(m^2-M^2-s)(\Lambda+st)-(2C_0+D_0t)\Lambda[2\Lambda+(m^2-M^2-s)t]}{8(\Lambda+st)^2} \\
\mathrm{Im}[D_{312}] &= \frac{-2B_0(m^2-M^2)(\Lambda+st)}{8(\Lambda+st)^2} \\
&- \frac{(2C_0+D_0t)\Lambda[\Lambda-(M^2-m^2-s)t]}{8(\Lambda+st)^2} \\
\mathrm{Im}[D_{313}] &= \frac{2B_0s(\Lambda+st)-(D_0t+2C_0)\Lambda^2}{8(\Lambda+st)^2}
\end{aligned} \tag{2.50}
$$

Looking at the integral with four powers of momenta in the numerator, we have:

$$
\begin{aligned}
D^{\alpha\beta\gamma\delta} &= D_{41}p_1^\alpha p_1^\beta p_1^\gamma p_1^\delta + D_{42}p_2^\alpha p_2^\beta p_2^\gamma p_2^\delta + D_{43}p_3^\alpha p_3^\beta p_3^\gamma p_3^\delta + D_{44}[p_1,p_1,p_1,p_2]^{\alpha\beta\gamma\delta} \\
&+ D_{45}[p_1,p_1,p_1,p_3]^{\alpha\beta\gamma\delta} + D_{46}[p_1,p_2,p_2,p_2]^{\alpha\beta\gamma\delta} + D_{47}[p_2,p_2,p_2,p_3]^{\alpha\beta\gamma\delta} \\
&+ D_{48}[p_1,p_3,p_3,p_3]^{\alpha\beta\gamma\delta} + D_{49}[p_2,p_3,p_3,p_3]^{\alpha\beta\gamma\delta} + D_{410}[p_1,p_1,p_2,p_2]^{\alpha\beta\gamma\delta} \\
&+ D_{411}[p_1,p_1,p_3,p_3]^{\alpha\beta\gamma\delta} + D_{412}[p_2,p_2,p_3,p_3]^{\alpha\beta\gamma\delta} + D_{413}[p_1,p_1,p_2,p_3]^{\alpha\beta\gamma\delta} \\
&+ D_{414}[p_1,p_2,p_2,p_3]^{\alpha\beta\gamma\delta} + D_{415}[p_1,p_2,p_3,p_3]^{\alpha\beta\gamma\delta} + D_{416}[p_1,p_1,g]^{\alpha\beta\gamma\delta} \\
&+ D_{417}[p_2,p_2,g]^{\alpha\beta\gamma\delta} + D_{418}[p_3,p_3,g]^{\alpha\beta\gamma\delta} + D_{419}[p_1,p_2,g]^{\alpha\beta\gamma\delta} \\
&+ D_{420}[p_1,p_3,g]^{\alpha\beta\gamma\delta} + D_{421}[p_2,p_3,g]^{\alpha\beta\gamma\delta} + D_{422}[g,g]^{\alpha\beta\gamma\delta}
\end{aligned} \tag{2.51}
$$

and after evaluating the coefficients, we get:

$$
\begin{aligned}
\mathrm{Im}[D_{41}] &= \frac{D_0}{2\Lambda(\Lambda+st)^4s^2} \\
&\Big[[m^8-4M^2m^6+(6M^4-4M^2s)m^4-4(M^3-Ms)^2m^2+(M^2-s)^4]t^4 \\
&+ 4\Lambda[m^6-4M^2m^4+(5M^4-4M^2s)m^2-(M^2-s)(2M^2-s)]t^3 \\
&+ 2\Lambda^2(3m^4-12M^2m^2+10M^2+3s^2-12M^2s)t^2 \\
&+ 4\Lambda^3(m^2-4M^2+s)t+2\Lambda^4\Big] \\
&+ \frac{C_0}{\Lambda(\Lambda+st)^4s^2} \\
&\Big[[(m^2-M^2)^4-s^4-4M^2s^3+2M^2(3M^2-2m^2)s^2-4(M^3-m^2M^2)s]t^3 \\
&+ 4\Lambda[m^6-4M^2m^2+(5M^4-4M^2s)m^2-2M^6-s^3-4M^2s^2+5M^4s]t^2 \\
&+ 2\Lambda^2(3m^4-12M^2m^2+10M^4-3s^2-12M^2s)t+4\Lambda^3(m^2-4M^2-s)\Big]
\end{aligned}
$$

$$
\begin{aligned}
&+ \quad \frac{B_0}{6\Lambda(\Lambda+st)^4 s^2}(\Lambda+st)\Big[2\Lambda^2[(m^2-M^2)^4+2(m^2-4M^2)s(m^2-M^2)^2 \\
&+ \quad 13s^4-2(11m^2-26M^2)s^3+6(m^4-6M^2m^2+6M^4)s^2] \\
&+ \quad s^2[11(m^2-M^2)^4-4(2m^2+7M^2)s(m^2-M^2)^2+11s^4 \\
&- \quad 4(2m^2-11M^2)s^3-6(m^4-2M^2m^2-M^4)^2s^2]t^2 \\
&+ \quad \Lambda s[7(m^2-M^2)^4+4(5m^2-17M^2)s(m^2-M^2)^2+31s^4 \\
&- \quad 4(7m^2-31M^2)s^3-6(5m^2-7M^2)(m^2+M^2)s^2]t\Big] \\
\mathrm{Im}[D_{42}] \quad &= \quad \frac{D_0}{2\Lambda(\Lambda+st)^4 s^2 t} \\
&\Big[\quad [m^8-4M^2m^6+(6M^4-4M^2s)m^4-4(M^3-Ms)^2m^2+(M^2-s)^4]t^4 \\
&- \quad 4\Lambda[M^2m^4-2(M^4-M^2s)m^2+(m^2-s)^3]t^3 \\
&+ \quad 2\Lambda^2[2m^2M^2-3(M^2-s)^2]t^2-4\Lambda^3(M^2-4s)t+\Lambda^4\Big] \\
&+ \quad \frac{C_0}{\Lambda(\Lambda+st)^4 s^2 t} \\
&\Big[\quad [(m^2-M^2)^4-4M^2s^3+2M^2(3M^2-2m^2)s^2-4(M^3-m^2M^2)s]t^3 \\
&- \quad 4\Lambda[(m^2-M^2)^2+3s^2+(2m^2-3M^2)s]M^2t^2 \\
&- \quad 2\Lambda^2(2m^2-3M^2+6s)M^2t-4\Lambda^3M^2\Big] \\
&+ \quad \frac{B_0}{6\Lambda(\Lambda+st)^4 s^2 t}(\Lambda+st)\Big[11s^3\Lambda^3 \\
&+ \quad [2(m^2-M^2)^4+33s^4+12M^2(3M^2-2m^2)^2s^2-12(M^3-m^2M)^2s]t\Lambda^2 \\
&+ \quad s^2[11(m^2-M^2)^4+11s^4+12M^2(3M^2-2m^2)s^2-36(M^3-m^2M)^2s]t^3 \\
&+ \quad s[7(m^2-M^2)^4+33s^4+24M^2(3M^2-2m^2)s^2-48(M^3-m^2M)^2s]\Lambda t^2\Big] \\
\mathrm{Im}[D_{43}] \quad &= \quad \frac{1}{6(\Lambda+st)^4}\Big[3[D_0\Lambda^4+2C_0s(-4\Lambda^3-6st\Lambda^2-4s^2t^2\Lambda-s^3t^3)] \\
&+ \quad \frac{B_0 s}{\Lambda t}(\Lambda+st)(11\Lambda^3+59st\Lambda^2+64s^2t^2\Lambda+22s^3t^3)\Big] \\
\mathrm{Im}[D_{44}] \quad &= \quad \frac{D_0}{2\Lambda(\Lambda+st)^4 s^2}\Big[[m^8-4M^2m^6+(6M^4-4M^2s)m^4 \\
&- \quad 4(M^3-Ms)^2m^2+(M^2-s)^4]t^4 \\
&+ \quad \Lambda[3m^6-13M^2m^4+(17M^4-14M^2s)m^2-(7M^2-4s)(m^2-s^2)]t^3 \\
&+ \quad \Lambda^2(3m^4-16M^2m^2+15M^2+6s^2-20M^2s)t^2+\Lambda^3(m^2-10M^2+4s)t+\Lambda^4\Big]
\end{aligned}
$$

$$
\begin{aligned}
&+ \quad \frac{C_0}{2\Lambda(\Lambda+st)^4 s^2} \\
&\Big[\quad 2[(m^2-M^2)^4 - 4M^2 s^3 + 2M^2(3M^2-2m^2)s^2 - 4(M^3 - m^2 M^2)s] \\
&+ \quad 2\Lambda[-15s^2M^2 + 2(9M^2-7m^2)sM^2 + (3m^2-7M^2)(m^2-M^2)^2]t^2 \\
&+ \quad \Lambda^2(6m^4 - 32M^2m^2 + 30M^4 - 40M^2 s)t + 2\Lambda^3(m^2-10M^2)\Big] \\
&+ \quad \frac{B_0}{6\Lambda(\Lambda+st)^4 s^2}(\Lambda+st)\Big[\Lambda^2[2(m^2-M^2)^4 + 3(m^2-5M^2)s(m^2-M^2)^2 \\
&- \quad (11m^2-47M^2)s^3 + 6(m^4 - 9M^2m^2 + 10M^4)s^2] \\
&+ \quad s^2[11(m^2-M^2)^4 - 6(m^2+5M^2)s(m^2-M^2)^2 \\
&- \quad 2(2m^2-13M^2)s^3 - 3(m^4-5M^4)s^2]t^2 \\
&+ \quad \Lambda s[7(m^2-M^2)^4 + 3(5m^2-21M^2)s(m^2-M^2)^2 \\
&- \quad (7m^2-67M^2)s^3 - 3(5m^4 + 6M^2m^2 - 19M^4)s^2]t\Big] \\
\mathrm{Im}[D_{45}] \quad &= \quad \frac{D_0}{2\Lambda(\Lambda+st)^4 s}[\Lambda^4 + 3\Lambda^3(m^2-2M^2)t \\
&+ \quad \Lambda^2(3m^4 - 8M^2m^2 + 5M^4 - 4M^2 s)t^2 + (m^2-M^2)^5 \\
&- \quad 2(m^2+2M^2)s(m^2-M^2)^3 - M^2 s^4 + 4M^4 s^3 + (m^6 + 5M^4m^2 - 6M^6)s^2] \\
&+ \quad \frac{C_0}{2\Lambda(\Lambda+st)^4 s}\Big[2\Lambda^3(3m^2 - 6M^2 - 4s) \\
&+ \quad 2\Lambda^2(3m^4 - 8M^2m^2 + 5M^4 - 6s^2 - 4M^2 s)t \\
&+ \quad 2\Lambda[(m^2-M^2)^3 - 4s^3 - M^2 s^2 + 2M^2(M^2-m^2)s]t^2 - 2s^4 t^3\Big] \\
&+ \quad \frac{B_0}{6\Lambda(\Lambda+st)^4 s^2}(\Lambda+st)\Big[\Lambda^2[(m^2-M^2)^3 + 26s^3 \\
&- \quad 3(11m^2-19M^2)s^2 + 6(m^4 - 3M^2m^2 + 2M^4)s] \\
&+ \quad s^2[2(M^2-m^2)^3 + 11s^3 - 6(m^2-3M^2)s^2 - 3(m^4 - 4M^2m^2 + 3M^4)s]t^2 \\
&+ \quad \Lambda s[5(m^2-M^2)^3 - 15s(m^2-M^2)^2 + 31s^3 - 3(7m^2-19M^2)s^2]t\Big] \\
\mathrm{Im}[D_{46}] \quad &= \quad \frac{D_0}{2(\Lambda+st)^4 \Lambda s^2 t}\Big[[m^8 - 4M^2m^6 + (6M^4 - 4M^2 s)m^4 \\
&- \quad 4(M^3 - Ms)^2 m^2 + (M^2-s)^4]t^4 \\
&+ \quad \Lambda[m^6 - 7M^2m^4 + (11M^4 - 10M^2 s)m^2 - (5M^2-4s)(M^2-s)^2]t^3 \\
&+ \quad 2\Lambda^2(4M^4 - 3m^2M^2 - 7sM^2 + 3s^2)t^2 - \Lambda^3(5M^2-4s)t + \Lambda^4\Big] \\
&+ \quad \frac{C_0}{(\Lambda+st)^4 \Lambda s^2 t^4}
\end{aligned}
$$

$$
\begin{aligned}
& \Big[\quad [(m^2-M^2)^4 - 4M^2 s^3 + 2M^2(3M^2-2m^2)s^2 - 4(M^3 - m^2M^2)s]t^3 \\
& + \quad \Lambda[-13s^2M^2 + 2(7M^2-5m^2)sM^2 + (m^2-5M^2)(m^2-M^2)^2]t^2 \\
& - \quad 2\Lambda^2 M^2(3m^2 - 4M^2 + 7s) - 5\Lambda^3 M^2 \Big] \\
& + \quad \frac{B_0}{6\Lambda(\Lambda+st)^3 s^2 t}\Big[9s^3\Lambda^3 + [2(m^2-M^2)^4 + (m^2-13M^2)s(m^2-M^2)^2 \\
& + \quad 27s^4 + 6M^2 s^3 + 6M^2(7M^2-5m^2)s^2]t\Lambda^2 \\
& + \quad s^2[11(m^2-M^2)^4 - 2(m^2+17M^2)s(m^2-M^2)^2 + 9s^4 + 6M^2 s^3 \\
& + \quad 6M^2(5M^2-3m^2)s^2]t^3 + \Lambda s[7(m^2-M^2)^4 \\
& + \quad (5m^2-53M^2)s(m^2-M^2)^2 + 27s^4 + 12M^2 s^3 + 24M^2(3M^2-2m^2)s^2]t^2\Big] \\
\mathrm{Im}[D_{47}] \quad = \quad & \frac{D_0\Lambda}{2\Lambda(\Lambda+st)^4 st}\Big[\Lambda^2 + [m^4 - 2M^2m^2 + (M^2-s)^2]t^2 \\
& - \quad 2\Lambda t(M^2-s)\Big[m^4 + [t-2(M^2+s)]m^2 + (M^2-s)(M^2-s-t)\Big]\Big] \\
& + \quad \frac{C_0}{\Lambda(\Lambda+st)^4 st} \\
& \Big[\quad \Lambda[(m^2-M^2)^3 - 3s^3 + (m^2-3M^2)s^2 + (m^4 - 4M^2m^2 + 3M^4)s]t^2 \\
& + \quad \Lambda^2[m^4 + (2s-4M^2)m^2 + 3(M^4 - 2sM^2 - s^2)]t + (m^2 - 3M^2 - s)\Lambda^3 - t^3 s^4\Big] \\
& + \quad \frac{B_0}{6\Lambda(\Lambda+st)^4 st}(\Lambda+st)\Big[11s^2\Lambda^3 \\
& + \quad [(m^2-M^2)^3 + 33s^3 - 6(m^2-3M^2)s^2 - 3(m^4 - 4M^2m^2 + 3M^2)^2 s]t\Lambda^2 \\
& + \quad \Lambda s[5(m^2-M^2)^3 + 33s^3 - 12(m^2-3M^2)s^2]t^2 \\
& + \quad s^2[2(M^2-m^2)^3 + 11s^3 - 6(m^2-3M^2)s^2 - 3(m^4 - 4M^2m^2 + 3M^4)s]t^3\Big] \\
\mathrm{Im}[D_{48}] \quad = \quad & \frac{D_0}{6(\Lambda+st)^4\Lambda t}3t\Lambda^4\Big[m^4 + [t-2(M^2+s)]m^2 + (M^2-s)^2 - M^2 t\Big] \\
& + \quad \frac{C_0}{6(\Lambda+st)^4}6[-t^3s^4 - 4\Lambda t^2 s^3 - 6\Lambda^2 t s^2 + (m^2 - M^2 - 4s)\Lambda^3] \\
& + \quad \frac{B_0 s}{6(\Lambda+st)^4\Lambda t}[9\Lambda^4 + (-11m^2 + 11M^2 + 62s)t\Lambda^3 \\
& + \quad 3s(-6m^2 + 6M^2 + 37s)t^2\Lambda^2 + 2s^3(-m^2 + M^2 + 10s)t^4 \\
& - \quad 3(3m^2 - 3M^2 - 26s)\Lambda s^2 t^3] \\
\mathrm{Im}[D_{49}] \quad = \quad & \frac{1}{12\Lambda(\Lambda+st)^4}\Big[6D_0\Lambda^4\Big[m^4 + [t-2(M^2+s)]m^2 + (M^2-s)(M^2-s-t)\Big]
\end{aligned}
$$

$$
\begin{aligned}
&+ \quad \frac{1}{t}\Big[C_0[12(m^2-M^2-3s)t\Lambda^4-72s^2t^2\Lambda^3-48s^3t^3\Lambda^2-12s^4t^4\Lambda] \\
&+ \quad B_0 s[22\Lambda^4+(-11m^2+11M^2+59s)t\Lambda^3-6s(6m^2-6M^2-35s)t^2\Lambda^2 \\
&- \quad 2s^2(9m^2-9M^2-77s)t^3\Lambda-4s^3(m^2-M^2-10s)\Big]\Big] \\
\mathrm{Im}[D_{410}] &= \quad \frac{D_0}{6(\Lambda+st)^4} \\
&\Big[\quad 3[m^8-4M^2m^6+(6M^4-4M^2s)m^4-4(M^3-Ms)^2m^2+(M^2-s)^4]t^4 \\
&+ \quad 6\Lambda[m^6-5M^2m^4+(7M^4-6M^2s)m^2-(3M^2-2s)(M^2-s)]t^3 \\
&+ \quad \Lambda^2(3m^4-30M^2m^2+33M^4+18s^2-50M^2s)-4(5M^2-3s)\Lambda^3t+3\Lambda^4\Big] \\
&+ \quad \frac{C_0}{6(\Lambda+st)^4} \\
&\Big[\quad 6[(m^2-M^2)^4-4M^2s^3+2M^2(3M^2-2m^2)s^2-4(M^3-m^2M)^2s]t^3 \\
&+ \quad 12\Lambda[-7s^2M^2+2(4M^2-3m^2)sM^2+(m^2-3M^2)(m^2-M^2)]t^2 \\
&+ \quad 2\Lambda^2(3m^4-30M^2m^2+33M^4-50M^2s)t-40M^2\Lambda^3\Big] \\
&+ \quad \frac{B_0}{6(\Lambda+st)^3\Lambda s^2t}\Big[6s^3\Lambda^3+2[(m^2-M^2)^4+(m^2-7M^2)s(m^2-M^2)^2 \\
&+ \quad 9s^4+9M^2s^3+(m^4-20M^2m^2+25M^4)s^2]t\Lambda^2+s^2[11(m^2-M^2)^4 \\
&- \quad 4(m^2+8M^2)s(m^2-M^2)^2+6s^4+14M^2s^3-(m^4+10M^2m^2-23M^4)s^2]t^3 \\
&+ \quad \Lambda s[7(m^2-M^2)^4+2(5m^2-29M^2)s(m^2-M^2)^2+18s^4+32M^2s^3 \\
&- \quad (5m^4+38M^2m^2-67M^4)s^2]t^2\Big] \\
\mathrm{Im}[D_{411}] &= \quad \frac{D_0}{6(\Lambda+st)^4}\Big[[3(m^2-M^2)^2-2M^2s]\Lambda^2+3\Lambda^4+2(3m^2-4M^2)t\Lambda^3\Big] \\
&+ \quad \frac{C_0}{6(\Lambda+st)^4}\Big[6t^3s^4-24s^3t^2\Lambda+4(3m^2-4M^2-6s)\Lambda^3 \\
&+ \quad 2[-2sM^2+3(m^2-M^2)^2-18s^2]t\Lambda^2\Big] \\
&+ \quad \frac{B_0}{6(\Lambda+st)^3\Lambda t}\Big[6s\Lambda^3+2[m^4-(2M^2+11s)m^2+M^4+22s^2+14M^2s]t\Lambda^2 \\
&- \quad s^2[4sm^2+(m^2-M^2)^2-17s^2-6M^2s]t^3 \\
&- \quad \Lambda s[5(m^2-M^2)^2-49s^2+2(7m^2-11M^2)s]t^2\Big] \\
\mathrm{Im}[D_{412}] &= \quad \frac{D_0}{12(\Lambda+st)^4}\Big[3\Lambda^4+2[3m^4+(4s-6M^2)m^2+3(M^2-s)^2]\Lambda^2
\end{aligned}
$$

$$
\begin{aligned}
&+ \quad 2\Lambda^3(2m^2-3M^2+3s)t\Big] \\
&+ \quad \frac{C_0}{6(\Lambda+st)^4}\Big[-12t^3s^4-48\Lambda s^3t^2+4[2m^2-3(M^2+s)]\Lambda^3 \\
&+ \quad 2\Lambda^2[4sm^2+3(m^2-M^2)^2-15s^2-6M^2s]t\Big] \\
&+ \quad \frac{B_0}{6(\Lambda+st)^3\Lambda t}2\Big[11s\Lambda^3 \\
&+ \quad [2m^4-4(M^2+3s)m^2+2M^4+39s^2+18M^2s]t\Lambda^2 \\
&- \quad s^2[4sm^2+(m^2-M^2)^2-17s^2-6M^2s]t^3 \\
&- \quad \Lambda s[5(m^2-M^2)^2-45s^2+8(2m^2-3M^2)s]t^2\Big] \\
\mathrm{Im}[D_{413}] &= \quad \frac{D_0}{6(\Lambda+st)^4}\Big[3\Lambda^4+2(3m^2-7M^2+3s)t\Lambda^3 \\
&+ \quad \Lambda^2[7m^4+4(s-5M^2)m^2+13M^4+4s^2-16M^2s]t^2 \\
&+ \quad \Lambda[3(m^2-M^2)^3+s^3+(m^2-5M^2)s^2+(m^4-8M^2m^2+7M^4)s]\Big] \\
&+ \quad \frac{C_0}{6(\Lambda+st)^4}\Big[4(3m^2-7M^2-3s)\Lambda^3 \\
&+ \quad 2[7m^4+4(s-5M^2)m^2+13M^4-14s^2-16M^2s]t\Lambda^2 \\
&+ \quad 2[3(m^2-M^2)^3-11s^3+(m^2-5M^2)s^2 \\
&+ \quad (m^4-8M^2m^2+7M^4)s]t^2\Lambda-6s^4t^3\Big] \\
&+ \quad \frac{B_0}{6(\Lambda+st)^3\Lambda st}\Big[6s^2\Lambda^3 \\
&+ \quad [(m^2-M^2)^3+25s^3-(19m^2-39M^2)s^2+(5m^4-16M^2m^2+11M^4)s]t\Lambda^2 \\
&+ \quad s^2[-2(m^2-M^2)^3+11s^3-6(m^2-3M^2)s^2-3(m^4-4M^2m^2+3M^4)s]t^3 \\
&+ \quad \Lambda s[5(m^2-M^2)^3-10s(m^2-M^2)^2+30s^3-(19m^2-51M^2)s^2]t^2\Big] \\
\mathrm{Im}[D_{414}] &= \quad \frac{D_0}{6(\Lambda+st)^4}\Big[3\Lambda^4+(4m^2-11M^2+8s)t\Lambda^3 \\
&+ \quad \Lambda^2[5m^4-16M^2m^2+11M^4+7s^2+6(m^2-3M^2)s]t^2 \\
&+ \quad \Lambda[3(m^2-M^2)^3+2s^3+(2m^2-7M^2)s^2+2(m^4-5M^2m^2+4M^4)s]t^3\Big] \\
&+ \quad \frac{C_0}{6(\Lambda+st)^4}\Big[2(4m^2-11M^2-4s)\Lambda^3 \\
&+ \quad 2[5m^4+(6s-16M^2)m^2+11M^4-11s^2-18M^2s]t\Lambda^2 \\
&+ \quad 2[3(m^2-M^2)^3-10s^3+(2m^2-7M^2)s^2
\end{aligned}
$$

$$
\begin{aligned}
&+ \quad 2(m^4 - 5M^2m^2 + 4M^4)s]t^2\Lambda - 6s^4t^3\Big] \\
&+ \quad \frac{B_0}{6(\Lambda+st)^3\Lambda st}\Big[9s^2\Lambda^3 \\
&+ \quad [(m^2-M^2)^3 + 29s^3 - 2(5m^2-13M^2)s^2 + 2(2m^4 - 7M^2m^2 + 5M^4)s]t\Lambda^2 \\
&+ \quad s^2[-2(m^2-M^2)^3 + 11s^3 - 6(m^2-3M^2)s^2 - 3(m^4 - 4M^2m^2 + 3M^4)s]t^3 \\
&+ \quad \Lambda s[5(m^2-M^2)^3 - 5s(m^2-M^2)^2 + 31s^3 - 4(4m^2-11M^2)s^2]t^2\Big] \\
\mathrm{Im}[D_{415}] \quad &= \quad \frac{D_0}{6(\Lambda+st)^4} \\
&[\quad 3(m^2-M^2)^2 + s^2 + 2(m^2-2M^2)s\Lambda^2 + 3\Lambda^4 + (5m^2 - 7M^2 + 4s)t\Lambda^3] \\
&+ \quad \frac{C_0}{6(\Lambda+st)^4}\Big[-6t^3s^4 - 24s^3t^2\Lambda + 2(5m^2 - 7M^2 - 8s)\Lambda^3 \\
&+ \quad [6(m^2-M^2)^2 - 34s^2 + 4(m^2-2M^2)s]t\Lambda^2\Big] \\
&+ \quad \frac{B_0}{6(\Lambda+st)^3\Lambda t}\Big[9s\Lambda^3 + [-17sm^2 + 2(m^2-M^2)^2 + 39s^2 + 23M^2s]t\Lambda^2 \\
&- \quad s^2[4sm^2 + (m^2-M^2)^2 - 17s^2 - 6M^2s]t^3 \\
&- \quad \Lambda s[5(m^2-M^2)^2 - 47s^2 + (15m^2 - 23M^2)s]t^2\Big] \\
\mathrm{Im}[D_{416}] \quad &= \quad \frac{1}{12s(\Lambda+st)^3}\Big[(D_0t + 2C_0)s\Lambda\Big[3\Lambda^2 + \Lambda(3m^2 - 4M^2 + 3s)t \\
&+ \quad [m^4 + (s-2M^2)m^2 + (M^2-s)^2]t^2\Big] \\
&+ \quad B_0(\Lambda+st)\Big[m^8 + (2s-4M^2)m^6 + 3[2M^4 - 4sM^2 + s(t-4s)]m^4 \\
&+ \quad [-4M^6 + 18sM^4 + 6s(2s-t)M^2 + 14s^3]m^2 + (M^2-s)^2(M^4 - 6sM^2 - 5s^2) \\
&+ \quad s(3M^4 - 2sM^2 - 3s^2)t\Big]\Big] \\
\mathrm{Im}[D_{417}] \quad &= \quad \frac{1}{12s(\Lambda+st)^3}\Big[(D_0t + 2C_0)s\Lambda\Big[\Lambda^2 + \Lambda(m^2 - 2M^2 + 2s)t \\
&+ \quad [m^4 + (s-2M^2)m^2 + (M^2-s)^2]t^2\Big] \\
&+ \quad B_0(\Lambda+st)\Big[m^8 - 4M^2m^6 + 3[2M^4 - 2sM^2 + s(t-s)]m^4 \\
&+ \quad 2[-2M^6 + 6sM^4 + s(s-3t)M^2 + s^2(s+t)]m^2 \\
&+ \quad M^2[M^6 - 6sM^4 + 3s(3s+t)M^2 - 4s^2(s+t)]\Big]\Big] \\
\mathrm{Im}[D_{418}] \quad &= \quad \frac{1}{12(\Lambda+st)^3}\Big[(D_0t + 2C_0)\Lambda^3 - B_0s(\Lambda+st)(3\Lambda+st)\Big]
\end{aligned}
$$

$$
\begin{aligned}
\mathrm{Im}[D_{419}] &= \frac{1}{24s(\Lambda+st)^3}\Bigg[(D_0t+2C_0)s\Lambda\Big[3\Lambda^2+\Lambda(4m^2-6M^2+5s)t \\
&+ 2[m^4+(s-2M^2)m^2+(M^2-s)^2]t^2\Big] \\
&+ 2B_0(\Lambda+st)\Big[m^8+(s-4M^2)m^6+3[2M^4-3sM^2+s(t-2s)]m^4 \\
&+ [-4M^6+15sM^4+2s(2s-3t)M^2+s^2(5s+t)]m^2+M^8-7M^6s \\
&- 3M^2s^2(s+t)-s^3(s+t)+M^4s(10s+3t)\Big]\Bigg] \\
\mathrm{Im}[D_{420}] &= \frac{1}{24(\Lambda+st)^3}\Big[(D_0t+2C_0)[3\Lambda+(2m^2-2M^2+s)t]\Lambda^2 \\
&+ 2B_0[-(m^2-M^2+2s)t^2s^2-6\Lambda ts^2+(m^2-M^2-4s)\Lambda^2]\Big] \\
\mathrm{Im}[D_{421}] &= \frac{1}{12(\Lambda+st)^3}\Bigg[(D_0t+2C_0) \\
&\Big[\ m^4+[t-2(M^2+s)]m^2+(M^2-s)(M^2-s-t)\Big]\Lambda^2 \\
&+ 2B_0[-(m^2-M^2+2s)t^2s^2-4\Lambda ts^2+(m^2-M^2-2s)\Lambda^2]\Bigg] \\
\mathrm{Im}[D_{422}] &= \frac{\Lambda}{96(\Lambda+st)^2}\Bigg[(D_0t+2C_0)\Big[-2m^6+[4(M^2+s)+t]m^4 \\
&- 2[(M^2-s)^2+(M^2+2s)t]m^2+(M^2-s)^2t\Big] \\
&+ 2B_0(\Lambda+st)\Bigg] \qquad (2.52)
\end{aligned}
$$

Chapter 3

Parity-Violating Electron-Deuteron Scattering

3.1 Introduction

An introduction to the parity-violating electron-deuteron scattering was presented in Section 1.3. This work was published in Physical Review C63, 2001, 044007 (nucl-th/0011034). This work also includes a numerical computation that was performed using software developed by Rocco Schiavilla at Thomas Jefferson National Accelerator Facility (TJNAF). The Thomas Jefferson National Accelerator Facility also provided computing time on their computing facility.

This chapter is organized as follows: a summary of the relevant formulas for the calculation of the asymmetry is given in Section 3.2. The computation of the current operators in EFT can be found in Section 3.3. Sections 3.4.1 and 3.4.2 contain a description of the inclusion of the one- and two-body currents into the phenomenological model. The numerical computation of the asymmetry is described in Section 3.5. Results and conclusions are presented in Section 3.6.

3.2 The Parity-Violating Asymmetry

Parity-violating electron-nucleus scattering results from the interference of amplitudes associated with photon and Z^0 exchanges as shown in Fig. 3.1. The initial

and final electron (nucleus) four-momenta are labeled by k^μ and k'^μ (P^μ and P'^μ), respectively, while the four-momentum transfer Q^μ is defined as $Q^\mu \equiv k^\mu - k'^\mu \equiv (\omega, \mathbf{q})$. The amplitudes for the processes in Fig. 3.1 are then given by [51]:

$$M = -\frac{4\pi\alpha}{Q^2}(M^\gamma + M^Z) \tag{3.1}$$

$$M^\gamma = \overline{u}'\gamma^\sigma u\, j^\gamma_{\sigma,fi} \tag{3.2}$$

$$M^Z = \frac{1}{4\pi\sqrt{2}}\frac{G_\mu Q^2}{\alpha}\overline{u}'\gamma^\sigma(g_V^{(e)} + g_A^{(e)}\gamma_5)u\, j^Z_{\sigma,fi} \tag{3.3}$$

where α and G_μ are the fine-structure constant and Fermi constant for muon decay, respectively, $g_V^{(e)} = -1 + 4\sin^2\theta_W$ and $g_A^{(e)} = 1$ are the Standard Model values for the neutral-current couplings to the electron given in terms of the Weinberg angle θ_W, u and u' are the initial and final electron spinors, and $j^{\gamma,\sigma}_{fi}$ and $j^{Z,\sigma}_{fi}$ denote nuclear matrix elements of the electromagnetic and weak neutral currents, i.e.:

$$j^{\gamma,\sigma}_{fi} \equiv \langle f|j^{\gamma,\sigma}(0)|i\rangle \equiv (\rho^\gamma_{fi}(\mathbf{q}), \mathbf{j}^\gamma_{fi}(\mathbf{q})) \tag{3.4}$$

and similarly for $j^{Z,\sigma}_{fi}$. Here $|i\rangle$ and $|f\rangle$ are the initial and final nuclear states. Note that in the amplitude M^Z the Q^2 dependence of the Z^0 propagator has been ignored, since here we restricted ourselves to $|Q^2| \ll m_Z^2$.

The parity-violating asymmetry in the quasi-elastic regime is given by:

$$A = \left(\frac{d\sigma^+}{d\Omega d\omega} - \frac{d\sigma^-}{d\Omega d\omega}\right) \Bigg/ \left(\frac{d\sigma^+}{d\Omega d\omega} + \frac{d\sigma^-}{d\Omega d\omega}\right) \tag{3.5}$$

where $d\sigma^h/d\Omega d\omega$ is the inclusive cross section for scattering of an incident electron with helicity $h = \pm 1$. It is easily seen that, to leading order:

$$A \propto \frac{\Re\,(M^\gamma M^{Z*})}{\mid M^\gamma \mid^2} \tag{3.6}$$

Standard manipulations then lead to the following expression for the asymmetry in the extreme relativistic limit for the electron [51]:

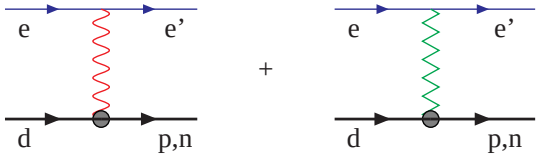

Figure 3.1: (a) Single photon-exchange and (b) Z-exchange diagrams in parity-violating quasi-elastic electron-deuteron scattering. The blobs denote the nuclear currents.

$$A = \frac{1}{2\sqrt{2}} \frac{G_\mu Q^2}{\alpha} \frac{g_A^{(e)} v_L R_L^{\gamma,0} + g_A^{(e)} v_T R_T^{\gamma,0} + g_V^{(e)} v'_T R_T^{\gamma,5}}{v_L R_L^{\gamma,\gamma} + v_T R_T^{\gamma,\gamma}} \tag{3.7}$$

where the v's are defined in terms of electron kinematical variables:

$$v_L = \frac{Q^4}{q^4} \tag{3.8}$$

$$v_T = \tan^2(\theta/2) + \frac{|Q^2|}{2\,q^2} \tag{3.9}$$

$$v'_T = \tan(\theta/2)\sqrt{\tan^2(\theta/2) + \frac{|Q^2|}{q^2}} \tag{3.10}$$

θ being the electron scattering angle in the laboratory, while the R's are the nuclear electro-weak response functions, which depend on q and ω, to be defined below. To this end, it is first convenient to separate the weak current $j^{Z,\sigma}$ into its vector $j^{0,\sigma}$ and axial-vector $j^{5,\sigma}$ components, and to write correspondingly:

$$j_{fi}^{Z,\sigma} = j_{fi}^{0,\sigma} + j_{fi}^{5,\sigma} \equiv (\rho_{fi}^0(\mathbf{q}), \mathbf{j}_{fi}^0(\mathbf{q})) + (\rho_{fi}^5(\mathbf{q}), \mathbf{j}_{fi}^5(\mathbf{q})) \tag{3.11}$$

The response functions can then be expressed as:

$$R_L^{\gamma,\mathrm{a}}(q,\omega) = \overline{\sum_i} \sum_f \delta(\omega + m_i - E_f)\, \Re\left[\rho^{\gamma}_{fi}(\mathbf{q})\rho^{\mathrm{a}*}_{fi}(\mathbf{q})\right] \tag{3.12}$$

$$R_T^{\gamma,\mathrm{a}}(q,\omega) = \overline{\sum_i} \sum_f \delta(\omega + m_i - E_f)\, \Re\left[j^{\gamma}_{x,fi}(\mathbf{q})j^{\mathrm{a}*}_{x,fi}(\mathbf{q}) + j^{\gamma}_{y,fi}(\mathbf{q})j^{\mathrm{a}*}_{y,fi}(\mathbf{q})\right] \tag{3.13}$$

$$R_T^{\gamma,5}(q,\omega) = \overline{\sum_i} \sum_f \delta(\omega + m_i - E_f)\, \Im\left[j^{\gamma}_{x,fi}(\mathbf{q})j^{5*}_{y,fi}(\mathbf{q}) - j^{\gamma}_{y,fi}(\mathbf{q})j^{5*}_{x,fi}(\mathbf{q})\right] \tag{3.14}$$

where m_i is the mass of the target (assumed at rest in the laboratory), E_f is the energy of the final nuclear state (in general, a scattering state), and in Eqs. (3.12) and (3.13) the superscript a is either γ or 0. Note that there is a sum over the final states and an average over the initial spin projection states of the target, as implied by the notation $\overline{\sum}_i$. In the expressions above for the R's, it has been assumed that the three-momentum transfer $\mathbf{q}$ is along the z-axis, which defines the spin quantization axis for the nuclear states.

3.3 Operators in Effective Field Theory

The purpose of this section is to obtain from EFT the one and two-body operators required in the computation. We consider only up and down quarks, in which case the QCD Lagrangian has an approximate $SU(2)_L \times SU(2)_R$ chiral symmetry. This symmetry is spontaneously broken by the vacuum to the diagonal $SU(2)_V$ subgroup, and three pseudoscalar Goldstone bosons, the pions π_a, appear in the spectrum. Chiral symmetry provides important constraints on the description of low-momentum processes involving pions. In particular, it allows one to estimate the relative size of various contributions.

To accomplish this, the most general effective Lagrangian with broken $SU(2)_L \times SU(2)_R$ is constructed. This effective Lagrangian includes terms with an arbitrary number of derivatives and powers of the quark masses; however, higher-dimension operators are suppressed by inverse powers of the characteristic mass scale of QCD, $M_\chi = 4\pi f_\pi \sim 1$ GeV. Thus, pion interactions are determined as a power series in

$(q, m_\pi)/M_\chi$, where q is the typical external three-momentum. At low energies this is a small number and hence only the lowest-order terms are considered here. The diagrams that need to be included at the next order in the expansion are shown but they are not evaluated.

We start with the $\pi\pi$ and πN Lagrangians. Details can be found, for example, in Refs. [3, 31]. As described in the introduction, the pions are described by the field $U = u^2 = 1 + \mathrm{i}\boldsymbol{\tau}\cdot\boldsymbol{\pi}/f_\pi - \boldsymbol{\pi}^2/2f_\pi^2 + ...$, where $f_\pi = 93$ MeV is the pion decay constant. We denote the nucleon field of velocity v_μ and spin S_μ by N. In order to obtain the currents required for the computation of the asymmetry we must use the proper covariant derivatives. The covariant derivatives on the pion and nucleon field are constructed in terms of external vector and axial-vector fields $\mathcal{V}_\mu$ and $\mathcal{A}_\mu$ in the usual manner. They are given by:

$$D_\mu U = \partial_\mu U - \mathrm{i}(\mathcal{V}_\mu + \mathcal{A}_\mu)U + \mathrm{i}\,U(\mathcal{V}_\mu - \mathcal{A}_\mu) \tag{3.15}$$

$$D_\mu N = \partial_\mu N + \frac{1}{2}[u^\dagger, \partial_\mu u]N - \frac{\mathrm{i}}{2}\left[u^\dagger(\mathcal{V}_\mu^{(3)} + \mathcal{A}_\mu^{(3)})u + u(\mathcal{V}_\mu^{(3)} - \mathcal{A}_\mu^{(3)})u^\dagger\right]N - 3\mathrm{i}\,\mathcal{V}_\mu^{(0)}N \tag{3.16}$$

where the superscripts (0) and (3) denote isoscalar and isovector components. It is convenient to construct also other quantities that transform covariantly. For example:

$$a_\mu = \mathrm{i}[u^\dagger, D_\mu u]_+, \tag{3.17}$$

$$f_{\mu\nu}^\dagger = u^\dagger F_{\mu\nu}^R u + u F_{\mu\nu}^L u^\dagger \tag{3.18}$$

where $F_{\mu\nu}^{R,L} = \partial_\mu F_\nu^{R,L} - \partial_\nu F_\mu^{R,L} - \mathrm{i}[F_\nu^{R,L}, F_\mu^{R,L}]$ with $F_\mu^R = \mathcal{V}_\mu + \mathcal{A}_\mu$ and $F_\mu^L = \mathcal{V}_\mu - \mathcal{A}_\mu$.

One can find the relation between the external fields and Z^0 or photon by considering the covariant derivative on the quark fields (see, e.g., Ref. [52]):

$$\mathcal{A}_\mu = \frac{g}{2\cos\theta_W}\frac{\tau_z}{2}Z_\mu \tag{3.19}$$

$$\mathcal{V}_\mu = \frac{g}{2\cos\theta_W}(\frac{\tau_z}{2} - 2\sin^2\theta_W Q_q)Z_\mu + eQ_qA_\mu \tag{3.20}$$

where Q_q is the quark-charge matrix.

From these building blocks we can write the chiral Lagrangians:

$$\mathcal{L}_{\pi\pi} = \frac{f_\pi^2}{4}\mathrm{Tr}[D_\mu U^\dagger D^\mu U] + \ldots \tag{3.21}$$

$$\begin{aligned}\mathcal{L}_{\pi N} &= N^\dagger[\mathrm{i}\, v\cdot D + g_A S\cdot a]N + \frac{1}{2m}N^\dagger\Big[(v\cdot D)^2 - D\cdot D - \mathrm{i}\, g_A[S\cdot D, v\cdot v]_+\Big]N \\ &- \frac{\mathrm{i}}{4m}N^\dagger[S^\mu, S^\nu]\Big[(1-\kappa_v)f^+_{\mu\nu} + \frac{1}{2}(\kappa_s-\kappa_v)\mathrm{Tr}(f^+_{\mu\nu})\Big]N + \ldots\end{aligned} \tag{3.22}$$

where $\kappa_s = -0.12$ and $\kappa_v = 3.71$, and $\ldots$ denote terms with more derivatives and/or powers of the pion mass. One can also write down interactions containing four or more nucleon fields [31, 53], which are important for a fully consistent description of systems involving two or more nucleons. One- and two-body currents can be obtained from these interactions.

3.3.1 Ordering of Terms

The symmetries allow an infinite number of interactions, so an ordering scheme is necessary for predictive power. We want to estimate the size of matrix elements of one- or two-body currents between NN wave functions. These matrix elements involve: the final NN wave function, a two-nucleon propagator, the current operator, another two-nucleon propagator, and the initial NN wave function. Let us now investigate the order of the current operators and the required diagrams.

Contributions to the amplitude M^γ start at $\mathcal{O}(e^2/q^2)$ with the tree-level one-body charge operator shown if Figure 3.2. First corrections come in tree-level one-body currents from $\mathcal{O}(q/\Lambda_\chi)$ magnetic corrections in the Lagrangian. These are shown in Figure 3.3. Second corrections are of two types: (i) one-loop corrections and $\mathcal{O}(q^2/\Lambda_\chi^2)$ interactions in one-body currents shown in Figure 3.4, and (ii) tree-level two-body currents of Figure 3.5. As such, we see that two-body currents

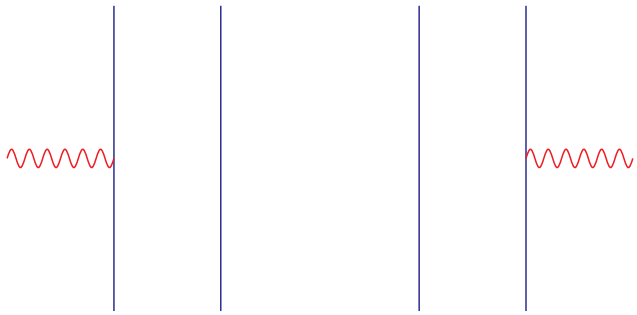

Figure 3.2: Electromagnetic charge one-body diagrams.

of interest in this work enter the calculation two orders below the leading order one-body currents.

Contributions to the amplitude M^Z follow the same pattern, but have an extra overall factor of $\mathcal{O}(q^2/M_Z^2) = \mathcal{O}(G_\mu q^2/e^2)$ due to the different coupling of the Z to the nucleon versus the photon.

Interesting also are the contributions to the asymmetry that come not from the exchange of a Z^0 between electron and deuteron, but from Z^0 exchange between hadrons (and photon exchange between electron and deuteron). Also, the contribution from PV interactions between the pion and the nucleon must be considered. Let us denote these contributions by $M^{\gamma(Z)}$. How does $M^{\gamma(Z)}$ compare to M^Z? The contributions from the pion nucleon PV interaction were discussed in [54] and a more recent computation of these contribution shows that they are small [36]. Direct Z exchange between nucleons (PV in the deuteron initial state) are not included in the computation. These have been recently calculated and shown to be small [37].

This calculation involves all other contributions suppressed by $\mathcal{O}(q^2/M_\chi^2)$ compared to the leading one-body term. The leading two-body currents in the am-

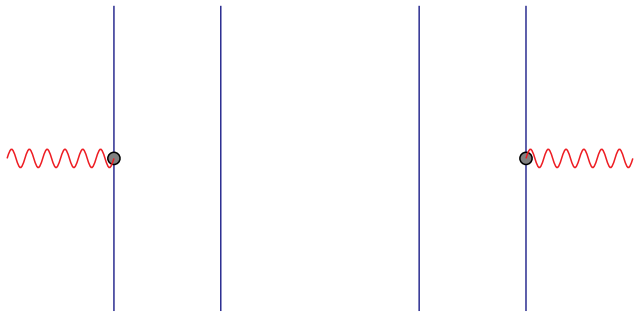

Figure 3.3: Electromagnetic one-body diagrams (magnetic corections) at $\mathcal{O}(q/M_\chi)$ relative to leading orger charge operators.

plitude M^Z stemming from pion exchange are being calculated here for the first time.

Figures 3.2 to 3.6 show the order by order contributions in the electromagnetic sector. The leading order term is the one-body charge operator shown in Figure 3.2. Figure 3.4 shows the first order correction (magnetic corrections) to the charge operator. Both these diagrams are included in the computation.

At the next order in the expansion, we have the one-body contributions from Figure. 3.4 which are not included and the leading order two-body diagrams of Figure 3.5 which are included. Finally, Figure 3.6 shows the first order corrections to the two-body contribution, however these are not included in the computation.

Figures 3.7 to 3.10 show the order by order contribution for the weak sector. They are exactly as the electromagnetic ones except for the overall factor of $\mathcal{O}(G_\mu q^2/e^2)$ as described above.

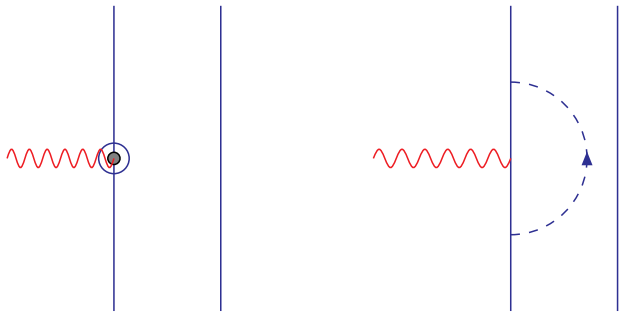

Figure 3.4: Electromagnetic one-body diagrams at $\mathcal{O}(q^2/M_\chi^2)$ relative to leading orger charge operators.

3.3.2 Connection with Phenomenological Model

The operators obtained from the EFT will be used in conjunction with a successful phenomenological Lagrangian. The reason for doing this is three-fold. First, the model and necessary software to perform the numerical computation already existed, and as such there was no need to generate an EFT description of the initial and final state. This in turn, allowed the results to be generated and communicated to the SAMPLE collaboration in a timely fashion. Second, the model allows for inclusion of higher-order terms as will be discussed in this section. Although this is not consistent with EFT, a sizable contribution from these terms would imply that the EFT was truncated too early in the expansion, and more terms need to be considered. Finally, the use of a phenomenological potential in conjunction with currents derived from EFT has already been proven to be successful [31].

As noted above, the phenomenological model used in this computation has the ability to include higher-order contribution through different techniques such as the Riska prescription [33] where the pion meson exchange currents are extended to account for heavier mesons. All these techniques, when translated into an

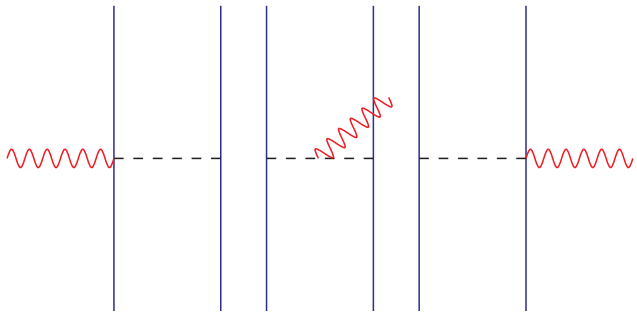

Figure 3.5: Electromagnetic two-body diagrams at $\mathcal{O}(eq^2/M_\chi^2)$ in EFT. Solid (dashed) lines denote nucleons (pions).

EFT language correspond to the inclusions of terms beyond the ones considered in the previous section. Furthermore, these techniques lack the systematic approach found in the EFT; that is to say they may include some of the terms at a given order in the expansion but not all. Nonetheless, their inclusion has been successful in past computations, and as such in this computation we will investigate their impact on the final result. As stated earlier, if they turn out to have a significant impact, the implication is that the EFT expansion was truncated too early. One would thus need to go back to the EFT expansion and rework the currents to include the next order terms. In this case, that would mean including the diagrams shown in Figure 3.6 and Figure 3.10.

After performing the computation, the results show that these higher-order contributions are negligible and, as such, there is no need to include the next order in the expansion.

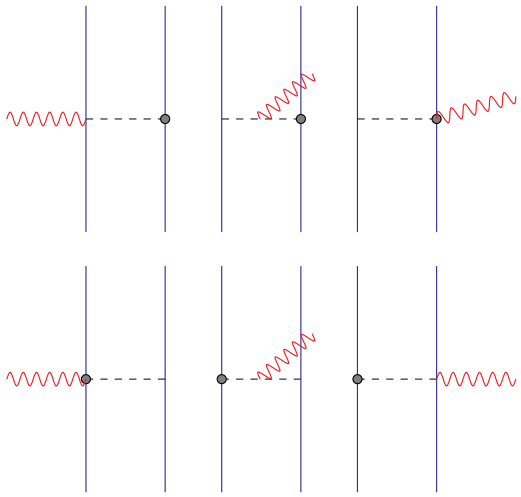

Figure 3.6: Electromagnetic two-body diagrams at $\mathcal{O}(eq^3/M_\chi^3)$ in EFT. Solid (dashed) lines denote nucleons (pions).

3.3.3 One- and Two-Body Currents

The one-body currents contributing to the processes in Fig. 3.1, depicted in Figs. 3.2, 3.3, 3.7 and 3.8, are given to $\mathcal{O}(eq/\Lambda_\chi)$ by:

$$\rho^{\rm a}(\mathbf{r}) = \frac{1}{2}\sum_i (g_E^S + g_E^V \tau_{z,i})\delta(\mathbf{r}-\mathbf{r}_i) \tag{3.23}$$

$$\mathbf{j}^{\rm a}(\mathbf{r}) = \frac{1}{4m}\sum_i \Big[(g_E^S + g_E^V \tau_{z,i})[\delta(\mathbf{r}-\mathbf{r}_i)\mathbf{p}_i + \mathbf{p}_i\delta(\mathbf{r}-\mathbf{r}_i)] + (g_M^S + g_M^V \tau_{z,i})\boldsymbol{\nabla}\delta(\mathbf{r}-\mathbf{r}_i)\times\boldsymbol{\sigma}_i\Big] \tag{3.24}$$

$$\rho^5(\mathbf{r}) = -\frac{1}{4m} g_A \sum_i [\boldsymbol{\sigma}_i\cdot\mathbf{p}_i\delta(\mathbf{r}-\mathbf{r}_i) + \delta(\mathbf{r}-\mathbf{r}_i)\boldsymbol{\sigma}_i\cdot\mathbf{p}_i]\tau_{z,i} \tag{3.25}$$

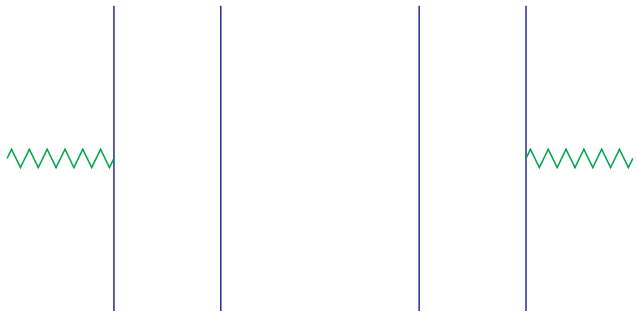

Figure 3.7: Leading order weak neutral one-body diagrams.

$$\mathbf{j}^5(\mathbf{r}) \quad = \quad -\frac{1}{2} g_A \sum_i \delta(\mathbf{r} - \mathbf{r}_i) \boldsymbol{\sigma}_i \tau_{z,i} \tag{3.26}$$

where a = γ or 0, the coupling constants $g_E^{(S,V)}$ and $g_M^{(S,V)}$ are given in Table 3.1, and g_A is the nucleon axial coupling constant. These results are in agreement with those presented in Ref. [27]. These coupling constants acquire, in higher orders, a Q^2 dependence, as described, for example, in Ref. [55]. In our calculation we use a phenomenological parametrization of the Q^2 dependence, as described in Secs. 3.4.1 and 3.4.2.

Form Factor	γ	Z
g_E^S	1	$-2\sin^2\theta_W$
g_E^V	1	$1-2\sin^2\theta_W$
g_M^S	$1+\kappa_s$	$-(1+\kappa_s)\sin^2\theta_W$
g_M^V	$1+\kappa_v$	$(1+\kappa_v)(1-2\sin^2\theta_W)$

Table 3.1: Coupling constants appearing in one-body currents to $\mathcal{O}(eq/\Lambda_\chi)$ in EFT.

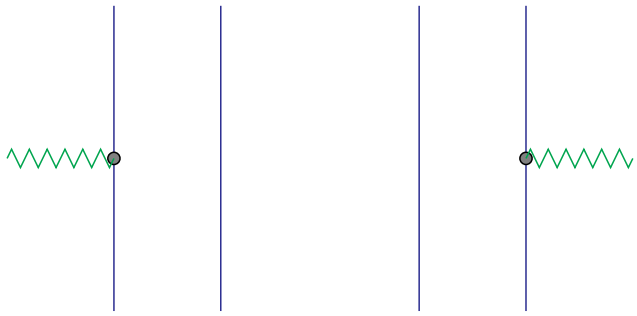

Figure 3.8: Next to leading order weak neutral one-body diagrams.

Note that $\mathcal{L}_{\pi\pi}$ contains a π-Z^0 mixing term in the form $Z \cdot \partial\pi^0$. The corresponding diagram is shown in Figure 3.11 which has a contribution proportional to Q_μ, the four-momentum transfer. Its contraction with the leptonic current produces a contribution proportional to the mass of the electron. In the extreme relativistic limit for the electron under consideration here, this contribution can be neglected.

The two-body contributions to the processes shown in Fig. 3.1 are depicted in Figs. 3.5 and 3.9, where again contributions from π-Z^0 mixing are neglected in the extreme relativistic limit. To $\mathcal{O}(eq^2/\Lambda_\chi^2)$, they are given in momentum space by:

$$\begin{aligned}\mathbf{j}^{\mathrm{a}}(\mathbf{k}_1,\mathbf{k}_2) &= 3\mathrm{i}\, g_E^V(\boldsymbol{\tau}_1\times\boldsymbol{\tau}_2)_z\Big[v_\pi(k_2)\boldsymbol{\sigma}_2\cdot\mathbf{k}_2\boldsymbol{\sigma}_1-v_\pi(k_1)\boldsymbol{\sigma}_1\cdot\mathbf{k}_1\boldsymbol{\sigma}_2 \\ &\quad -\frac{v_\pi(k_2)-v_\pi(k_1)}{{k_1}^2-{k_2}^2}(\mathbf{k}_1-\mathbf{k}_2)\boldsymbol{\sigma}_1\cdot\mathbf{k}_1\boldsymbol{\sigma}_2\cdot\mathbf{k}_2\Big] \quad (3.27)\end{aligned}$$

where $\mathbf{k}_i = \mathbf{p}_i' - \mathbf{p}_i$ with $\mathbf{p}_i$ ($\mathbf{p}_i'$) denoting the initial (final) momentum of nucleon

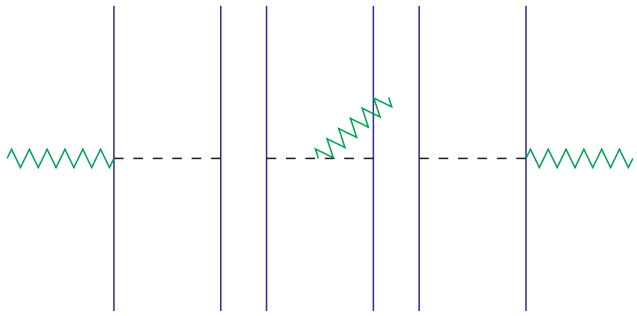

Figure 3.9: Weak neutral two-body diagrams at $\mathcal{O}(eq^2/M_\chi^2)$ in EFT.

i. In the formula above:

$$v_\pi(k) = -\frac{1}{3}\left(\frac{g_A}{4f_\pi}\right)^2 \frac{1}{{m_\pi}^2 + k^2} \tag{3.28}$$

Note that there is no contribution to the axial current operator or the electromagnetic charge operator up to the order considered here. There is a contribution to the axial charge operator which, however, does not enter in the asymmetry computation. These results are in agreement with Ref. [56], where the Fourier transform of the above expressions are also given in detail.

In higher order other currents appear. There exist shorter-range currents, which are expected to be smaller than the ones from pion exchange with leading-order interactions. These higher-order effects are parameterized in our calculation through the Riska prescription as outlined in Sections 3.4.1 and 3.4.2. In particular, we do not use Eq. (3.28) for $v_\pi(k)$, but the pseudoscalar component of the v_{18} potential.

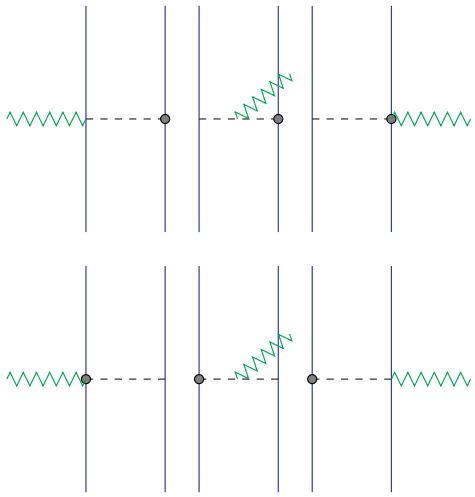

Figure 3.10: Weak neutral two-body diagrams at $\mathcal{O}(eq^3/M_\chi^3)$ in EFT.

3.4 Phenomenological Model

This section describes how the model incorporates the different currents.

3.4.1 Electromagnetic Operators

The nuclear charge and current operators consist of one- and two-body terms that operate on the nucleon degrees of freedom:

$$\rho^\gamma(\mathbf{q}) = \sum_i \rho_i^{\gamma,1}(\mathbf{q}) + \sum_{i<j} \rho_{ij}^{\gamma,2}(\mathbf{q}) \tag{3.29}$$

$$\mathbf{j}^\gamma(\mathbf{q}) = \sum_i \mathbf{j}_i^{\gamma,1}(\mathbf{q}) + \sum_{i<j} \mathbf{j}_{ij}^{\gamma,2}(\mathbf{q}) \tag{3.30}$$

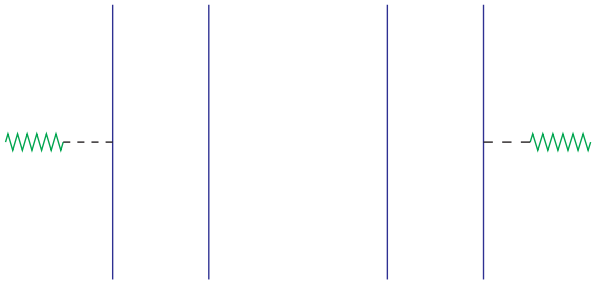

Figure 3.11: Contributions from pion-Z mixing.

The one-body operators $\rho_i^{\gamma,1}$ and $\mathbf{j}_i^{\gamma,1}$ have the standard expressions obtained from a relativistic reduction of the covariant single-nucleon current and are listed below for convenience. The charge operator is written as:

$$\rho_i^{\gamma,1}(\mathbf{q}) = \rho_{i,\mathrm{NR}}^{\gamma,1}(\mathbf{q}) + \rho_{i,\mathrm{RC}}^{\gamma,1}(\mathbf{q}) \tag{3.31}$$

with:

$$\rho_{i,\mathrm{NR}}^{\gamma,1}(\mathbf{q}) = \epsilon_i \, \mathrm{e}^{\mathrm{i}\mathbf{q}\cdot\mathbf{r}_i} \tag{3.32}$$

$$\rho_{i,\mathrm{RC}}^{\gamma,1}(\mathbf{q}) = \left(\frac{1}{\sqrt{1+|Q^2|/4m^2}} - 1 \right) \epsilon_i \mathrm{e}^{\mathrm{i}\mathbf{q}\cdot\mathbf{r}_i} - \frac{\mathrm{i}}{4m^2} \left(2\,\mu_i - \epsilon_i\right) \mathbf{q}\cdot(\boldsymbol{\sigma}_i \times \mathbf{p}_i) \mathrm{e}^{\mathrm{i}\mathbf{q}\cdot\mathbf{r}_i} \tag{3.33}$$

where $|Q^2| = q^2 - \omega^2 > 0$ is the four-momentum transfer defined earlier, and m is the nucleon mass. The current operator is expressed as:

$$\mathbf{j}_i^{\gamma,1}(\mathbf{q}) = \frac{1}{2m} \epsilon_i \left[\mathbf{p}_i \, , \, \mathrm{e}^{\mathrm{i}\mathbf{q}\cdot\mathbf{r}_i}\right]_+ - \frac{\mathrm{i}}{2m} \mu_i \, \mathbf{q} \times \boldsymbol{\sigma}_i \, \mathrm{e}^{\mathrm{i}\mathbf{q}\cdot\mathbf{r}_i} \tag{3.34}$$

where $[\cdots \, , \, \cdots]_+$ denotes the anticommutator. The following definitions have been introduced:

$$\epsilon_i \equiv \frac{1}{2}\left[G_E^S(|Q^2|) + G_E^V(|Q^2|)\tau_{z,i}\right] \tag{3.35}$$

$$\mu_i \equiv \frac{1}{2}\left[G_M^S(|Q^2|) + G_M^V(|Q^2|)\tau_{z,i}\right] \tag{3.36}$$

and $\mathbf{p}$, $\boldsymbol{\sigma}$, and $\boldsymbol{\tau}$ are the nucleon's momentum, Pauli spin, and isospin operators, respectively. The two terms proportional to $1/m^2$ in $\rho_{i,\mathrm{RC}}^{\gamma,1}$ are the well-known Darwin-Foldy and spin-orbit relativistic corrections [57], respectively. The dipole parameterization is used for the isoscalar (S) and isovector (V) combinations of the electric and magnetic nucleon form factors (including the Galster form for the electric neutron form factor [58]).

The most important features of the two-body parts of the electromagnetic current operator are summarized below. The reader is referred to Refs. [56, 59, 60] for a derivation and listing of their explicit expressions.

Two-body current operators

The two-body current operator has "model-independent" and "model-dependent" components, in the classification scheme of Riska [33]. The model-independent terms are obtained from the two-nucleon interaction (in the present study the Argonne v_{18} interaction [34] is employed) and by construction satisfy current conservation with it. The leading operator is the isovector "π-like" current obtained from the isospin-dependent spin-spin and tensor interactions. The latter also generate an isovector "ρ-like" current, while additional model-independent isoscalar and isovector currents arise from the isospin-independent and isospin-dependent central and momentum-dependent interactions. These currents are short-ranged and numerically far less important than the π-like current.

The model-dependent currents are purely transverse and, therefore, cannot be directly linked to the underlying two-nucleon interaction. The present calculation includes the isoscalar $\rho\pi\gamma$ and isovector $\omega\pi\gamma$ transition currents as well as the isovector current associated with excitation of intermediate Δ-isobar reso-

nances (for the values of the various coupling constants and cutoff masses in the monopole form factors at the meson-baryon vertices, see Ref. [61]). Among the model-dependent currents, those associated with the Δ-isobar are the most important ones. In the present calculation, these currents are treated within the static Δ approximation. While this is sufficiently accurate for our purposes here, it is important to realize that such an approach can lead to a gross overestimate of Δ contributions in electro-weak transitions (see Refs. [62, 63, 64] for a discussion of this issue within the context of neutron and proton radiative captures on deuteron and ^{3}He, and the proton weak capture on ^{3}He).

Finally, it is worth pointing out that the contributions associated with the $\rho\pi\gamma$, $\omega\pi\gamma$, and Δ-excitation mechanisms are, in the regime of low to moderate momentum-transfer values of interest here ($q \leq 2$ fm^{-1}), typically much smaller than those due to the leading model-independent π-like current [65] as expected from power counting.

Two-body charge operators

While the main parts of the two-body currents are linked to the form of the two-nucleon interaction through the continuity equation, the most important two-body charge operators are model-dependent and should be considered as relativistic corrections. Indeed, a consistent calculation of two-body charge effects in nuclei would require the inclusion of relativistic effects in both the interaction models and nuclear wave functions. There are nevertheless rather clear indications for the relevance of two-body charge operators from the failure of the impulse approximation in predicting the deuteron tensor polarization observable [66] and charge form factors of the three- and four-nucleon systems [65, 67]. The model commonly used [59] includes the π-, ρ-, and ω-meson exchange charge operators with both isoscalar and isovector components, as well as the (isoscalar) $\rho\pi\gamma$ and (isovector) $\omega\pi\gamma$ charge transition couplings, in addition to the single-nucleon Darwin-Foldy and spin-orbit relativistic corrections. The π- and ρ-meson exchange charge operators are constructed from the isospin-dependent spin-spin and tensor interactions

(those of the Argonne v_{18} here), using the same prescription adopted for the corresponding current operators.

It should be emphasized, however, that for $q \leq 2$ fm^{-1} the contributions due to these two-body charge operators are very small when compared to those from the one-body operator. This is because as shown previously they enter at $\mathcal{O}(p/M)^2$ relative to the leading term and for small p they become very small.

3.4.2 Weak Operators

In the Standard Model the vector part of the neutral weak current is related to the isoscalar (S) and isovector (V) components of the electromagnetic current, denoted respectively as $j_S^{\gamma,\sigma}$ and $j_V^{\gamma,\sigma}$, via:

$$j^{0,\sigma} = -2\sin^2\theta_W\, j_S^{\gamma,\sigma} + (1 - 2\sin^2\theta_W)\, j_V^{\gamma,\sigma} \tag{3.37}$$

and, therefore, the associated one- and two-body weak charge and current operators are easily obtained from those given in the preceding section.

The axial charge and current operators also have one- and two-body terms. Only the axial current:

$$\mathbf{j}^5(\mathbf{q}) = \sum_i \mathbf{j}_i^{5,1}(\mathbf{q}) + \sum_{i<j} \mathbf{j}_{ij}^{5,2}(\mathbf{q}) \tag{3.38}$$

enters in the calculation of the asymmetry. The axial charge operator is not needed in the present work. The one-body axial current is given, to lowest order in $1/m$, by:

$$\mathbf{j}_i^{5,1}(\mathbf{q}) = -G_A(|Q^2|)\frac{\tau_{z,i}}{2}\boldsymbol{\sigma}_i\, \mathrm{e}^{\mathrm{i}\mathbf{q}\cdot\mathbf{r}_i} \tag{3.39}$$

where the nucleon axial form factor is parametrized as:

$$G_A(|Q^2|) = \frac{g_A}{(1 + |Q^2|/\Lambda_A^2)^2} \tag{3.40}$$

Here g_A is the nucleon axial coupling constant, $g_A = 1.2654$, and the cutoff mass

Λ_A is taken to be 1 GeV/c^2, as obtained from an analysis of pion electroproduction data [68] and measurements of the reaction $\nu_\mu\, p \to \mu^+\, n$ [69].

There are relativistic corrections to $\mathbf{j}^{5,1}$ as well as two-body contributions arising from π-, ρ-, $\rho\pi$-exchange mechanisms and Δ excitation [64]. All these effects, however, are neglected in the present study. The reasons for doing so are twofold: firstly, axial current contributions to the asymmetry are small, since they are proportional to the electron neutral weak coupling $g_V^{(e)} \simeq -0.074$ (see Eq. (3.7)); secondly, axial contributions from two-body operators are expected to be at the $\simeq 1$ % level of those due to the one-body operator in Eq. (3.39). For example, in the proton weak capture on proton at KeV energies [70] (this process is induced by the charge-changing axial weak current) the π, ρ, $\rho\pi$, and Δ two-body operators increase the predicted one-body cross section by 1.5%. Such an estimate is expected to hold up also in the quasi-elastic regime being considered here.

3.5 Calculation

In this section we describe the calculation of the deuteron response functions given in Eqs. (3.12)–(3.14). The deuteron wave function is written as:

$$|d, M_d\rangle = \left[\frac{u(r)}{r}\mathcal{Y}^{M_d}_{011} + \frac{w(r)}{r}\mathcal{Y}^{M_d}_{211}\right]\chi^0_0 \tag{3.41}$$

where the $\mathcal{Y}^{M_J}_{LSJ}$ are standard spin-angle functions, $\chi^T_{M_T}$ is a two-nucleon T, M_T isospin state, and $u(r)$ and $w(r)$ are the S- and D-wave radial functions. In the ^{2}H$(\vec{e}, e')pn$ reaction the final state is in the continuum, and its wave function is written as:

$$|\mathbf{q}; \mathbf{p}, SM_S, TM_T\rangle = \mathrm{e}^{\mathrm{i}\mathbf{q}\cdot\mathbf{R}}\, \psi^{(-)}_{\mathbf{p},SM_S,TM_T}(\mathbf{r}) \tag{3.42}$$

where $\mathbf{r} = \mathbf{r}_1 - \mathbf{r}_2$ and $\mathbf{R} = (\mathbf{r}_1 + \mathbf{r}_2)/2$ are the relative and center-of-mass coordinates. The incoming-wave scattering-state wave function of the two nucleons having relative momentum $\mathbf{p}$ and spin-isospin states SM_S, TM_T is approximated

as [71]:

$$\psi^{(-)}_{\mathbf{p},SM_S,TM_T}(\mathbf{r}) \simeq \frac{1}{\sqrt{2}}\Big[e^{\mathrm{i}\mathbf{p}\cdot\mathbf{r}} - (-1)^{S+T}e^{-\mathrm{i}\mathbf{p}\cdot\mathbf{r}}\Big]\chi^S_{M_S}\chi^T_{M_T} + \frac{4\pi}{\sqrt{2}}\sum_{\substack{JM_J \\ J\le J_{\max}}}\sum_{LL'}\mathrm{i}^L\,\delta_{LST}$$
$$[Z^{JM_J}_{LSM_S}(\hat{\mathbf{p}})]^*\left[\frac{1}{r}u^{(-)}_{L'L}(r;p,JST) - \delta_{L'L}\;j_L(pr)\right]\mathcal{Y}^{M_J}_{L'SJ}\chi^T_{M_T} \tag{3.43}$$

where:

$$\delta_{LST} = 1-(-1)^{L+S+T} \tag{3.44}$$

$$Z^{JM_J}_{LSM_S}(\hat{\mathbf{p}}) = \sum_{M_L}\langle LM_L, SM_S|JM_J\rangle Y_{LM_L}(\hat{\mathbf{p}}) \tag{3.45}$$

The δ_{LST} factor ensures the antisymmetry of the wave function, while the Clebsch-Gordan coefficients restrict the sum over L and L'. The radial functions $u^{(-)}_{L'L}$ are obtained by solving the Schrödinger equation in the JST channel, and behave asymptotically as:

$$\frac{1}{r}u^{(-)}_{L'L}(r;p,JST) \underset{r\to\infty}{\sim} \frac{1}{2}\left[\delta_{L'L}h^{(1)}_L(pr) + (S^{JST}_{L'L})^*h^{(2)}_{L'}(pr)\right] \tag{3.46}$$

where $S^{JST}_{L'L}$ is the S-matrix in the JST channel, and the Hankel functions are defined as $h^{(1,2)}_L(x)=j_L(x)\pm\mathrm{i}\,n_L(x)$, j_l and n_L being the spherical Bessel and Neumann functions, respectively. In the absence of interactions, $u^{(-)}_{L'L}(r;p,JST)/r \longrightarrow \delta_{L'L}\;j_L(pr)$, and $\psi^{(-)}(\mathbf{r})$ reduces to an antisymmetric plane wave. Interaction effects are retained in all partial waves with $J\le J_{\max}$. In the quasi-elastic regime of interest here, it is found that these interaction effects are negligible for $J_{\max}>7$.

The response functions are written as (only $R^{\gamma,\gamma}_L$ is given below for illustration):

$$R^{\gamma,\gamma}_L(q,\omega) = \sum_{S,T=0,1} R^{\gamma,\gamma}_L(q,\omega;S,T) \tag{3.47}$$

where the contributions from the individual spin-isospin states are:

$$R_L^{\gamma,\gamma}(q,\omega;S,T) = \frac{1}{3}\sum_{M_d M_S}\int\frac{d\mathbf{p}}{(2\pi)^3}\frac{1}{2}|A_{ST}^{\gamma}(\mathbf{q},\mathbf{p};M_S M_d)|^2\delta\left(\omega + E_d - \frac{q^2}{6\,m} - \frac{p^2}{m}\right) \tag{3.48}$$

with A_{ST}^{γ} defined as:

$$A_{ST}^{\gamma}(\mathbf{q},\mathbf{p};M_S M_d) \equiv \langle \mathbf{q};\mathbf{p},SM_S T,M_T=0|\rho^{\gamma}(\mathbf{q})|d,M_d\rangle \tag{3.49}$$

Here $E_d = -2.225$ MeV is the deuteron ground-state energy, the factor $1/2$ in Eq. (3.48) is included to avoid double counting, and the states $|d,M_d\rangle$ and $|\mathbf{q};\mathbf{p},SM_S T,M_T=0\rangle$ are represented by the wave functions in Eqs. (3.41) and (3.43), respectively. By integrating out the energy-conserving δ-function one finds:

$$R_L^{\gamma,\gamma}(q,\omega;S,T) = \frac{m\,p}{48\,\pi^2}\sum_{M_d,M_S}\int_{-1}^{+1} d(\cos\theta_{\mathbf{p}})\,|A_{ST}^{\gamma}(q,p,\cos\theta_{\mathbf{p}};M_S M_d)|^2 \tag{3.50}$$

where the magnitude of the relative momentum $\mathbf{p}$ is fixed by $p=\sqrt{m(\omega+E_d)-q^2/4}$, and $\theta_{\mathbf{p}}$ is the angle between $\mathbf{q}$ and $\mathbf{p}$. The initial- and final-state wave functions are written as vectors in the spin-isospin space of the two nucleons for any given spatial configuration $\mathbf{r}$. For the given $\mathbf{r}$ the state vector $\rho^{\gamma}(\mathbf{q})|d,M_d\rangle$ is calculated with the same methods used in quantum Monte Carlo calculations of, for example, the charge and magnetic form factors of the trinucleons [65]. The $\mathbf{r}$ and $\theta_{\mathbf{p}}$ integrations required to calculate the amplitudes and response function are then performed by means of Gaussian quadratures.

Finally, note that, since the deuteron is a $T=0$ state, one finds:

$$R_L^{\gamma,0}(q,\omega;S,T=0) = -2\sin^2\theta_W\, R_L^{\gamma,\gamma}(q,\omega;S,T=0) \tag{3.51}$$

$$R_L^{\gamma,0}(q,\omega;S,T=1) = (1-2\sin^2\theta_W)\, R_L^{\gamma,\gamma}(q,\omega;S,T=1) \tag{3.52}$$

with similar relations holding between the transverse response functions.

3.6 Results and Conclusions

The asymmetry has been calculated at the kinematics relevant to the SAMPLE experiment. The incident electron energy was set to $E = 193$ MeV. SAMPLE measures the asymmetry at four different angles ($\theta = 138.4^o, 145.9^o, 154.0^o, 160.4^o$). Different electron final energies E' correspond to different momentum transfers Q^2, $|Q^2| \simeq 0.1$ GeV^2 in the SAMPLE experiment, which is small enough to justify the use of a non-relativistic formalism with leading interactions obtained from EFT.

The calculated asymmetries, as functions of the electron final energy, are shown in Figs. 3.12, 3.13, 3.14, and 3.15, for the four different electron scattering angles. For each set of kinematics, the left panels display the asymmetry and the total inclusive cross section, with different curves representing one-body contributions, one- plus two-body contributions from pion-exchange currents only, and the sum of all contributions. The ratios of one- plus two-body contributions from pion-exchange only and full currents to one-body contributions for both asymmetries and cross sections are displayed in the right panels.

As is apparent from the figures, the results at all angles are qualitatively similar. Near the quasi-elastic peak two-body effects in the asymmetry are negligible, less than 1%, while away from the quasi-elastic peak they become relatively more important, increasing the asymmetry by at most 3%. Note, however, that the two-body current contributions are large in the inclusive cross section, indeed dominant in the left-hand side of the quasielastic peak. In this region the contribution associated with the currents of pion range is more than 50% of the total two-body contribution.

It is interesting to examine more closely the reasons for the relative unimportance of two-body current contributions in the asymmetry. At backward angles, the expression for the asymmetry can be approximated as:

$$\frac{A}{G_\mu Q^2/(2\sqrt{2}\alpha)} \simeq \frac{R_T^{\gamma,0} + (-1+4\sin^2\theta_W) R_T^{\gamma,5}}{R_T^{\gamma,\gamma}} \tag{3.53}$$

where terms proportional to the longitudinal response functions are suppressed by the factor $v_L/v_T \leq 1/\tan^2(\theta/2)$, a small number at the angles under consideration here (note that the $R_L^{\gamma,\mathrm{a}}$ and $R_T^{\gamma,\mathrm{a}}$ response functions are of the same order of magnitude). It is useful to identify the contributions from $T=0$ and $T=1$ pn final states, and to use Eqs. (3.51) and (3.52), relating the $R_T^{\gamma,0}(T=0,1)$ to $R_T^{\gamma,\gamma}(T=0,1)$. One then finds:

$$\frac{A}{G_\mu Q^2/(2\sqrt{2}\alpha)} = \frac{1-2\sin^2\theta_W(1+r^{\gamma,\gamma}) + (-1+4\sin^2\theta_W)\, r^{\gamma,5}}{1+r^{\gamma,\gamma}} \tag{3.54}$$

$$r^{\gamma,\gamma} = R_T^{\gamma,\gamma}(T=0)/R_T^{\gamma,\gamma}(T=1) \tag{3.55}$$

$$r^{\gamma,5} = R_T^{\gamma,5}(T=1)/R_T^{\gamma,\gamma}(T=1) \tag{3.56}$$

Note that the $R_T^{\gamma,5}$ response function only receives contributions from $T=1$ pn final states, since the current $\mathbf{j}^{5,1}$ is isovector. The ratio $r^{\gamma,\gamma}$ is much smaller than one, since the transverse response is predominantly isovector. For example, at $E'=55$ MeV and $\theta=160.5^o$, $R_T^{\gamma,\gamma}(T=0) = 0.769\times10^{-5}(0.935\times10^{-5})$ MeV^{-1} and $R_T^{\gamma,\gamma}(T=1) = 10.3\times10^{-5}(25.9\times10^{-5})$ MeV^{-1}, and hence $r^{\gamma,\gamma}=0.0748$ (0.0361) with one-body (full) currents. In contrast, the ratio $r^{\gamma,5}$ is of order one; again at $E'=55$ MeV and $\theta=160.5^o$, $R_T^{\gamma,5}(T=1) = -18.3\times10^{-5}(-26.0\times10^{-5})$ MeV^{-1}, and hence $r^{\gamma,5}=-1.78$ (-1.00) with one-body (full) currents. However, it is multiplied by the small factor $(-1+4\sin^2\theta_W) = -0.074$, and so the asymmetry turns out to be largely independent of nuclear structure details.

Finally, if A^0 denotes the asymmetry obtained by ignoring the contribution of the axial current, one finds:

$$\frac{|A|}{|A^0|} = 1 + \frac{(-1+4\sin^2\theta_W)\, r^{\gamma,5}}{1-2\sin^2\theta_W(1+r^{\gamma,\gamma})} \tag{3.57}$$

The computed value for this ratio is shown in Fig. 3.16 for one of the kinematics of

the SAMPLE experiment. The contribution of the axial current to the asymmetry is of the order of 13% to 24% throughout the kinematical range considered. Note that in Fig. 3.16 we have included the small contribution from the longitudinal response.

As a last remark, we should emphasize that the calculated transverse ($R_T^{\gamma,\gamma}$) and longitudinal ($R_L^{\gamma,\gamma}$) response functions-including one- and two-body operators-reproduce [72] existing Bates data [73].

Since we have performed the computations at the SAMPLE kinematics, the above results may be used to account for two-body current corrections in the analysis of the experimental data. The SAMPLE experiment measures a convolution of the asymmetry A and the cross section ($d\sigma/d\Omega dE'$) over a certain range of electron final energies:

$$A_{total} = \frac{\int A\,(d\sigma/d\Omega dE')\,dE'}{\int (d\sigma/d\Omega dE')\,dE'} \tag{3.58}$$

The goal of the experiment is to extract the one-body part of A_{total}. To accomplish this, a model that includes only one-body contributions is used to generate the cross section. One can now use our results for the ratios of total to one-body contributions in the asymmetry and cross section to adjust for two-body effects in the experiment.

In conclusion, we have presented a calculation of the asymmetry in quasi-elastic electron-deuteron scattering arising from Z^0 exchange. The calculation includes one- and two-body contribution to both the electromagnetic and weak currents up to $\mathcal{O}(p/M)^2$ relative to the leading one-body charge current. Parity violation in the deuteron initial state or in the pion-nucleon vertex (anapole moment) are not included. Since we find that, when the cross section is large at the quasi-elastic peak, the change in the asymmetry due to two-body currents is negligible, we expect that these two-body corrections will produce a modification in the analysis of the SAMPLE experiment at the percent level, too small to affect significantly the extraction of the strange and axial form factors of the nucleon. As discussed earlier

the work to examined whether the same holds for effects from Z^0 exchange that manifest themselves within the two-nucleon system through the parity-violating pion-nucleon coupling has been completed since the completion of this computation [36], [37].

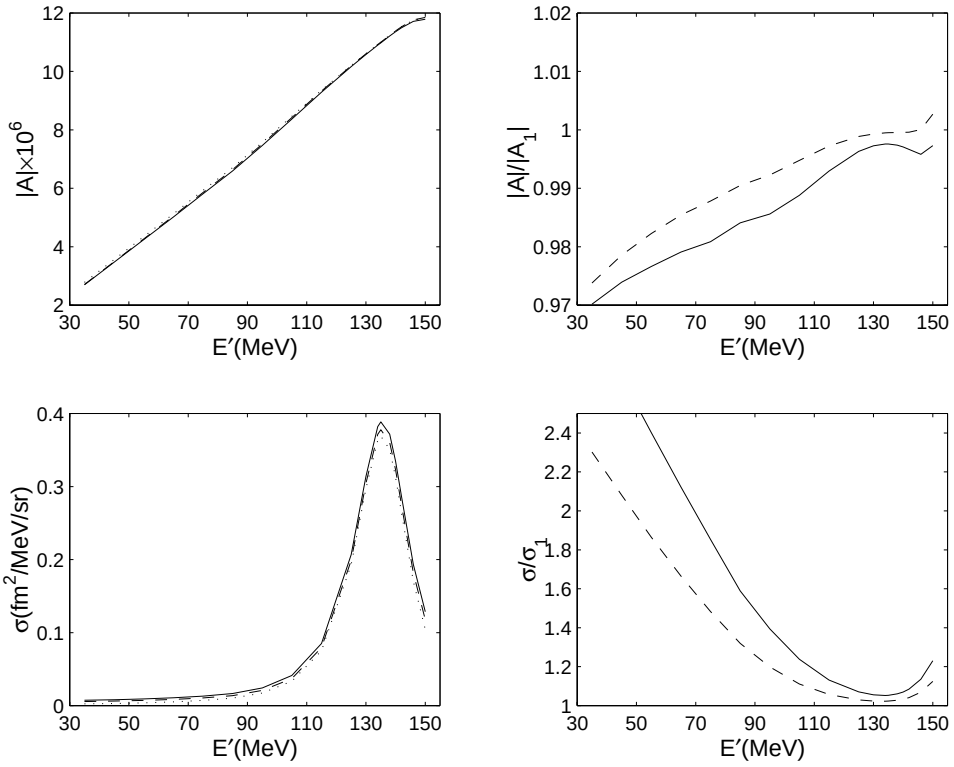

Figure 3.12: Results for scattering of an electron with incident energy $E = 193$ MeV on a deuteron at rest, as function of the electron final energy E' in MeV, for a scattering angle $\theta = 160.5^o$. Left panels: longitudinal asymmetry $|A|$ (top) and cross section σ in fm^2/MeV/sr (bottom). Shown are one-body contributions (dotted line), one- plus two-body contributions from pion-exchange currents only (dashed line), and the sum of all contributions (solid line). Right panels: ratios of one- plus two-body contributions from pion only (dashed line) and full currents (solid line) to one-body contributions for the asymmetry $|A|/|A_1|$ (top) and cross section σ/σ_1 (bottom).

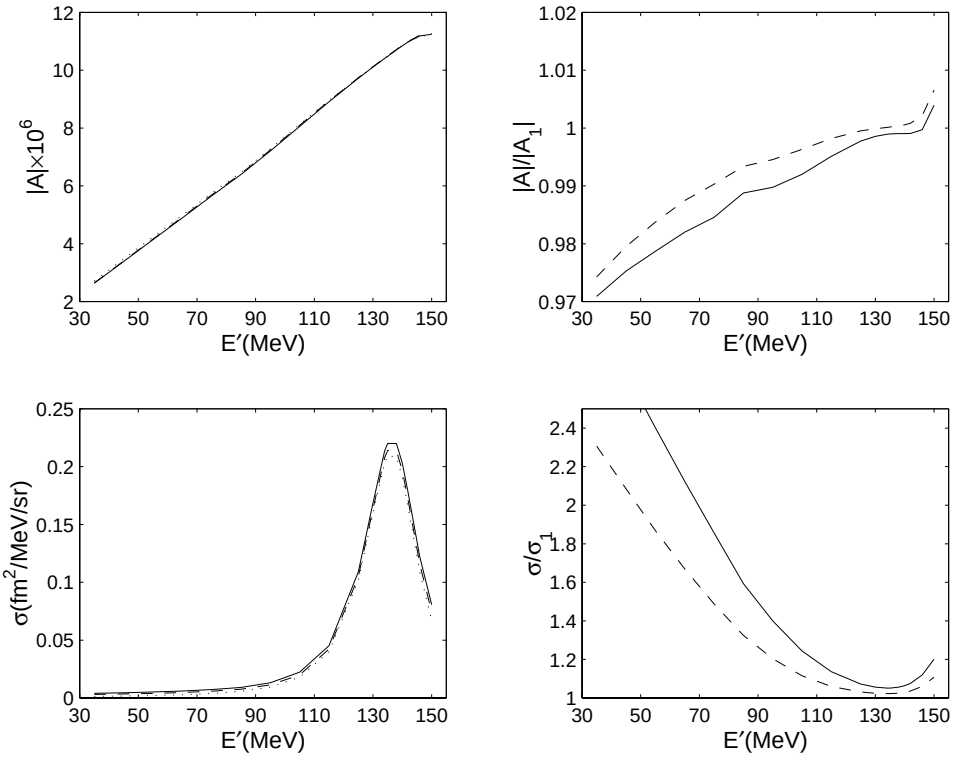

Figure 3.13: Same as Fig. 3.12, but for $\theta = 154.0^o$.

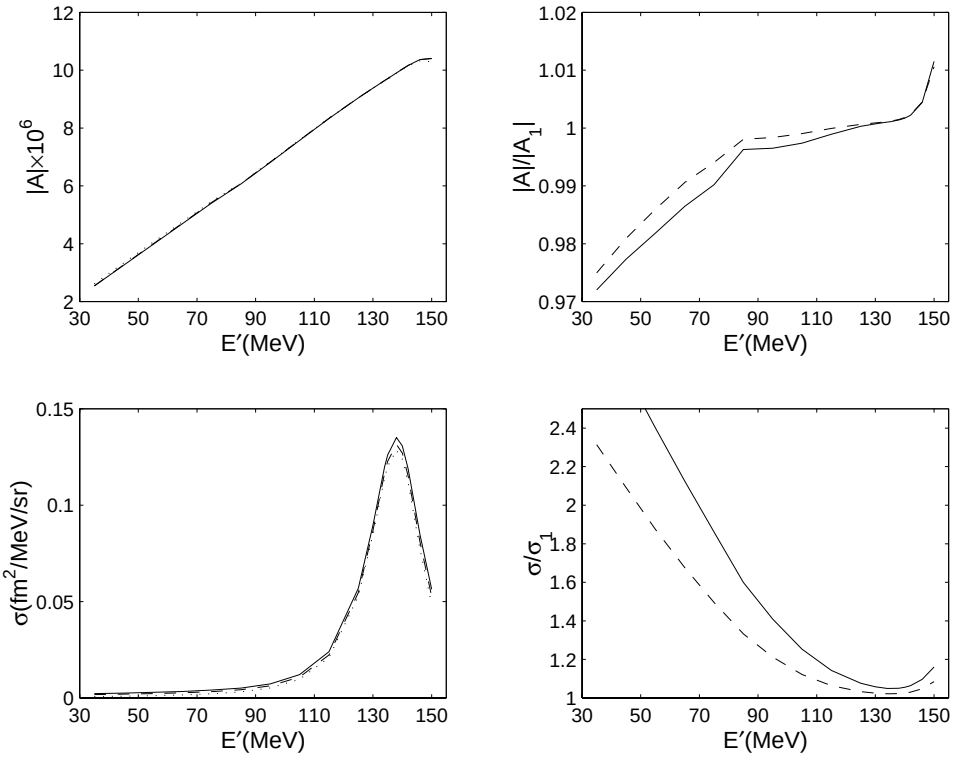

Figure 3.14: Same as Fig. 3.12, but for $\theta = 145.9^o$.

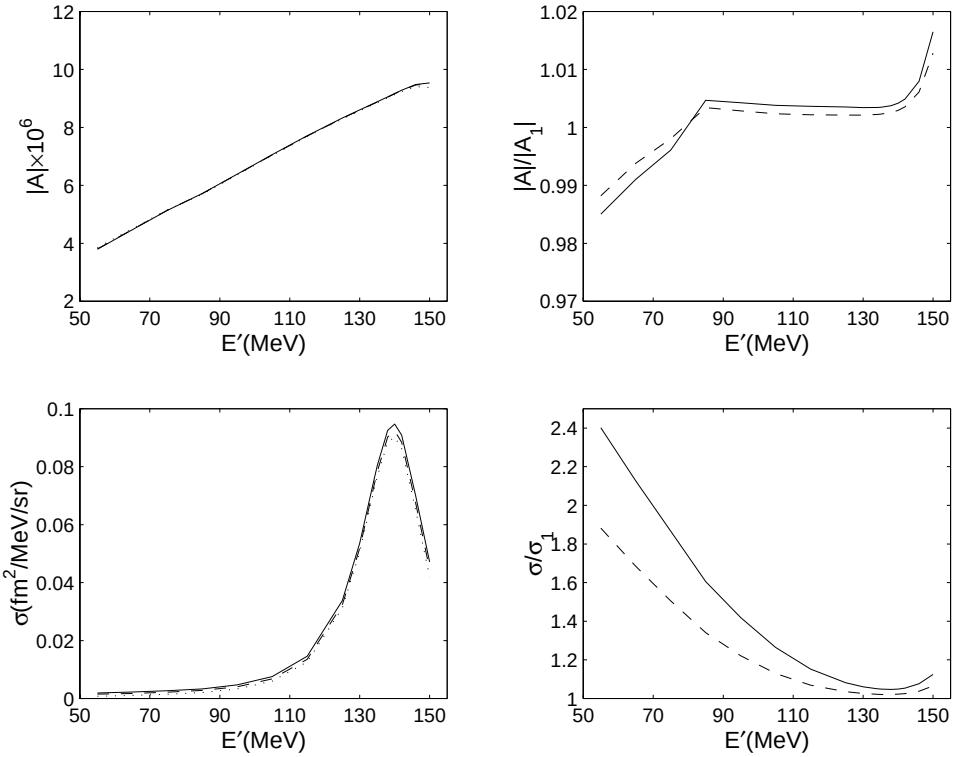

Figure 3.15: Same as Fig. 3.12, but for $\theta = 138.4^o$.

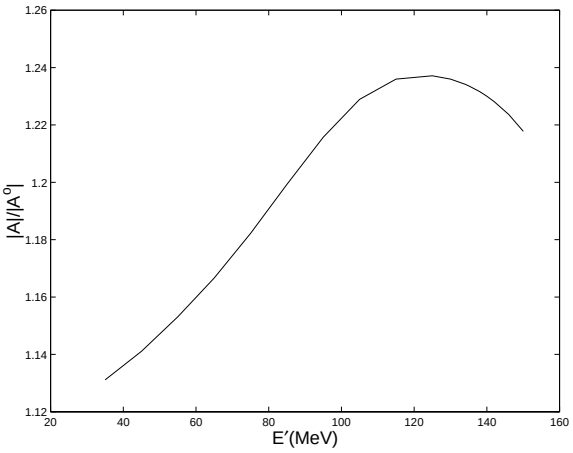

Figure 3.16: The ratio $|A|/|A^0|$ where $|A|$ is the full asymmetry and $|A^0|$ is the asymmetry without the axial contribution for scattering of an electron with incident energy $E = 193$ MeV on a deuteron at rest, as function of the electron final energy E' in MeV, for a scattering angle $\theta = 160.5^o$.

Bibliography

[1] S. Weinberg, Phys. Rev. **166**, 1568 (1968).

[2] E. Jenkins and A.V. Manohar, Phys. Lett. **B255**, 558 (1991).

[3] V. Bernard, N. Kaiser, and U.-G. Meißner, Int. J. Mod. Phys. **E4**, 193 (1995).

[4] S.P. Wells *et al.*, SAMPLE Collaboration, Phys. Rev. C **63** (2001).

[5] N.F. Mott, Proc. Roy. Soc. (London) **A 135**, 429 (1932) .

[6] F. Maas, talk given at ECT$*$, Trento, Italy, April 2004, and F. Maas, private communication.

[7] D.T. Spayde *et al.* (SAMPLE Collaboration), Phys. Rev. Lett. **84**, 1106 (2000).

[8] T.M. Ito *et al.* (SAMPLE Collaboration), Phys. Rev. Lett. **92**, 102003 (2004).

[9] L. J. Lising *et al.* [emiT Collaboration], Phys. Rev. C **62**, 055501 (2000) [arXiv:nucl-ex/0006001].

[10] P. Herczeg, "Time Reversal Violation in Nuclear Processes," in *Symmetries and Fundamental Interactions in Nuclei*, W.C. Haxton and E.M. Henley, eds., World Scientific (1995), p. 89 and references therein.

[11] F. Boehm, "Time Reversal Tests in Nuclei," in *Symmetries and Fundamental Interactions in Nuclei*, W.C. Haxton and E.M. Henley, eds., World Scientific (1995), p.67 and references therein.

[12] A. Kurylov, G. C. McLaughlin, and M. J. Ramsey-Musolf, Phys. Rev. D **63**, 076007 (2001) [arXiv:hep-ph/0011185].

[13] M. J. Ramsey-Musolf, Phys. Rev. Lett. **83**, 3997 (1999) [Erratum-ibid. **84**, 5681 (2000)] [arXiv:hep-ph/9905429].

[14] J. Engel, P. H. Frampton, and R. P. Springer, Phys. Rev. D **53**, 5112 (1996) [arXiv:nucl-th/9505026].

[15] R. S. Conti and I. B. Khriplovich, Phys. Rev. Lett. **68** (1992) 3262.

[16] I. B. Khriplovich, Nucl. Phys. B **352**, 385 (1991).

[17] B.R. Davis, S.E. Koonin, and P. Vogel, Phys. Rev. C **22**, 1233 (1980).

[18] P. G. Blunden, W. Melnitchouk, and J. A. Tjon, Phys. Rev. Lett. **91**, 142304 (2003) [arXiv:nucl-th/0306076].

[19] R. D. McKeown and M. J. Ramsey-Musolf, Mod. Phys. Lett. A **18**, 75 (2003) [arXiv:hep-ph/0203011].

[20] P. A. M. Guichon and M. Vanderhaeghen, Prog. Part. Nucl. Phys. **41** 125 (1998).

[21] P. L. Anthony et al. [SLAC E158 Collaboration], hep-ex/0312035; K. Kumar and Y. Kolomensky, private communication.

[22] A.O. Barut and C. Fronsdal, Phys. Rev. **120**, 1871 (1960).

[23] L.L. DeRaad and Y. J. Ng, Phys. Rev. **D10**, 683 (1974); Phys. Rev. **D 10**, 3440 (1974); Phys. Rev. **D 11**, 1586 (1975).

[24] L. Dixon and M. Schreiber, hep-ph/0402221.

[25] E. Beise and M. Pitt (Spokespersons), MIT-Bates Proposal.

[26] R.D. McKeown, private communication (2000).

[27] S. Ying, W.C. Haxton, and E.M. Henley, Phys. Rev. D **40**, 3211 (1989).

[28] E. Hadjimichel, G.I. Poulis, and T.W. Donnelly, Phys. Rev. C **45**, 2666 (1992).

[29] S. Schram and C.J. Horowitz, Phys. Rev. C **49**, 2777 (1994).

[30] W-Y.P. Hwang, E.M. Henley, and G.A. Miller, Ann. Phys. (N.Y.) **137**, 378 (1981).

[31] U. van Kolck, Prog. Part. Nucl. Phys. **43**, 409 (1999); S.R. Beane *et al.*, nucl-th/0008064.

[32] J. Carlson and R. Schiavilla, Rev. Mod. Phys. **70**, 1 (1998).

[33] D.O. Riska, Phys. Rep. **181**, 207 (1989).

[34] R.B. Wiringa, V.G.J. Stoks, and R. Schiavilla, Phys. Rev. C **51**, 38 (1995).

[35] Shi-Lin Zhu *et al.* nucl-th/0407088.

[36] C.-P. Liu, G. Prezeau, and M.J. Ramsey-Musolf, Phys. Rev. C **67**, (2003).

[37] R. Schiavilla, J. Carlson, and M. Paris, nucl-th/0404082

[38] T.M. Ito (Spokesperson), MIT-Bates Proposal.

[39] G0 Collaboration, www.npl.uiuc.edu/exp/G0/G0Main.html

[40] G. G. Simon, C. Schmitt, F. Borkowski, and V. H. Walther, Nucl. Phys. A **333**, 381 (1980).

[41] R.K. Bhaduri, "Models of the Nucleon," Addison-Wesley, Redwood City, CA (1988).

[42] G. 't Hooft and M. Veltman, Nucl. Phys. **B 153**, 365-401 (1979).

[43] G. Passarino and M. Veltman, Nucl. Phys. **B 160**, 151-207 (1979).

[44] S. L. Zhu, S. Puglia, and M. J. Ramsey-Musolf, Phys. Rev. D **63**, 034002 (2001) [arXiv:hep-ph/0009159].

[45] P. van Nieuwenhuizen, Nucl. Phys. **B 28**, 429-454 (1971).

[46] A. Afanasev, I. Akushevich, and N. P. Merenkov, arXiv:hep-ph/0208260.

[47] Y. C. Chen, A. Afanasev, S. J. Brodsky, C. E. Carlson, and M. Vanderhaeghen, arXiv:hep-ph/0403058.

[48] B. Pasquini, D. Drechsel, M. Vanderhaeghen, M. Gorchtein, and A. Metz, AIP Conf. Proc. **675** (2003) 646.

[49] J. Bernabeu and J.A. Penarrocha, Phys. Rev. **D22**, 1082 (1980).

[50] D. Bardin, Lectures at the European School of High Energy Physics, Slovakia Aug.-Sept. 1999

[51] M.J. Musolf and T.W. Donnelly, Nucl. Phys. **A546**, 509 (1992).

[52] M.E. Peskin and D.V Schroeder, *An Introduction to Quantum Field Theory* (Addison-Wesley, 1997).

[53] C. Ordóñez and U. van Kolck, Phys. Lett. **B291**, 459 (1992); L. Ray, C. Ordóñez, and U. van Kolck, Phys. Rev. C **53**, 2086 (1996).

[54] C.M. Maekawa and U. van Kolck, Phys. Lett. **B478**, 73 (2000); C.M. Maekawa, J.S. Veiga, and U. van Kolck, Phys. Lett. **B488**, 167 (2000).

[55] V. Bernard, H.W. Fearing, T.R. Hemmert, and U.-G. Meißner, Nucl. Phys. **A635**, 121 (1998); **A642**, 563 (1998) (E).

[56] R. Schiavilla, V.R. Pandharipande, and D.O. Riska, Phys. Rev. C **40**, 2294 (1989).

[57] J.L. Friar, Ann. Phys. (N.Y.) **81**, 332 (1973).

[58] S. Galster *et al.*, Nucl. Phys. **B32**, 221 (1971).

[59] R. Schiavilla, V.R. Pandharipande, and D.O. Riska, Phys. Rev. C **41**, 309 (1990).

[60] J. Carlson, D.O. Riska, R. Schiavilla, and R.B. Wiringa, Phys. Rev. C **42**, 830 (1990).

[61] M. Viviani, A. Kievsky, L.E. Marcucci, S. Rosati, and R. Schiavilla, Phys. Rev. C **61**, 064001 (2000).

[62] M. Viviani, R. Schiavilla, and A. Kievsky, Phys. Rev. C **54**, 534 (1996).

[63] R. Schiavilla, R.B. Wiringa, V.R. Pandharipande, and J. Carlson, Phys. Rev. C **45**, 2628 (1992).

[64] L.E. Marcucci *et al.*, Phys. Rev. C63 (2001) 044603.

[65] L.E. Marcucci, D.O. Riska, and R. Schiavilla, Phys. Rev. C **58**, 3069 (1998).

[66] D. Abbott *et al.*, Phys. Rev. Lett. **84**, 5053 (2000).

[67] R.B. Wiringa, Phys. Rev. C **43**, 1585 (1991).

[68] E. Amaldi, S. Fubini, and G. Furlan, *Electroproduction at Low Energy and Hadron Form Factors* (Springer Tracts in Modern Physics No. 83).

[69] T. Kitagaki *et al.*, Phys. Rev. D **28**, 436 (1983).

[70] R. Schiavilla *et al.*, Phys. Rev. C **58**, 1263 (1998).

[71] R. Schiavilla and D.O. Riska, Phys. Rev. C **43**, 437 (1991).

[72] J. Carlson and R. Schiavilla, Phys. Rev. Lett. **68**, 3682 (1992).

[73] S.A. Dytman *et al.*, Phys. Rev. C **38**, 800 (1988).